Finite stacked microstrip arrays with thick substrates

tu/e
Research Report
ISSN 0167-9708
Coden: TEUEDE

Eindhoven
University of Technology
Netherlands

Faculty of Electrical Engineering

Finite Stacked Microstrip Arrays with Thick Substrates

by
A.B. Smolders

EUT Report 93-E-273
ISBN 90-6144-273-7
May 1993

Eindhoven University of Technology Research Reports
EINDHOVEN UNIVERSITY OF TECHNOLOGY

Faculty of Electrical Engineering
Eindhoven The Netherlands

ISSN 0167-9708 Coden: TEUEDE

Finite Stacked Microstrip Arrays with Thick Substrates

by

A.B. Smolders

EUT Report 93-E-273
ISBN 90-6144-273-7

EINDHOVEN
MAY 1993

CIP-DATA KONINKLIJKE BIBLIOTHEEK, DEN HAAG

Smolders, A.B.

Finite stacked microstrip arrays with thick substrates /
by A.B. Smolders. - Eindhoven : Eindhoven University of
Technology, Faculty of Electrical Engineering. - Fig.,
photos. - (EUT report, ISSN 0167-9708 ; 93-E-273)
With bibliogr.
ISBN 90-6144-273-7
NUGI 832
Subject heading: microstrip antennas.

Abstract

This report deals with a method for the analysis of phased arrays of rectangular stacked microstrip antennas. The method of moments is used in combination with the exact spectral domain Green's function in order to calculate the unknown currents on each array element. First arrays based on electrically thin dielectric substrates are investigated. Lateron this model is extended to the case of arrays on electrically thick substrates. In this case a proper model for the feeding coaxial cables has to be used including an attachment mode that ensures continuity of current at the probe/patch transitions.

When analysing arrays it is extremely important that the asymptotic-form extraction technique is used. Without this analytical method it is almost impossible to analyse large arrays accurately with an acceptable computation time. More computation time can be saved if interactions in the method of moments matrices between basis functions that are located far away from each other are neglected. In this way these matrices become sparse matrices.

Mutual coupling measurements were made on a 7×7 array with a single patch layer. The measurements agreed fairly well with our calculations. Two broadband configurations have been investigated, namely a stacked microstrip array on a thick substrate and an array with electromagnetically coupled (EMC) microstrip elements. The mutual coupling level is relatively high in both configurations. Despite of this, it seems that an EMC-microstrip antenna is a very good candidate for the design of broadband microstrip arrays.

Smolders, A.B.
FINITE STACKED MICROSTRIP ARRAYS WITH THICK SUBSTRATES
Eindhoven: Faculty of Electrical Engineering, Eindhoven University of Technology, The Netherlands, 1993.
EUT Report 93-E-273, ISBN 90-6144-273-7

Address of the author
Electromagnetics Division
Faculty of Electrical Engineering, Eindhoven University of Technology
P.O. Box 513
5600 MB Eindhoven
The Netherlands

Acknowledgements

This research was supported by the Technology foundation (STW). The author wishes to thank Dr. M.E.J. Jeuken and Ir. E.S.A.M. Lepelaars for the helpful discussions.

Contents

Chapter 1

Introduction

Over the past few decades microstrip antennas and -arrays have become very popular due to features such as light weight, conformability and potentially low production costs. There are many applications of microstrip arrays ranging from mobile communications (see figure 1.1) to phased array radar systems. For some of these applications input impedance bandwidths of only a few percent suffices. However, in most practical systems a larger bandwidth is needed in order to fulfil the overall system requirements. For mobile satellite communications, an impedance bandwidth of at least 6.5 percent is required whereas for certain radar systems bandwidth requirements of more than 20% can be expected.

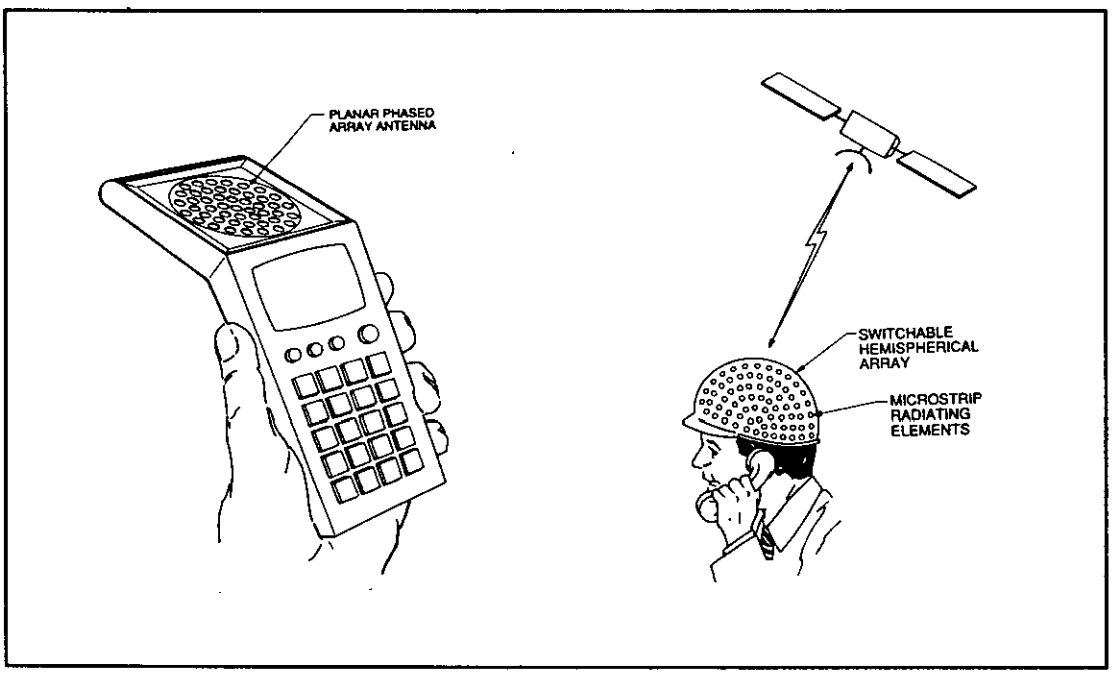

Figure 1.1: *Mobile satellite communication with microstrip arrays*

One way to improve the bandwidth of microstrip arrays is by using an electrically thick

dielectric substrate. Another way is by using stacked structures. Both configurations will be investigated in this report. In order to be able to compute the input characteristics and the radiation pattern of electrically thick microstrip arrays a rigorous model for the feeding coaxial cables has to be used in the analysis. Particularly the non-uniform nature of the current distribution on the probes must be incorporated in our model. For that purpose the Electrical Field Integral Equation (EFIE) on all patches and probes is solved with the method of moments. The same approach has already been used in [1,2,3,4,6] for the analysis of isolated microstrip antennas based on electrically thin substrates. In [5] this method has been applied to the case of isolated microstrip antennas on electrically thick substrates.

Microstrip arrays can be analysed with two approaches: 1) element by element approach (finite array approach) and 2) infinite array approach. Small arrays and edge-array elements can only be analysed in a proper way by using an element by element approach.

The organisation of this report is as follows. Chapter 2 looks at stacked-element microstrip arrays on electrically thin substrates. A simple model for the feeding coaxial cables is used. The currents on the patches are calculated with a method of moments procedure. Once these currents are known, the scattering matrix and the radiation pattern can be calculated. Chapter 3 deals with stacked-element microstrip arrays on electrically thick substrates. A sophisticated model for the coaxial cables will be included in the analysis. In the last section of chapter 2 and 3 some results are presented. Calculated data will be compared with measurements. Chapter 4 includes a paper about finite arrays of monopoles that was previously published by the author in Electronics Letters [october 1992].

Chapter 2

Finite stacked microstrip arrays with a thin substrate

2.1 Introduction

In [1],[2] and [3] a method was presented for the analysis of isolated microstrip antennas with an electrically thin substrate. They all used a spectral domain method of moments in order to calculate the unknown current distribution on the patch. Because the substrate was assumed to be electrically thin, a simple model for the feeding coaxial cable could be used. In this chapter we shall extend this model to the case of a finite array of stacked microstrip antennas build on an electrically thin substrate. The technique which was used in [4] to reduce the computation time needed to evaluate certain infinite integrals for the isolated microstrip antenna case, shall be extended in this chapter to the microstrip stacked-patch array situation.

2.2 Model description

The geometry of a finite array of identical stacked rectangular microstrip patches, fed by a coaxial cable, is shown in figure 2.1 along with the notation to be used. Both patches of each array element are assumed to be embedded in the grounded dielectric slab. The centre of both the lower and upper patch of antenna element 1 ($k = l = 1$) is located at $(x, y) = (0, 0)$. The infinite groundplane and all patches are perfect electric conductors ($\sigma \to \infty$). The dielectric material extends to infinity in the xy-plane and is isotropic, homogeneous and lossy material. The permittivity of the substrate is complex:

$$\epsilon_r = \epsilon' - j\epsilon'' = \epsilon'(1 - j \tan \delta), \tag{2.1}$$

where $\tan \delta$ is the loss-tangent of the dielectric substrate. The permeability μ of the material is the same as the permeability in vacuum: $\mu = \mu_0$.
Only the rectangular array-grid situation is studied here, but an extension to other grid forms is straightforward. The x- respectively y-dimensions of the lower patches ($z = z_1'$) are W_{x1} and W_{y1} and the x- resp. y-dimensions of the upper patches ($z = z_2'$) are W_{x2} and

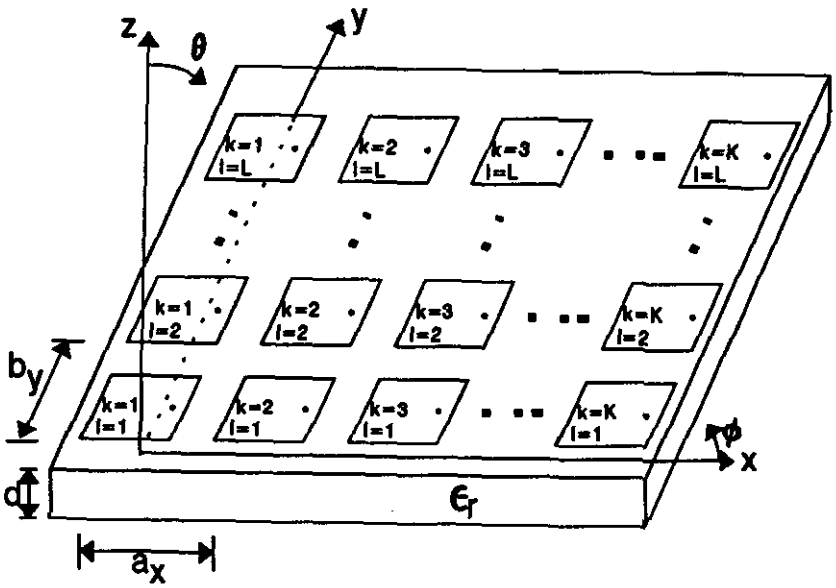

a. Top view

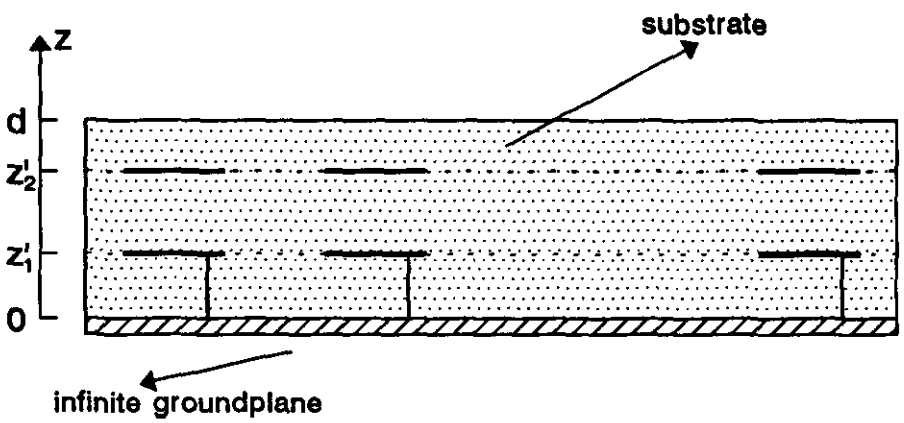

b. Side view

Figure 2.1: *Geometry of a finite array of stacked microstrip antennas embedded in a grounded dielectric slab*

W_{y2}. The feeding coaxial cables with inner radius a and outer radius b, are connected to the lower patches at a distance (x_s, y_s) from the centre of each lower patch. The number of array elements in x- and y-direction is K and L respectively and the array element index is represented by $j = (l-1) \times K + k$. We shall assume that the distance between the lower patches and the groundplane is small compared to the wavelength in the substrate ($z_1' \ll \lambda_\epsilon$). In this case the current along the coaxial probes will be almost constant. However, when the substrate is electrically thick, the current distribution along the probes will be z-dependent and therefore a more sophisticated model has to be used. Arrays on thick substrates are discussed in chapter 3 of this report. Now let's assume the substrate to be electrically thin. The probe is represented by a cylinder with radius a. The z-independent current distribution on the probe of antenna element 1 ($j = 1$) is then given by

$$\vec{\mathcal{J}}^{tot}_{probe1}(x,y,z) = I_1^p \vec{\mathcal{J}}_{probe1}(x,y,z) = \vec{e}_z \frac{I_1^p}{2\pi a} \delta\left(\sqrt{(x-x_s)^2+(y-y_s)^2} - a\right) \quad 0 \le z \le z_1' \tag{2.2}$$

where I_1^p is the port current of antenna element 1.

2.3 Green's function

A Green's function is the vector potential or the electric and magnetic field created by a unit source. The fields resulting from a general electric current distribution can then be found by dividing this current distribution into an infinite number of elementary electric dipoles and then integrating the contributions of all the elementary dipoles. The problem shall be formulated in the spectral domain, because a closed form expression of the Green's function can be found in the spectral domain. So all quantities are transformed according to $\{x,y\} \longrightarrow \{k_x, k_y\}$:

$$\begin{aligned} F(k_x,k_y) &= \int_{-\infty}^{\infty}\int_{-\infty}^{\infty} \mathcal{F}(x,y) e^{jk_x x} e^{jk_y y}\, dxdy, \\ \mathcal{F}(x,y) &= \frac{1}{4\pi^2}\int_{-\infty}^{\infty}\int_{-\infty}^{\infty} F(k_x,k_y) e^{-jk_x x} e^{-jk_y y}\, dk_x dk_y. \end{aligned} \tag{2.3}$$

In [5],[6] the spectral domain Green's function was given of an electric dipole embedded in a substrate above an infinite and perfectly conducting groundplane. Using these results, the electric field in the substrate at (x,y,z) due to a general current distribution in the substrate is given by

$$\begin{aligned} \vec{\mathcal{E}}(x,y,z) &= \frac{1}{4\pi^2}\int_{-\infty}^{\infty}\int_{-\infty}^{\infty} \vec{E}(k_x,k_y,z) e^{-jk_x x} e^{-jk_y y} dk_x dk_y \\ &= \frac{1}{4\pi^2}\int_{-\infty}^{\infty}\int_{-\infty}^{\infty}\int_{z_0} \bar{\bar{Q}}_E(k_x,k_y,z_0,z)\cdot \vec{J}(k_x,k_y,z_0) dz_0 e^{-jk_x x} e^{-jk_y y} dk_x dk_y, \end{aligned}$$

with

$$\bar{\bar{Q}}_E(k_x, k_y, z_0, z) = \begin{pmatrix} Q_{Exx} & Q_{Exy} & Q_{Exz} \\ Q_{Eyx} & Q_{Eyy} & Q_{Eyz} \\ Q_{Ezx} & Q_{Ezy} & Q_{Ezz} \end{pmatrix} \quad \text{for} \quad z \le d \text{ and } z_0 \le d, \tag{2.4}$$

$$Q_{Exx}(k_x, k_y, z_0, z) = \begin{cases} \frac{\omega\mu_0 \sin k_1 z_0}{\epsilon_r k_0^2 k_1 TeTm} \left[\jmath(k_x^2 - k_0^2\epsilon_r)Ne(z)Tm - k_x^2 k_1^2(\epsilon_r - 1)\sin k_1 z\right] & z_0 \le z \\ \frac{\omega\mu_0 \sin k_1 z}{\epsilon_r k_0^2 k_1 TeTm} \left[\jmath(k_x^2 - k_0^2\epsilon_r)Ne(z_0)Tm - k_x^2 k_1^2(\epsilon_r - 1)\sin k_1 z_0\right] & z \le z_0 \end{cases},$$

$$Q_{Exy}(k_x, k_y, z_0, z) = Q_{Eyx} = \begin{cases} \frac{\omega\mu_0 k_x k_y \sin k_1 z_0}{\epsilon_r k_0^2 k_1 TeTm} \left[\jmath Ne(z)Tm - k_1^2(\epsilon_r - 1)\sin k_1 z\right] & z_0 \le z \\ \frac{\omega\mu_0 k_x k_y \sin k_1 z}{\epsilon_r k_0^2 k_1 TeTm} \left[\jmath Ne(z_0)Tm - k_1^2(\epsilon_r - 1)\sin k_1 z_0\right] & z \le z_0 \end{cases},$$

$$Q_{Eyy}(k_x, k_y, z_0, z) = \begin{cases} \frac{\omega\mu_0 \sin k_1 z_0}{\epsilon_r k_0^2 k_1 TeTm} \left[\jmath(k_y^2 - k_0^2\epsilon_r)Ne(z)Tm - k_y^2 k_1^2(\epsilon_r - 1)\sin k_1 z\right] & z_0 \le z \\ \frac{\omega\mu_0 \sin k_1 z}{\epsilon_r k_0^2 k_1 TeTm} \left[\jmath(k_y^2 - k_0^2\epsilon_r)Ne(z_0)Tm - k_y^2 k_1^2(\epsilon_r - 1)\sin k_1 z_0\right] & z \le z_0 \end{cases},$$

$$Q_{Exz}(k_x, k_y, z_0, z) = -Q_{Ezx} = \begin{cases} \frac{\omega\mu_0 k_x \cos k_1 z_0}{k_0^2 \epsilon_r Tm} \left[\epsilon_r k_2 \cos k_1(d - z) + \jmath k_1 \sin k_1(d - z)\right] & z_0 \le z \\ \frac{\omega\mu_0 k_x \cos k_1 z}{k_0^2 \epsilon_r Tm} \left[\epsilon_r k_2 \cos k_1(d - z_0) + \jmath k_1 \sin k_1(d - z_0)\right] & z \le z_0 \end{cases},$$

$$Q_{Eyz}(k_x, k_y, z_0, z) = -Q_{Ezy} = \begin{cases} \frac{\omega\mu_0 k_y \cos k_1 z_0}{k_0^2 \epsilon_r Tm} \left[\epsilon_r k_2 \cos k_1(d - z) + \jmath k_1 \sin k_1(d - z)\right] & z_0 \le z \\ \frac{\omega\mu_0 k_y \cos k_1 z}{k_0^2 \epsilon_r Tm} \left[\epsilon_r k_2 \cos k_1(d - z_0) + \jmath k_1 \sin k_1(d - z_0)\right] & z \le z_0 \end{cases},$$

$$Q_{Ezz}(k_x, k_y, z_0, z) = \frac{\jmath\omega\mu_0}{\epsilon_r k_0^2}\delta(z - z_0) - \frac{\jmath\omega\mu_0(k_x^2 + k_y^2)}{k_0^2 \epsilon_r k_1 Tm} \begin{cases} \cos k_1 z_0 \left[\epsilon_r k_2 \sin k_1(d - z) - \jmath k_1 \cos k_1(d - z)\right] & z_0 \le z \\ \cos k_1 z \left[\epsilon_r k_2 \sin k_1(d - z_0) - \jmath k_1 \cos k_1(d - z_0)\right] & z_0 \ge z \end{cases},$$

and

$$Ne(z_0) = k_1 \cos k_1(d - z_0) + \jmath k_2 \sin k_1(d - z_0),$$

$$Tm = k_2\epsilon_r \cos k_1 d + \jmath k_1 \sin k_1 d,$$

$$Te = k_1 \cos k_1 d + \jmath k_2 \sin k_1 d,$$

$$k_1^2 = \epsilon_r k_0^2 - k_x^2 - k_y^2,$$

$$k_2^2 = k_0^2 - k_x^2 - k_y^2, \qquad (Im(k_2) < 0),$$

where $k_0 = \omega\sqrt{\epsilon_0\mu_0}$ is the free space wave number and $\omega = 2\pi f$ is the radial frequency. The restriction that $Im(k_2) < 0$ follows from the radiation condition that the fields are outward propagating waves, decaying with distance from the source. The corresponding magnetic field at (x, y, z) is given by

$$\begin{aligned}\vec{\mathcal{H}}(x,y,z) &= \frac{1}{4\pi^2}\int_{-\infty}^{\infty}\int_{-\infty}^{\infty}\vec{H}(k_x,k_y,z)e^{-\jmath k_x x}e^{-\jmath k_y y}dk_x dk_y \\ &= \frac{1}{4\pi^2}\int_{-\infty}^{\infty}\int_{-\infty}^{\infty}\int_{z_0}\bar{\bar{Q}}_H(k_x,k_y,z_0,z)\cdot\vec{J}(k_x,k_y,z_0)dz_0 e^{-\jmath k_x x}e^{-\jmath k_y y}dk_x dk_y,\end{aligned}$$

with

$$\bar{\bar{Q}}_H(k_x,k_y,z_0,z) = \begin{pmatrix} Q_{Hxx} & Q_{Hxy} & Q_{Hxz} \\ Q_{Hyx} & Q_{Hyy} & Q_{Hyz} \\ Q_{Hzx} & Q_{Hzy} & Q_{Hzz}, \end{pmatrix} \quad \text{for } z \le d \text{ and } z_0 \le d, \qquad (2.5)$$

$$
\begin{aligned}
Q_{Hxx}(k_x,k_y,z_0,z) &= \frac{jk_xk_y(\epsilon_r-1)\sin k_1z_0\cos k_1z}{TeTm} && z\le z_0,\\
Q_{Hxy}(k_x,k_y,z_0,z) &= -\frac{Ne\cos k_1z}{Te}+\frac{jk_y^2(\epsilon_r-1)\sin k_1z_0\cos k_1z}{TeTm} && z\le z_0,\\
Q_{Hyx}(k_x,k_y,z_0,z) &= \frac{Ne\cos k_1z}{Te}-\frac{jk_x^2(\epsilon_r-1)\sin k_1z_0\cos k_1z}{TeTm} && z\le z_0,\\
Q_{Hyy}(k_x,k_y,z_0,z) &= -\frac{jk_xk_y(\epsilon_r-1)\sin k_1z_0\cos k_1z}{TeTm} && z\le z_0,\\
Q_{Hxz}(k_x,k_y,z_0,z) &= -\frac{jk_y\cos k_1z}{k_1Tm}[\epsilon_rk_2\sin k_1(d-z_0)-jk_1\cos k_1(d-z_0)] && z\le z_0,\\
Q_{Hyz}(k_x,k_y,z_0,z) &= \frac{jk_x\cos k_1z}{k_1Tm}[\epsilon_rk_2\sin k_1(d-z_0)-jk_1\cos k_1(d-z_0)] && z\le z_0,\\
Q_{Hzx}(k_x,k_y,z_0,z) &= \frac{jk_yNe(z_0)\sin k_1z}{k_1Te} && z\le z_0,\\
Q_{Hzy}(k_x,k_y,z_0,z) &= -\frac{jk_xNe(z_0)\sin k_1z}{k_1Te} && z\le z_0,\\
Q_{Hzz}(k_x,k_y,z_0,z) &= 0
\end{aligned}
$$

In this chapter the magnetic field shall not be used. However, in chapter 3 where a sophisticated model for the feeding coaxial cable is presented, the magnetic field will be used, with $z \le z_0$. The roots of the functions Te and Tm correspond to solutions of the characteristic equation for TE respectively TM surface waves in a grounded dielectric slab [7]. These roots correspond to first order poles in the Green's function and are therefore a source for numerical problems. In paragraph 2.6 a method is discussed that avoids these numerical problems.

2.4 Method of moments formulation

The boundary conditions on all the $2 \times K \times L$ patches of the stacked microstrip array are used to formulate an integral equation for the unknown current distribution on each patch. This integral equation is then solved by applying the method of moments. We will start with the boundary condition that on all the patches of the array the total tangential electric field has to be zero, i.e.

$$\vec{\mathcal{E}}^{tot}_{tan}(x,y,z) = \vec{\mathcal{E}}^{ex}_{tan}(x,y,z) + \vec{\mathcal{E}}^{s}_{tan}(x,y,z) = \vec{0} \quad \text{on each patch,} \tag{2.6}$$

where $\vec{\mathcal{E}}^{ex}_{tan}(x,y,z)$ and $\vec{\mathcal{E}}^{s}_{tan}(x,y,z)$ represents the excitation field and scattered field respectively. The scattered field results from the induced currents on all the patches of the array. The excitation field is the electric field due to the $K \times L$ coaxial probes. The next step in the method of moments formulation is the expansion of the unknown current distribution on each patch into a set of basis functions

$$\vec{\mathcal{J}}(x,y,z) = \sum_{j=1}^{K\times L} \vec{\mathcal{J}}_j(x,y,z) = \sum_{j=1}^{K\times L}\sum_{m=1}^{N_1+N_2} I_{mj}\vec{\mathcal{J}}_{mj}(x,y,z_m) \tag{2.7}$$

$$\times\left\{U(x+(k-1)a_x+\tfrac{W_{xt}}{2})-U(x+(k-1)a_x-\tfrac{W_{xt}}{2})\right\}\left\{U(y+(l-1)b_y+\tfrac{W_{yt}}{2})-U(y+(l-1)b_y-\tfrac{W_{yt}}{2})\right\},$$

with

$$U(x) = 0 \quad \text{for} \quad x < 0$$

$$U(x) = 1 \quad \text{for} \quad x \geq 0,$$

and

$$W_{xt} = \begin{cases} W_{x1} & m \leq N_1 \\ W_{x2} & m > N_1 \end{cases} \quad W_{yt} = \begin{cases} W_{y1} & m \leq N_1 \\ W_{y2} & m > N_1 \end{cases} \quad z_m = \begin{cases} z_1' & m \leq N_1 \\ z_2' & m > N_1 \end{cases}.$$

N_1 is the number of basis functions used on each lower patch of an antenna element and N_2 the number of basis functions used on each upper patch. So the total number of basis functions is $N_{max} = K \times L \times (N_1 + N_2)$. $\vec{\mathcal{J}}_{mj}$ represents the m-th basis function on antenna element j and I_{mj} the corresponding unknown mode coefficient. On each antenna element the same set of basis functions will be used. The scattered electric field $\vec{\mathcal{E}}^s_{tan}(x,y,z)$ can now be expressed in terms of the unknown mode coefficients, because we may use the superposition principle. This then gives

$$\vec{\mathcal{E}}^s(x,y,z) = \sum_{i=1}^{K\times L}\sum_{n=1}^{N_1+N_2} I_{ni}\vec{\mathcal{E}}^s_{ni}(x,y,z). \tag{2.8}$$

Substituting expansion (2.8) in (2.6) gives

$$\vec{e}_z \times \left(\sum_{i=1}^{K\times L}\sum_{n=1}^{N_1+N_2} I_{ni}\vec{\mathcal{E}}^s_{ni} + \vec{\mathcal{E}}^{ex}\right) = \vec{0} \quad \text{on each patch.} \tag{2.9}$$

Introduce a residue according to

$$\vec{R} = \vec{e}_z \times \left(\sum_{i=1}^{K\times L}\sum_{n=1}^{N_1+N_2} I_{ni}\vec{\mathcal{E}}^s_{ni} + \vec{\mathcal{E}}^{ex}\right) \doteq \vec{0} \quad \text{on each patch.} \tag{2.10}$$

The above equation has to be satisfied at all points of each patch. We shall relax this condition a little bit. The residue is now weighted to zero with respect to some weighting functions, $\vec{\mathcal{J}}_{mj}$, such that

$$\langle \vec{R}\ ;\ \vec{\mathcal{J}}_{mj}\rangle_{S_{mj}} = \int\int_{S_{mj}} \vec{R}.\vec{\mathcal{J}}_{mj}\, dS_{mj} \doteq 0 \quad \text{for} \quad m = 1,2...,N_1+N_2 \quad j = 1,2,...,K\times L, \tag{2.11}$$

where S_{mj} represents the surface of the lower patch of array element j if $m \leq N_1$ and S_{mj} represents the surface of the upper patch of array element j if $m > N_1$. Note that the set of weighting functions is the same as the set of expansion functions. This choice is known as Galerkin's method. Inserting (2.10) in (2.11) gives a set of linear equations:

$$\sum_{i=1}^{K\times L}\sum_{n=1}^{N_1+N_2} I_{ni}\int\int_{S_{mj}} \vec{\mathcal{E}}^{s}_{ni}\cdot\vec{\mathcal{J}}_{mj}\,dS_{mj} + \int\int_{S_{mj}} \vec{\mathcal{E}}^{ex}\cdot\vec{\mathcal{J}}_{mj}\,dS_{mj} = 0, \qquad (2.12)$$

for $m = 1,2...,N_1+N_2,\quad j = 1,2,...,K\times L.$

The excitation field $\vec{\mathcal{E}}^{ex}$, excited by the $K \times L$ probes, can be written in terms of the contribution from each probe:

$$\sum_{i=1}^{K\times L}\sum_{n=1}^{N_1+N_2} I_{ni}\int\int_{S_{mj}} \vec{\mathcal{E}}^{s}_{ni}\cdot\vec{\mathcal{J}}_{mj}\,dS_{mj} + \sum_{i=1}^{K\times L} I^{p}_{i}\int\int_{S_{mj}} \vec{\mathcal{E}}^{ex}_{i}\cdot\vec{\mathcal{J}}_{mj}\,dS_{mj} = 0, \qquad (2.13)$$

for $m = 1,2...,N_1+N_2,\quad j = 1,2,...,K\times L.$

This set of linear equations can be written in a matrix form

$$[Z][I] + [V0][I^p] = [0]. \qquad (2.14)$$

with

$$\begin{aligned} Z_{mj,ni} &= 4\pi^2\int\int_{S_{mj}} \vec{\mathcal{E}}^{s}_{ni}(x,y,z_m)\cdot\vec{\mathcal{J}}_{mj}(x,y,z_m)\,dxdy, \\ V0_{mj,i} &= 4\pi^2\int\int_{S_{mj}} \vec{\mathcal{E}}^{ex}_{i}(x,y,z_m)\cdot\vec{\mathcal{J}}_{mj}(x,y,z_m)\,dxdy \\ &= 4\pi^2\int\int\int_{probe\ i} \vec{\mathcal{E}}^{s}_{mj}(x,y,z)\cdot\vec{\mathcal{J}}_{probe\ i}(x,y,z)\,dxdydz, \end{aligned} \qquad (2.15)$$

where the reaction concept was used [7] to rewrite $V0_{mj,i}$. $\vec{\mathcal{J}}_{probe\ i}(x,y,z)$ represents the current distribution along the coaxial probe of antenna element i and is given in (2.2). The matrix $[Z]$ contains $N_{max} \times N_{max}$ elements ($N_{max} = K \times L \times (N_1 + N_2)$), $[I]$ is a vector containing the N_{max} unknown mode coefficients of the basis functions, $[V0]$ is an $N_{max} \times (K \times L)$ matrix and $[I^p]$ is the $K \times L$-element column vector of port currents. In paragraph 2.3 a closed form expression was given for the dielectric slab Green's function in the spectral domain. The elements of $[Z]$ and $[V0]$ can be expressed in terms of this spectral domain Green's function:

$$
\begin{aligned}
Z_{mj,ni} &= 4\pi^2 \int\int_{S_{mj}} \vec{\mathcal{E}}^s_{ni}(x,y,z_m)\cdot\vec{\mathcal{J}}_{mj}(x,y,z_m)\,dxdy \\
&= 4\pi^2 \int\int_{S_{mj}} \left[\frac{1}{4\pi^2}\int_{-\infty}^{\infty}\int_{-\infty}^{\infty} \bar{\bar{Q}}_E(k_x,k_y,z_n,z_m)\cdot\vec{J}_{ni}(k_x,k_y,z_n)e^{-\jmath k_x x}e^{-\jmath k_y y}dk_x dk_y\right] \\
&\quad \cdot\vec{\mathcal{J}}_{mj}(x,y,z_{mj})dxdy \\
&= \int_{-\infty}^{\infty}\int_{-\infty}^{\infty}\left[\bar{\bar{Q}}_E(k_x,k_y,z_n,z_m)\cdot\vec{J}_{ni}(k_x,k_y,z_n)\right] \\
&\quad \cdot\left[\int\int_{S_{mj}} \vec{\mathcal{J}}_{mj}(x,y,z_m)e^{-\jmath k_x x}e^{-\jmath k_y y}dxdy\right]dk_x dk_y \\
&= \int_{-\infty}^{\infty}\int_{-\infty}^{\infty}\left[\bar{\bar{Q}}_E(k_x,k_y,z_n,z_m)\cdot\vec{J}_{ni}(k_x,k_y,z_n)\right]\cdot\vec{J}^*_{mj}(k_x,k_y,z_m)dk_x dk_y \\
&= \int_{-\infty}^{\infty}\int_{-\infty}^{\infty}\left[\bar{\bar{Q}}_E(k_x,k_y,z_n,z_m)\cdot\vec{J}_{n1}(k_x,k_y,z_n)\right]\cdot\vec{J}^*_{m1}(k_x,k_y,z_m)e^{-\jmath k_x S_{xji}}e^{-\jmath k_y S_{yji}}dk_x dk_y,
\end{aligned}
$$

$$
\begin{aligned}
V0_{mj,i} &= 4\pi^2 \int\int\int_{probe\ i} \vec{\mathcal{E}}^s_{mj}(x,y,z)\cdot\vec{\mathcal{J}}_{probe\ i}(x,y,z)\,dxdydz \\
&= 4\pi^2 \int\int\int_{probe\ i}\left[\frac{1}{4\pi^2}\int_{-\infty}^{\infty}\int_{-\infty}^{\infty}\bar{\bar{Q}}_E(k_x,k_y,z_m,z)\cdot\vec{J}_{mj}(k_x,k_y,z_m)e^{-\jmath k_x x}e^{-\jmath k_y y}dk_x dk_y\right] \\
&\quad \cdot\vec{\mathcal{J}}_{probe\ i}(x,y,z)dxdydz \\
&= \int_{-\infty}^{\infty}\int_{-\infty}^{\infty}\left[\int_0^{z_1'}\bar{\bar{Q}}_E(k_x,k_y,z_m,z)dz\cdot\vec{J}_{mj}(k_x,k_y,z_m)\right]\cdot\vec{J}^*_{probe\ i}(k_x,k_y)dk_x dk_y \\
&= \int_{-\infty}^{\infty}\int_{-\infty}^{\infty}\left[\int_0^{z_1'}\bar{\bar{Q}}_E(k_x,k_y,z_m,z)dz\cdot\vec{J}_{m1}(k_x,k_y,z_m)\right]\cdot\vec{e}_z J_0(a\sqrt{k_x^2+k_y^2}) \\
&\qquad e^{\jmath k_x(S_{xji}-x_s)}e^{\jmath k_y(S_{yji}-y_s)}dk_x dk_y,
\end{aligned}
\tag{2.16}
$$

with

$$
\vec{J}^*_{probe\ i}(k_x,k_y) = \vec{e}_z J_0(a\sqrt{k_x^2+k_y^2})e^{-\jmath k_x(x_s+(k_i-1)a_x)}e^{-\jmath k_y(y_s+(l_i-1)b_y)},
$$

$$
\text{with}\quad i=(l_i-1)K+k_i,
$$

where $\vec{J}_{mj}(k_x,k_y,z_m)$ is the Fourier transform of the m-th basis function on antenna element j and $J_0(x)$ is a Bessel function of the first kind of order 0. We will only use real basis functions, i.e. $\vec{\mathcal{J}}^*_{mj}(x,y,z_m)=\vec{\mathcal{J}}_{mj}(x,y,z_m)$. $\vec{J}^*_{mj}(k_x,k_y,z_m)$ is the complex conjugate of

$\vec{J}_{mj}(k_x, k_y, z_m)$. S_{xji} and S_{yji} are the distances in x- respectively y-direction between the centre of antenna element j and antenna element i. $\bar{\bar{Q}}_E(k_x, k_y, z_0, z)$ is the dyadic Green's function given by (2.4). The z-integral in (2.16) can be performed analytically. From (2.16) it is clear that $[Z]$ and $[V0]$ have a Toeplitz-type of symmetry. So only the $Z_{mj,ni}$ elements with $m = 1, .., N_1 + N_2$, $n = 1, .., N_1 + N_2$ and $i = 1, .., K \times L$ have to be calculated. Similarly, only the $V0_{mj,1}$ elements of $[V0]$ have to be evaluated for a maximum of 4 probe locations namely 1) probe at (x_s, y_s) 2) $(x_s, -y_s)$ 3) $(-x_s, y_s)$ and 4) $(-x_s, -y_s)$.

2.5 Basis functions

In general two types of basis functions can be distinguished: 1) entire domain basis functions and 2) subdomain basis functions. With subdomain basis functions arbitrarily shaped patches can be analysed whereas with a set of entire domain basis functions usually only one patch shape can be analysed. From a computationally point of view however, entire domain basis functions are more efficient, because usually only a few basis functions have to be used in order to obtain accurate results from a moment method procedure. We shall only consider microstrip patches with a rectangular shape and therefore a set of entire domain basis functions shall be used. These basis functions are solutions obtained from a cavity model analysis [8]. They form a complete and orthogonal set that exists on each patch of the array. The m-th basis function on antenna element 1 ($j = 1$) is then given by

Lower patch $(z_m = z_1')$, $m = 1, ..., N_1$

$$\vec{J}_{m1}(x, y, z_1') = \vec{J}_{m_x m_y}(x, y, z_1') = \vec{e}_x \frac{m_x \pi}{W_{x1}} \sin\left(\frac{m_x \pi}{W_{x1}}(x + \frac{W_{x1}}{2})\right) \cos\left(\frac{m_y \pi}{W_{y1}}(y + \frac{W_{y1}}{2})\right)$$
$$+\vec{e}_y \frac{m_y \pi}{W_{y1}} \cos\left(\frac{m_x \pi}{W_{x1}}(x + \frac{W_{x1}}{2})\right) \sin\left(\frac{m_y \pi}{W_{y1}}(y + \frac{W_{y1}}{2})\right),$$

with $|x| \leq \frac{W_{x1}}{2}$, $|y| \leq \frac{W_{y1}}{2}$, $m_x = 0, 1, 2, ..., \quad m_y = 0, 1, 2, ..., \quad$

Upper patch$(z_m = z_2')$, $m = N_1 + 1, ..., N_1 + N_2$

$$\vec{J}_{m1}(x, y, z_2') = \vec{J}_{m_x m_y}(x, y, z_2') = \vec{e}_x \frac{m_x \pi}{W_{x2}} \sin\left(\frac{m_x \pi}{W_{x2}}(x + \frac{W_{x2}}{2})\right) \cos\left(\frac{m_y \pi}{W_{y2}}(y + \frac{W_{y2}}{2})\right)$$
$$+\vec{e}_y \frac{m_y \pi}{W_{y2}} \cos\left(\frac{m_x \pi}{W_{x2}}(x + \frac{W_{x2}}{2})\right) \sin\left(\frac{m_y \pi}{W_{y2}}(y + \frac{W_{y2}}{2})\right),$$

with $|x| \leq \frac{W_{x2}}{2}$, $|y| \leq \frac{W_{y2}}{2}$, $m_x = 0, 1, 2, ..., \quad m_y = 0, 1, 2, ...$

(2.17)

For every m we have to choose a certain combination (m_x, m_y). The Fourier transforms of the basis functions for antenna element 1 are given by

Lower patch $(z_m = z_1')$, $m = 1, ..., N_1$,

$$\vec{J}_m(k_x, k_y, z_1') = \vec{J}_{m_x m_y}(k_x, k_y, z_1')$$

$$= \vec{e}_x \frac{m_x \pi}{W_{x1}} F_s(m_x, k_x, W_{x1}) F_c(m_y, k_y, W_{y1}) + \vec{e}_y \frac{m_y \pi}{W_{y1}} F_c(m_x, k_x, W_{1x}) F_s(m_y, k_y, W_{y1}),$$

Upper patch $(z_m = z_2')$, $m = N_1 + 1, ..., N_1 + N_2$,

$$\vec{J}_m(k_x, k_y, z_2') = \vec{J}_{m_x m_y}(k_x, k_y, z_2')$$

$$= \vec{e}_x \frac{m_x \pi}{W_{x2}} F_s(m_x, k_x, W_{x2}) F_c(m_y, k_y, W_{y2}) + \vec{e}_y \frac{m_y \pi}{W_{y2}} F_c(m_x, k_x, W_{x2}) F_s(m_y, k_y, W_{y2}),$$

with $m_x = 0, 1, 2, ...$, $m_y = 0, 1, 2, ...$, (2.18)

and

$$F_s(m_x, k_x, W_{xt}) = \begin{cases} \dfrac{2 m_x \pi W_{xt} \cos \frac{k_x W_{xt}}{2}}{(m_x \pi)^2 - (k_x W_{xt})^2} & m_x \text{ odd} \\ \dfrac{-j 2 m_x \pi W_{xt} \sin \frac{k_x W_{xt}}{2}}{(m_x \pi)^2 - (k_x W_{xt})^2} & m_x \text{ even} \end{cases}$$

$$F_c(m_y, k_y, W_{yt}) = \begin{cases} \dfrac{-2j W_{yt} k_y \cos \frac{k_y W_{yt}}{2}}{(m_y \pi)^2 - (k_y W_{yt})^2} & m_y \text{ odd} \\ \dfrac{-2 W_y k_y \sin \frac{k_y W_{yt}}{2}}{(m_y \pi)^2 - (k_y W_{yt})^2} & m_y \text{ even} \end{cases} .$$

The definition of the Fourier transformation is given by (2.3). From convergence tests it was shown in [9] that the x-directed modes with $m_y = 0$ and the y-directed modes with $m_x = 0$ give good results for linearly polarised patch antennas. The other modes do not significantly improve the overall result. Therefore we shall use a sub-set of (2.17). For antenna element 1 this sub-set has the form

$$
\begin{aligned}
&\text{Lower patch } (z_m = z_1'), \quad m = 1, ..., N_1 \\
&\vec{J}_{m1}(x, y, z_1') = \vec{J}_{m_x m_y}(x, y, z_1') \\
&\qquad = \vec{e}_x \tfrac{m_x \pi}{W_{x1}} \sin\left(\tfrac{m_x \pi}{W_{x1}}(x + \tfrac{W_{x1}}{2})\right) + \vec{e}_y \tfrac{m_y \pi}{W_{y1}} \sin\left(\tfrac{m_y \pi}{W_{y1}}(y + \tfrac{W_{y1}}{2})\right), \\
&\text{with} \quad |x| \le \tfrac{W_{x1}}{2}, \ |y| \le \tfrac{W_{y1}}{2}, \ m_x = 0, 1, 2, ..., \ m_y = 0, 1, 2, ..., \\
&\text{Upper patch}(z_m = z_2'), \quad m = N_1 + 1, ..., N_1 + N_2 \\
&\vec{J}_{m1}(x, y, z_2') = \vec{J}_{m_x m_y}(x, y, z_2') \\
&\qquad = \vec{e}_x \tfrac{m_x \pi}{W_{x2}} \sin\left(\tfrac{m_x \pi}{W_{x2}}(x + \tfrac{W_{x2}}{2})\right) + \vec{e}_y \tfrac{m_y \pi}{W_{y2}} \sin\left(\tfrac{m_y \pi}{W_{y2}}(y + \tfrac{W_{y2}}{2})\right), \\
&\text{with} \quad |x| \le \tfrac{W_{x2}}{2}, \ |y| \le \tfrac{W_{y2}}{2}, \ m_x = 0, 1, 2, ..., \ m_y = 0, 1, 2, ...
\end{aligned}
\tag{2.19}
$$

And the corresponding Fourier transforms of these basis functions are given by

$$
\begin{aligned}
&\text{Lower patch}(z_m = z_1'), \quad m = 1, ..., N_1, \\
&\vec{J}_m(k_x, k_y, z_1') = \vec{J}_{m_x m_y}(k_x, k_y, z_1') \\
&= \vec{e}_x \frac{m_x \pi}{W_{x1}} F_s(m_x, k_x, W_{x1}) F_c(0, k_y, W_{y1}) + \vec{e}_y \frac{m_y \pi}{W_{y1}} F_c(0, k_x, W_{1x}) F_s(m_y, k_y, W_{y1}), \\
&\text{Upper patch } (z_m = z_2'), \quad m = N_1 + 1, ..., N_1 + N_2, \\
&\vec{J}_m(k_x, k_y, z_2') = \vec{J}_{m_x m_y}(k_x, k_y, z_2') \\
&= \vec{e}_x \frac{m_x \pi}{W_{x2}} F_s(m_x, k_x, W_{x2}) F_c(0, k_y, W_{y2}) + \vec{e}_y \frac{m_y \pi}{W_{y2}} F_c(0, k_x, W_{x2}) F_s(m_y, k_y, W_{y2}), \\
&\text{with} \quad m_x = 0, 1, 2, ..., \ m_y = 0, 1, 2, ...
\end{aligned}
\tag{2.20}
$$

2.6 Efficient evaluation of the matrix $[Z]$

In (2.16) an element of the moment method matrix $[Z]$ was expressed in terms of a two dimensional infinite integral. These integrals have to be evaluated numerically. Several numerical problems occur when calculating these integrals. Before we shall discuss these problems, a change to polar coordinates is introduced:

$$k_x = k_0\beta\cos\alpha,$$
$$k_y = k_0\beta\sin\alpha. \tag{2.21}$$

This change to polar coordinates transforms one infinite integral into a finite integral. An element of $[Z]$ then takes the form

$$Z_{mj,ni} = \int_{-\pi}^{\pi}\int_{0}^{\infty}\left[\bar{\bar{Q}}_E(\beta,\alpha,z_n,z_m)\cdot\vec{J}_{n1}(\beta,\alpha,z_n)\right]\cdot\vec{J}^{*}_{m1}(\beta,\alpha,z_m) \tag{2.22}$$
$$e^{-jk_0\beta\cos\alpha S_{xji}}e^{-jk_0\beta\sin\alpha S_{yji}}k_0^2\beta d\beta d\alpha$$

The α integration range of the above integral can be reduced to $[0,\frac{\pi}{2}]$ if one uses the even and odd properties of the dyadic Green's function $\bar{\bar{Q}}_E$ and of the basis functions $\vec{J}_{m1}$, $\vec{J}_{n1}$. Using these properties, an element of $[Z]$ can be written in the following form

$$\begin{aligned} Z_{mj,ni} &= \int_{0}^{\frac{\pi}{2}}\int_{0}^{\infty}\left[\bar{\bar{Q}}_E(\beta,\alpha,z_n,z_m)\cdot\vec{J}_{n1}(\beta,\alpha,z_n)\right]\cdot\vec{J}^{*}_{m1}(\beta,\alpha,z_m)\; S_x(m,j,n,i,\beta,\alpha)k_0^2\beta d\beta d\alpha \\ &= \int_{0}^{\frac{\pi}{2}}\int_{0}^{\infty} f(\beta,\alpha)d\beta d\alpha. \end{aligned} \tag{2.23}$$

with

1. $m_y = n_y = 0$, i.e. $\vec{J}_{m1} = J_{m1}\vec{e}_x$ and $\vec{J}_{n1} = J_{n1}\vec{e}_x$.

$$S_z(m,j,n,i,\beta,\alpha) = \begin{cases} 4\cos k_x S_{xji}\cos k_y S_{yji} & m_x \text{ odd, } n_x \text{ odd} \\ -4\jmath\sin k_x S_{xji}\cos k_y S_{yji} & m_x \text{ odd, } n_x \text{ even} \\ -4\jmath\sin k_x S_{xji}\cos k_y S_{yji} & m_x \text{ even, } n_x \text{ odd} \\ 4\cos k_x S_{xji}\cos k_y S_{yji} & m_x \text{ even, } n_x \text{ even} \end{cases}$$

2. $m_y = n_x = 0$, i.e. $\vec{J}_{m1} = J_{m1}\vec{e}_x$ and $\vec{J}_{n1} = J_{n1}\vec{e}_y$.

$$S_z(m,j,n,i,\beta,\alpha) = \begin{cases} -4\sin k_x S_{xji}\sin k_y S_{yji} & m_x \text{ odd, } n_y \text{ odd} \\ -4\jmath\sin k_x S_{xji}\cos k_y S_{yji} & m_x \text{ odd, } n_y \text{ even} \\ -4\jmath\cos k_x S_{xji}\sin k_y S_{yji} & m_x \text{ even, } n_y \text{ odd} \\ 4\cos k_x S_{xji}\cos k_y S_{yji} & m_x \text{ even, } n_y \text{ even} \end{cases}$$

3. $m_x = n_y = 0$, i.e. $\vec{J}_{m1} = J_{m1}\vec{e}_y$ and $\vec{J}_{n1} = J_{n1}\vec{e}_x$.

$$S_z(m,j,n,i,\beta,\alpha) = \begin{cases} -4\sin k_x S_{xji}\sin k_y S_{yji} & m_y \text{ odd, } n_x \text{ odd} \\ -4\jmath\cos k_x S_{xji}\sin k_y S_{yji} & m_y \text{ odd, } n_x \text{ even} \\ -4\jmath\sin k_x S_{xji}\cos k_y S_{yji} & m_y \text{ even, } n_x \text{ odd} \\ 4\cos k_x S_{xji}\cos k_y S_{yji} & m_y \text{ even, } n_x \text{ even} \end{cases}$$

4. $m_x = n_x = 0$, i.e. $\vec{J}_{m1} = J_{m1}\vec{e}_y$ and $\vec{J}_{n1} = J_{n1}\vec{e}_y$.

$$S_z(m,j,n,i,\beta,\alpha) = \begin{cases} 4\cos k_x S_{xji}\cos k_y S_{yji} & m_x \text{ odd, } n_x \text{ odd} \\ -4\jmath\cos k_x S_{xji}\sin k_y S_{yji} & m_x \text{ odd, } n_x \text{ even} \\ -4\jmath\cos k_x S_{xji}\sin k_y S_{yji} & m_x \text{ even, } n_x \text{ odd} \\ 4\cos k_x S_{xji}\cos k_y S_{yji} & m_x \text{ even, } n_x \text{ even} \end{cases}$$

The infinite β integration interval can be divided into three sub intervals, i.e. $[0,1]$, $[1,\sqrt{\epsilon_r}]$,

and $[\sqrt{\epsilon_r'}, \infty]$. In the first interval the integrand has an infinite derivative at $\beta = 1$. So much integration points are needed near this point in order to obtain a good accuracy in the numerical integration. This infinite derivative can be avoided by introducing a change of variables [10] with $\beta = \cos t$:

$$\int_0^{\frac{\pi}{2}} \int_0^1 f(\beta, \alpha) d\beta d\alpha = \int_0^{\frac{\pi}{2}} \int_0^{\frac{\pi}{2}} f(\cos t, \alpha) \sin t dt d\alpha. \tag{2.24}$$

In the second integration interval this infinite derivative also occurs. With a change of variables $\beta = \cosh t$ this infinite derivative can be eliminated [10]:

$$\int_0^{\frac{\pi}{2}} \int_1^{\sqrt{\epsilon_r'}} f(\beta, \alpha) d\beta d\alpha = \int_0^{\frac{\pi}{2}} \int_0^{arccosh\sqrt{\epsilon_r'}} f(\cosh t, \alpha) \sinh t dt d\alpha. \tag{2.25}$$

In the integration interval $[1, \sqrt{\epsilon_r'}]$ another numerical problem arises due to surface waves that exist in the grounded dielectric slab. The roots of the functions Tm and Te in (2.4) correspond to solutions of the characteristic equation for TM and TE surface waves in the dielectric slab. The roots of Tm and Te correspond to poles in the dyadic Green's function. In [6] it was shown that these poles in the dyadic Green's function are first order poles and are located just below the real β-axis if the substrate is not lossless. Although the poles are not located on the real β-axis, they do cause numerical problems when integrating along the real β-axis. In most practical situations there will only be one pole, corresponding to the TM_0 mode with a zero cut-off frequency. A second mode will occur if $k_0 d\sqrt{\epsilon_r' - 1} \geq \frac{\pi}{2}$. Now lets assume only Tm has one root located at $\beta = \beta_p = \beta_0 + j\,\nu$ with $1 \leq \beta_0 \leq \sqrt{\epsilon_r'}$ and $\nu \leq 0$. The β-integrand in (2.23) may be written in the form

$$f(\beta, \alpha) = \frac{h(\beta, \alpha)}{Tm(\beta)}. \tag{2.26}$$

Because the function Tm has a first order zero at $\beta = \beta_p$, $f(\beta, \alpha)$ will have a first order pole at this point. In the neighbourhood of this pole $f(\beta, \alpha)$ can be expanded in a Laurent series. The singular part of this series is given by

$$f_{sing}(\beta, \alpha) = \frac{R(\alpha)}{\beta - \beta_p}, \tag{2.27}$$

where $R(\alpha)$ is the residue of f at $\beta = \beta_p$:

$$R(\alpha) = \lim_{\beta \to \beta_p} (\beta - \beta_p) f(\beta, \alpha) = h(\beta_p, \alpha) \lim_{\beta \to \beta_p} \frac{(\beta - \beta_p)}{Tm(\beta)}. \tag{2.28}$$

$Tm(\beta)$ can be expanded into a Taylor series in the heighbourhood of $\beta = \beta_p$:

$$Tm(\beta) = \left.\frac{dTm(\beta)}{d\beta}\right|_{\beta=\beta_p} (\beta - \beta_p) + \text{....higher order terms} \tag{2.29}$$

Substituting this expansion in expression (2.28) and neglecting the higher order terms yields

$$R(\alpha) = \frac{h(\beta_p, \alpha)}{Tm'(\beta_p)} \tag{2.30}$$

Numerical problems associated with surface waves can be avoided by extracting the singular part, denoted by f_{sing}, from the original integrand f:

$$\int_0^{\frac{\pi}{2}} \int_1^{\sqrt{\epsilon_r'}} f(\beta,\alpha)d\beta d\alpha = \int_0^{\frac{\pi}{2}} \left\{ \int_1^{\sqrt{\epsilon_r'}} (f(\beta,\alpha) - f_{sing}(\beta,\alpha))d\beta + \int_1^{\sqrt{\epsilon_r'}} f_{sing}(\beta,\alpha)d\beta \right\} d\alpha. \tag{2.31}$$

The β integration over f_{sing} can be performed analytically:

$$\begin{aligned} \int_1^{\sqrt{\epsilon_r'}} f_{sing}(\beta,\alpha)d\beta = \; & \frac{R}{2}\ln\left[\frac{(\sqrt{\epsilon_r'}-\beta_0)^2+\nu^2}{(1-\beta_0)^2+\nu^2}\right] \\ & + jR\arctan\left[\frac{\sqrt{\epsilon_r'}-\beta_0}{\nu}\right] + jR\arctan\left[\frac{\beta_0-1}{\nu}\right] \end{aligned} \tag{2.32}$$

In the case of a lossless substrate ($\nu \uparrow 0$) the integral over f_{sing} takes the form

$$\int_1^{\sqrt{\epsilon_r'}} f_{sing}(\beta,\alpha)d\beta = R\ln\left[\frac{\sqrt{\epsilon_r'}-\beta_0}{(\beta_0-1)}\right] - j\pi R \tag{2.33}$$

The remaining β integral in (2.31) is well-behaved and can be calculated with a standard numerical integration routine.

In the third integration interval, i.e. $[\sqrt{\epsilon_r'}, \infty]$, no poles or infinite derivatives occur. Several authors [1],[2] perform this integration numerically for a certain upper integration limit β_{max}. A great disadvantage of this direct integration strategy is the fact that the β-integrand is a slowly decaying and strongly oscillating function. The direct integration strategy works well for isolated microstrip antennas. However, if one wants to analyse arrays, this strategy will be very time consuming and not very accurate. Because of the $e^{jk_x S_{xji}} e^{jk_y S_{yji}}$ term in the β-integrand of (2.22), the number of oscillations increase if the distance between the two patches under consideration increases. In [4] a technique was proposed (source term extraction technique) that was applied to the case of an isolated microstrip antenna. In this report we shall extend this method to the case of an array with stacked-patch elements. Now let $\bar{\bar{\tilde{Q}}}_E$ be the asymptotic form of the dyadic Green's function $\bar{\bar{Q}}_E$ for large β values. Then an element of the matrix $[Z]$ may be written as

$$\begin{aligned} Z_{mj,ni} &= \int_0^{\frac{\pi}{2}} \int_0^{\infty} \left[\bar{\bar{Q}}_E(\beta,\alpha,z_n,z_m)\cdot\vec{J}_{n1}(\beta,\alpha,z_n)\right]\cdot\vec{J}^*_{m1}(\beta,\alpha,z_m)\; S_z(m,j,n,i,\beta,\alpha)k_0^2\beta d\beta d\alpha \\ &= \int_0^{\frac{\pi}{2}} \left\{ \int_0^{\infty} \left[(\bar{\bar{Q}}_E(\beta,\alpha,z_n,z_m) - \bar{\bar{\tilde{Q}}}_E(\beta,\alpha,z_n,z_m))\cdot\vec{J}_{n1}(\beta,\alpha,z_n)\right]\cdot \right. \\ &\qquad \left. \vec{J}^*_{m1}(\beta,\alpha,z_m)\; S_z(m,j,n,i,\beta,\alpha)k_0^2\beta d\beta \right. \\ &\quad \left. + \int_0^{\infty} \left[\bar{\bar{\tilde{Q}}}_E(\beta,\alpha,z_n,z_m)\cdot\vec{J}_{n1}(\beta,\alpha,z_n)\right]\cdot\vec{J}^*_{m1}(\beta,\alpha,z_m)\; S_z(m,j,n,i,\beta,\alpha)k_0^2\beta d\beta \right\} d\alpha \\ &= \left(Z_{mj,ni} - \tilde{Z}_{mj,ni}\right) + \tilde{Z}_{mj,ni}, \end{aligned} \tag{2.34}$$

with

$$\widetilde{Z}_{mj,ni} = \int_0^{\frac{\pi}{2}} \int_0^{\infty} \left[\overline{\overline{\widetilde{Q}}}_E(\beta,\alpha,z_n,z_m)\cdot\vec{J}_{n1}(\beta,\alpha,z_n)\right]\cdot\vec{J}^*_{m1}(\beta,\alpha,z_m)\, S_z(m,j,n,i,\beta,\alpha)k_0^2\beta d\beta d\alpha. \tag{2.35}$$

Note that $\overline{\overline{\widetilde{Q}}}_E$ is extracted from the original integrand for all β-values. The asymptotic form of the Green's function can be found by substituting $k_1 = -\jmath k_0\beta$ and $k_2 = -\jmath k_0\beta$ in expression (2.4). In this chapter only x- and y-directed basis functions are used. So only Q_{Exx}, Q_{Eyy}, Q_{Eyx} and Q_{Exy} are used.

$$\overline{\overline{\widetilde{Q}}}_E(k_x,k_y,z_0,z) = \begin{pmatrix} \widetilde{Q}_{Exx} & \widetilde{Q}_{Exy} & \widetilde{Q}_{Exz} \\ \widetilde{Q}_{Eyx} & \widetilde{Q}_{Eyy} & \widetilde{Q}_{Eyz} \\ \widetilde{Q}_{Ezx} & \widetilde{Q}_{Ezy} & \widetilde{Q}_{Ezz} \end{pmatrix}, \tag{2.36}$$

with

$$\widetilde{Q}_{Exx} = \begin{cases} \dfrac{-\jmath\omega\mu_0}{2k_0\beta}\left[1-\dfrac{2\beta^2\cos^2\alpha}{\epsilon_r+1}\right] & z=z_0=d \\ \dfrac{-\jmath\omega\mu_0}{2k_0\beta}\left[1-\dfrac{\beta^2\cos^2\alpha}{\epsilon_r}\right] & z=z_0<d \\ 0 & z\neq z_0 \end{cases}$$

$$\widetilde{Q}_{Eyy} = \begin{cases} \dfrac{-\jmath\omega\mu_0}{2k_0\beta}\left[1-\dfrac{2\beta^2\sin^2\alpha}{\epsilon_r+1}\right] & z=z_0=d \\ \dfrac{-\jmath\omega\mu_0}{2k_0\beta}\left[1-\dfrac{\beta^2\sin^2\alpha}{\epsilon_r}\right] & z=z_0<d \\ 0 & z\neq z_0 \end{cases}$$

$$\widetilde{Q}_{Eyx} = \widetilde{Q}_{Exy} = \begin{cases} \dfrac{\jmath\omega\mu_0\beta\sin 2\alpha}{2k_0\beta(\epsilon_r+1)} & z=z_0=d \\ \dfrac{\jmath\omega\mu_0\beta\sin 2\alpha}{4k_0\beta\epsilon_r} & z=z_0<d \\ 0 & z\neq z_0 \end{cases} .$$

Note that the asymptotic form is not continuous for $z = z_0 = d$. From (2.36) it is clear that $\widetilde{Z}_{mj,ni}$ is unequal zero only if the basis functions $\vec{J}_{mj}(\beta,\alpha,z_m)$ and $\vec{J}_{nj}(\beta,\alpha,z_n)$ are located both at the same z-coordinate, i.e. if $z_m = z_n$. Our task is now to find a closed form expression for the infinite β-integration over the extracted part of the integrand. We shall present this method here only for the case of two x-directed basis functions, so $\vec{J}_{mj} = J_{mj}\vec{e}_x$ and $\vec{J}_{nj} = J_{nj}\vec{e}_x$ with m_x and n_x both odd. The procedure of determining $\widetilde{Z}_{mj,ni}$ for the remaining basis functions is analogeous. Substituting (2.4) and (2.20) in expression (2.35) yields

$$\widetilde{Z}_{mj,ni} = 4A \int_0^{\frac{\pi}{2}} \frac{1}{\sin^2\alpha} \int_0^{\infty} \left[1 - \frac{\beta^2 \cos^2\alpha}{\epsilon_{rh}}\right] \frac{\cos^2\frac{\beta\gamma}{2} \sin^2\frac{\beta\xi}{2} \cos\beta\zeta \cos\beta\eta}{(n_x\pi - \beta\gamma)(n_x\pi + \beta\gamma)(m_x\pi - \beta\gamma)(m_x\pi + \beta\gamma)\beta^2} d\beta d\alpha, \tag{2.37}$$

with

$$A = \frac{-8j\omega\mu_0\pi^4 m_x^2 n_x^2 W_{yt}}{k_0^2}$$

$$\gamma = k_0 \cos\alpha W_{xt}$$

$$\xi = k_0 \sin\alpha W_{yt}$$

$$\zeta = k_0 \cos\alpha S_{xji}$$

$$\eta = k_0 \sin\alpha S_{yji}$$

$$W_{xt} = \begin{cases} W_{x1} & \text{if } z_m = z_n = z_1' \\ W_{x2} & \text{if } z_m = z_n = z_2' \end{cases}$$

$$W_{yt} = \begin{cases} W_{y1} & \text{if } z_m = z_n = z_1' \\ W_{y2} & \text{if } z_m = z_n = z_2' \end{cases}$$

$$\epsilon_{rh} = \begin{cases} \epsilon_r & \text{if } z_m = z_n < d \\ \frac{\epsilon_r+1}{2} & \text{if } z_m = z_n = d \end{cases}$$

The $\cos^2\frac{\beta\gamma}{2} \sin^2\frac{\beta\xi}{2} \cos\beta\zeta \cos\beta\eta$ term in (2.37) can be expanded into a set of exponential functions:

$$\cos^2\frac{\beta\gamma}{2} \sin^2\frac{\beta\xi}{2} \cos\beta\zeta \cos\beta\eta = \frac{-1}{64} \{g(\beta) + g(-\beta)\}, \tag{2.38}$$

with

$$\begin{aligned} g(\beta) = \; & -4e^{\jmath\beta(\zeta+\eta)} - 4e^{\jmath\beta(\zeta-\eta)} - 2e^{\jmath\beta(\gamma+\zeta+\eta)} \\ & -2e^{\jmath\beta(\gamma+\zeta-\eta)} - 2e^{\jmath\beta(\gamma-\zeta+\eta)} - 2e^{\jmath\beta(\gamma-\zeta-\eta)} \\ & +2e^{\jmath\beta(\xi+\zeta+\eta)} + 2e^{\jmath\beta(\xi+\zeta-\eta)} + 2e^{\jmath\beta(\xi-\zeta+\eta)} \\ & +2e^{\jmath\beta(\xi-\zeta-\eta)} + e^{\jmath\beta(\gamma+\xi+\zeta+\eta)} + e^{\jmath\beta(\gamma+\xi+\zeta-\eta)} \\ & +e^{\jmath\beta(\gamma+\xi-\zeta+\eta)} + e^{\jmath\beta(\gamma+\xi-\zeta-\eta)} + e^{\jmath\beta(\gamma-\xi+\zeta+\eta)} \\ & +e^{\jmath\beta(\gamma-\xi+\zeta-\eta)} + e^{\jmath\beta(\gamma-\xi-\zeta+\eta)} + e^{\jmath\beta(\gamma-\xi-\zeta-\eta)}. \end{aligned}$$

Because of the fact that the β-integrand of $\widetilde{Z}_{mj,ni}$ is an even function of β, the integration interval can be extended to the range $[-\infty,\infty]$. This then results in

$$\begin{aligned} \widetilde{Z}_{mj,ni} &= 2A\int_0^{\frac{\pi}{2}} \frac{1}{\sin^2\alpha}\int_{-\infty}^{\infty}\left[1-\frac{\beta^2\cos^2\alpha}{\epsilon_{rh}}\right] \\ &\quad \frac{\cos^2\frac{\beta\gamma}{2}\sin^2\frac{\beta\xi}{2}\cos\beta\zeta\cos\beta\eta}{(n_x\pi-\beta\gamma)(n_x\pi+\beta\gamma)(m_x\pi-\beta\gamma)(m_x\pi+\beta\gamma)\beta^2}d\beta d\alpha \\ &= 2A\int_0^{\frac{\pi}{2}}\frac{1}{\sin^2\alpha}I_\beta(\alpha)d\alpha, \end{aligned} \tag{2.39}$$

with

$$I_\beta(\alpha)=\int_{-\infty}^{\infty}\left[1-\frac{\beta^2\cos^2\alpha}{\epsilon_{rh}}\right]\frac{\cos^2\frac{\beta\gamma}{2}\sin^2\frac{\beta\xi}{2}\cos\beta\zeta\cos\beta\eta}{(n_x\pi-\beta\gamma)(n_x\pi+\beta\gamma)(m_x\pi-\beta\gamma)(m_x\pi+\beta\gamma)\beta^2}d\beta. \tag{2.40}$$

Two situations can be distinguished: 1) $m_x \neq n_x$ and 2) $m_x = n_x$. We shall now take a closer look at both situations.

1. $m_x \neq n_x$

The integrand of $I_\beta(\alpha)$ is analytical for all β values. We may, therefore, modify the β-integration path as was done in figure 2.2. This figure shows the modified integration path in the complex β-plane.
Using this modified integration path, the integral $I_\beta(\alpha)$ is given by

$$I_\beta(\alpha)=\int_{-\infty}^{\infty}\left[1-\frac{\beta^2\cos^2\alpha}{\epsilon_{rh}}\right]\frac{\cos^2\frac{\beta\gamma}{2}\sin^2\frac{\beta\xi}{2}\cos\beta\zeta\cos\beta\eta}{(n_x\pi-\beta\gamma)(n_x\pi+\beta\gamma)(m_x\pi-\beta\gamma)(m_x\pi+\beta\gamma)\beta^2}d\beta, \tag{2.41}$$

where $\int_{-\infty}^{\infty}$ denotes the integration path of figure 2.2. If we substitute expansion (2.38) into expression (2.41) and then divide the β-integral in 36 parts, we have to determine 36 integrals with the general form

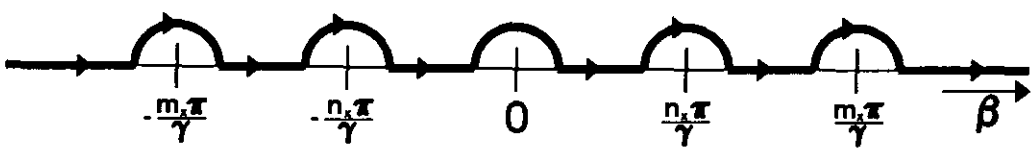

Figure 2.2: *Modified integration path if* $m_x \neq n_x$

$$G_1(t) = \int_{-\infty}^{\infty} \left[1 - \frac{\beta^2 \cos^2 \alpha}{\epsilon_{rh}}\right] \frac{e^{j\beta t}}{(n_x\pi - \beta\gamma)(n_x\pi + \beta\gamma)(m_x\pi - \beta\gamma)(m_x\pi + \beta\gamma)\beta^2} d\beta \quad (2.42)$$

The integrand of the above integral has 4 poles of order 1 at $\beta = \pm\frac{m_x\pi}{\gamma}$ and $\beta = \pm\frac{n_x\pi}{\gamma}$ and 1 pole of order 2 at $\beta = 0$. A closed form expression can be found of the integral $G_1(t)$ if the residue theorem of Cauchy and Jordan's Lemma [11] are being used. Two situations have to be distinguished in this case namely i) $t \geq 0$ and ii) $t < 0$.

i) $t \geq 0$

The original integration path of figure 2.2 will be closed with C_ρ^+ as is shown in figure 2.3. If $t > 0$ the integral over C_ρ^+ vanishes if $\rho \longrightarrow \infty$ according to Jordan's Lemma. If $t = 0$ the integral over C_ρ^+ is also zero if $\rho \longrightarrow \infty$, because the integrand has a $\frac{1}{\rho^4}$ behavior for large ρ values. The integral $G_1(t)$ is equal to zero for $t \geq 0$, because no poles are located within the area enclosed by the integration path of figure 2.3:

$$G_1(t) = 0 \quad \text{for} \quad t \geq 0. \quad (2.43)$$

ii) $t < 0$

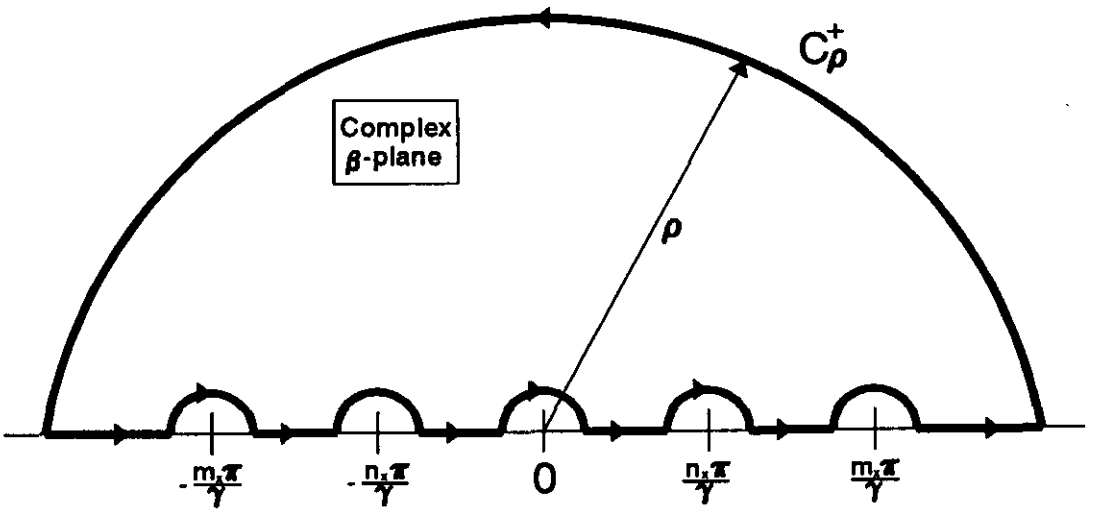

Figure 2.3: *Integration path for* $t \geq 0$

Our integration path is now closed with C_ρ^-, shown in fig. 2.4. Within the area enclosed by the integration path 5 poles are located. According to Jordan's Lemma the integral over C_ρ^- equals zero if $\rho \longrightarrow \infty$. Then $G_1(t)$ can be expressed in terms of the 5 residues:

$$G_1(t) = -2\pi j \left(\underset{\beta=\frac{-m_x\pi}{\gamma}}{\text{Res}} + \underset{\beta=\frac{-n_x\pi}{\gamma}}{\text{Res}} + \underset{\beta=0}{\text{Res}} + \underset{\beta=\frac{n_x\pi}{\gamma}}{\text{Res}} + \underset{\beta=\frac{m_x\pi}{\gamma}}{\text{Res}} \right) \tag{2.44}$$

$$\frac{\left[1 - \frac{\beta^2 \cos^2\alpha}{\epsilon_{rh}}\right] e^{j\beta t}}{(n_x\pi - \beta\gamma)(n_x\pi + \beta\gamma)(m_x\pi - \beta\gamma)(m_x\pi + \beta\gamma)\beta^2}.$$

The residue of a function $\frac{f(z)}{(z-a)^p}$ with $p \epsilon N$ at the point $z = a$, where f is an analytical function in $z = a$, can be calculated with the formula

$$\underset{z=a}{\text{Res}} \frac{f(z)}{(z-a)^p} = \frac{f^{(p-1)}(a)}{(p-1)!}. \tag{2.45}$$

Using this formula, the residues in (2.44) are given by

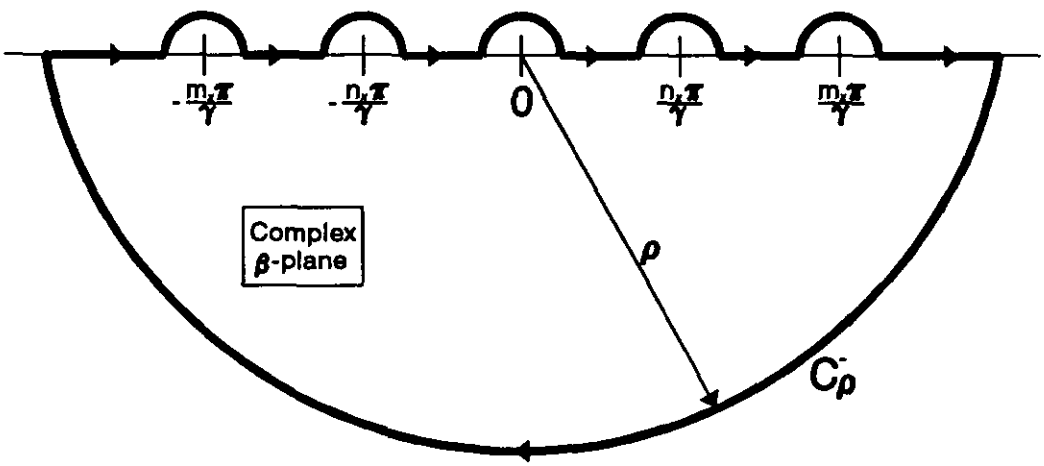

Figure 2.4: *Integration path for $t < 0$*

$$
\begin{aligned}
\operatorname*{Res}_{\beta=\frac{-m_x\pi}{\gamma}}() &= \frac{\gamma e^{-\frac{jm_x\pi t}{\gamma}}}{2\pi^5 m_x^3[n_x^2-m_x^2]}\left[1-\frac{m_x^2\pi^2\cos^2\alpha}{\gamma^2\epsilon_{rh}}\right] \\
\operatorname*{Res}_{\beta=\frac{-n_x\pi}{\gamma}}() &= \frac{\gamma e^{-\frac{jn_x\pi t}{\gamma}}}{2\pi^5 n_x^3[m_x^2-n_x^2]}\left[1-\frac{n_x^2\pi^2\cos^2\alpha}{\gamma^2\epsilon_{rh}}\right] \\
\operatorname*{Res}_{\beta=0}() &= \frac{jt}{m_x^2 n_x^2\pi^4} \\
\operatorname*{Res}_{\beta=\frac{n_x\pi}{\gamma}}() &= \frac{-\gamma e^{\frac{jn_x\pi t}{\gamma}}}{2\pi^5 n_x^3[m_x^2-n_x^2]}\left[1-\frac{n_x^2\pi^2\cos^2\alpha}{\gamma^2\epsilon_{rh}}\right] \\
\operatorname*{Res}_{\beta=\frac{m_x\pi}{\gamma}}() &= \frac{-\gamma e^{\frac{jm_x\pi t}{\gamma}}}{2\pi^5 m_x^3[n_x^2-m_x^2]}\left[1-\frac{m_x^2\pi^2\cos^2\alpha}{\gamma^2\epsilon_{rh}}\right]
\end{aligned}
\tag{2.46}
$$

Substituting these results in expression (2.44) gives a closed form expression for the integral $G_1(t)$:

$$G_1(t) = \frac{2t}{m_x^2 n_x^2 \pi^3} - \frac{2\gamma}{m_x^3\pi^4[n_x^2 - m_x^2]}\left[1 - \frac{m_x^2\pi^2\cos^2\alpha}{\gamma^2\epsilon_{rh}}\right]\sin\frac{m_x\pi t}{\gamma}$$

$$-\frac{2\gamma}{n_x^3\pi^4[m_x^2 - n_x^2]}\left[1 - \frac{n_x^2\pi^2\cos^2\alpha}{\gamma^2\epsilon_{rh}}\right]\sin\frac{n_x\pi t}{\gamma} \qquad t < 0. \tag{2.47}$$

Define a help function $G_1'(t)$ with $G_1'(t) = G_1(t) + G_1(-t)$. Then according to (2.47) and (2.43) $G_1'(t)$ is given by

$$G_1'(t) = \frac{-2|t|}{m_x^2 n_x^2 \pi^3} + \frac{2\gamma}{m_x^3\pi^4[n_x^2 - m_x^2]}\left[1 - \frac{m_x^2\pi^2\cos^2\alpha}{\gamma^2\epsilon_{rh}}\right]\sin\frac{m_x\pi|t|}{\gamma}$$

$$+\frac{2\gamma}{n_x^3\pi^4[m_x^2 - n_x^2]}\left[1 - \frac{n_x^2\pi^2\cos^2\alpha}{\gamma^2\epsilon_{rh}}\right]\sin\frac{n_x\pi|t|}{\gamma} \tag{2.48}$$

Now that $G_1'(t)$ is known, we can also calculate the original integral I_β. I_β can be expressed in terms of the function $G_1'(t)$:

$$I_\beta(\alpha) = \int_{-\infty}^{\infty}\left[1 - \frac{\beta^2\cos^2\alpha}{\epsilon_{rh}}\right]\frac{\cos^2\frac{\beta\gamma}{2}\sin^2\frac{\beta\xi}{2}\cos\beta\zeta\cos\beta\eta}{(n_x\pi - \beta\gamma)(n_x\pi + \beta\gamma)(m_x\pi - \beta\gamma)(m_x\pi + \beta\gamma)\beta^2}d\beta$$

$$= \tfrac{-1}{64}\{-4G_1'(\zeta+\eta) - 4G_1'(\zeta-\eta) - 2G_1'(\gamma+\zeta+\eta) - 2G_1'(\gamma+\zeta-\eta)$$

$$-2G_1'(\gamma-\zeta+\eta) - 2G_1'(\gamma-\zeta-\eta) + 2G_1'(\xi+\zeta+\eta) + 2G_1'(\xi+\zeta-\eta)$$

$$+2G_1'(\xi-\zeta+\eta) + 2G_1'(\xi-\zeta-\eta) + G_1'(\gamma+\xi+\zeta+\eta) + G_1'(\gamma+\xi+\zeta-\eta)$$

$$+G_1'(\gamma+\xi-\zeta+\eta) + G_1'(\gamma+\xi-\zeta-\eta) + G_1'(\gamma-\xi+\zeta+\eta)$$

$$+G_1'(\gamma-\xi+\zeta-\eta) + G_1'(\gamma-\xi-\zeta+\eta) + G_1'(\gamma-\xi-\zeta-\eta)\}$$

with $m_x \neq n_x$ (2.49)

2. $m_x = n_x$

The procedure used in the $m_x \neq n_x$ situation will also be used in this case. The integrand of I_β, given by (2.40), is in this case also analytical for all β-values. We may therefore use the modified integration path of figure 2.5 in order to determine I_β. I_β is then given by

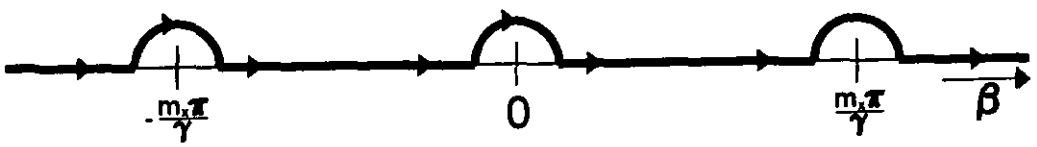

Figure 2.5: *Modified integration path for the case that* $m_x = n_x$

$$I_\beta(\alpha) = \int_{-\infty}^{\infty} \left[1 - \frac{\beta^2 \cos^2\alpha}{\epsilon_{rh}}\right] \frac{\cos^2\frac{\beta\gamma}{2}\sin^2\frac{\beta\xi}{2}\cos\beta\zeta\cos\beta\eta}{(m_x\pi - \beta\gamma)^2(m_x\pi + \beta\gamma)^2\beta^2} d\beta, \tag{2.50}$$

where the symbol $\int_{-\infty}^{\infty}$ is used to indicate that the integration path of figure 2.5 is used. Substitute expansion (2.38) in (2.50) and divide this integral in 36 parts. We then have to evaluate 36 integrals of the form

$$G_2(t) = \int_{-\infty}^{\infty} \left[1 - \frac{\beta^2 \cos^2\alpha}{\epsilon_{rh}}\right] \frac{e^{j\beta t}}{(m_x\pi - \beta\gamma)^2(m_x\pi + \beta\gamma)^2\beta^2} d\beta \tag{2.51}$$

The integrand of $G_2(t)$ has in this case 3 poles of order 2 at $\beta = \pm\frac{m_x\pi}{\gamma}$ and $\beta = 0$. If we want to use Jordan's Lemma to find an analytical solution for $G_2(t)$, two situations have to be distinguished, i.e. i) $t \geq 0$ and ii) $t < 0$.

i) $t \geq 0$

The integration path is now closed with C_ρ^+, shown in fig. 2.6.
According to Jordan's Lemma the integral over C_ρ^+ vanishes if $\rho \longrightarrow \infty$. There are no poles within the closed integration path of fig. 2.6, so $G_2(t)$ will be zero in this case.

$$G_2(t) = 0 \quad \text{for} \quad t \geq 0. \tag{2.52}$$

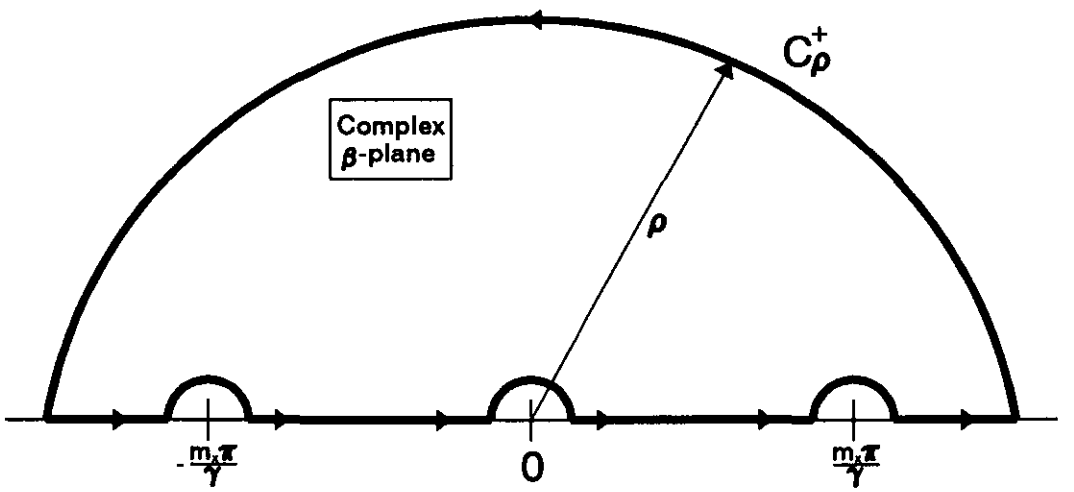

Figure 2.6: *Modified integration path if* $t \geq 0$

ii) $t < 0$

Close the integration path with C_ρ^- as shown in fig. 2.7.

Again Jordan's Lemma is used to eliminate the contribution of the integral over C_ρ^- for $\rho \longrightarrow \infty$. $G_2(t)$ can then be calculated from

$$G_2(t) = -2\pi j \left(\underset{\beta = \frac{-m_x\pi}{\gamma}}{\text{Res}} + \underset{\beta = 0}{\text{Res}} + \underset{\beta = \frac{m_x\pi}{\gamma}}{\text{Res}} \right) \frac{\left[1 - \frac{\beta^2 \cos^2 \alpha}{\epsilon_{rh}}\right] e^{j\beta t}}{(m_x\pi - \beta\gamma)^2 (m_x\pi + \beta\gamma)^2 \beta^2}. \tag{2.53}$$

The residues of the three poles can be determined with formula (2.45). Doing this one finally gets

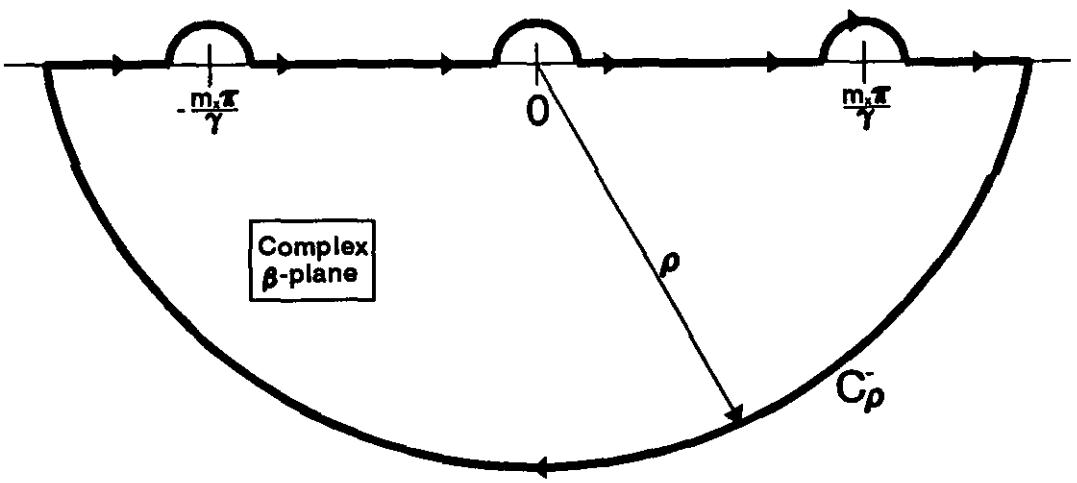

Figure 2.7: *Modified integration path if* $t < 0$

$$\begin{aligned}
\operatorname*{Res}_{\beta=\frac{-m_x\pi}{\gamma}}() &= \frac{e^{-\frac{jm_x\pi t}{\gamma}}}{4\gamma^2}\left\{\frac{\gamma^3}{m_x^5\pi^5}\left[\frac{jtm_x\pi}{\gamma}+3\right]-\frac{\gamma\cos^2\alpha}{m_x^3\pi^3\epsilon_{rh}}\left[\frac{jtm_x\pi}{\gamma}+1\right]\right\} \\
\operatorname*{Res}_{\beta=0}() &= \frac{jt}{m_x^4\pi^4} \\
\operatorname*{Res}_{\beta=\frac{m_x\pi}{\gamma}}() &= \frac{e^{\frac{jm_x\pi t}{\gamma}}}{4\gamma^2}\left\{\frac{\gamma^3}{m_x^5\pi^5}\left[\frac{jtm_x\pi}{\gamma}-3\right]-\frac{\gamma\cos^2\alpha}{m_x^3\pi^3\epsilon_{rh}}\left[\frac{jtm_x\pi}{\gamma}-1\right]\right\}
\end{aligned} \tag{2.54}$$

Substituting these results in expression (2.53) finally gives

$$\begin{aligned}
G_2(t) = {} & \frac{2t}{m_x^4\pi^3}+\frac{t}{m_x^4\pi^3}\left[1-\frac{m_x^2\pi^2\cos^2\alpha}{\gamma^2\epsilon_{rh}}\right]\cos\frac{m_x\pi t}{\gamma} \\
& -\frac{\gamma}{m_x^5\pi^4}\left[3-\frac{m_x^2\pi^2\cos^2\alpha}{\gamma^2\epsilon_{rh}}\right]\sin\frac{m_x\pi t}{\gamma} \qquad t<0.
\end{aligned} \tag{2.55}$$

Introduce the help function $G_2'(t) = G_2(t) + G_2(-t)$:

$$G_2'(t) = \frac{-2|t|}{m_x^4\pi^3} - \frac{|t|}{m_x^4\pi^3}\left[1 - \frac{m_x^2\pi^2\cos^2\alpha}{\gamma^2\epsilon_{rh}}\right]\cos\frac{m_x\pi t}{\gamma}$$

$$+\frac{\gamma}{m_x^5\pi^4}\left[3 - \frac{m_x^2\pi^2\cos^2\alpha}{\gamma^2\epsilon_{rh}}\right]\sin\frac{m_x\pi|t|}{\gamma} \tag{2.56}$$

I_β can now be expressed in terms of the functions G_2':

$$I_\beta(\alpha) = \int_{-\infty}^{\infty}\left[1 - \frac{\beta^2\cos^2\alpha}{\epsilon_{rh}}\right]\frac{\cos^2\frac{\beta\gamma}{2}\sin^2\frac{\beta\xi}{2}\cos\beta\zeta\cos\beta\eta}{(m_x\pi - \beta\gamma)^2(m_x\pi + \beta\gamma)^2\beta^2}d\beta$$

$$\begin{aligned}
&= \tfrac{-1}{64}\{-4G_2'(\zeta+\eta) - 4G_2'(\zeta-\eta) - 2G_2'(\gamma+\zeta+\eta) - 2G_2'(\gamma+\zeta-\eta)\\
&-2G_2'(\gamma-\zeta+\eta) - 2G_2'(\gamma-\zeta-\eta) + 2G_2'(\xi+\zeta+\eta) + 2G_2'(\xi+\zeta-\eta)\\
&+2G_2'(\xi-\zeta+\eta) + 2G_2'(\xi-\zeta-\eta) + G_2'(\gamma+\xi+\zeta+\eta) + G_2'(\gamma+\xi+\zeta-\eta)\\
&+G_2'(\gamma+\xi-\zeta+\eta) + G_2'(\gamma+\xi-\zeta-\eta) + G_2'(\gamma-\xi+\zeta+\eta)\\
&+G_2'(\gamma-\xi+\zeta-\eta) + G_2'(\gamma-\xi-\zeta+\eta) + G_2'(\gamma-\xi-\zeta-\eta)\}
\end{aligned} \tag{2.57}$$

with $m_x = n_x$

Note that the remaining α-integration in (2.39) has to be evaluated numerically. If one divides the α-integration interval properly into sub-intervals, only a few integration points are needed in order to obtain a good accuracy. The boundaries of these sub-intervals correspond to zeros in the arguments of $G_1'(t)$ or $G_2'(t)$. Fortunately these α integrals need only to be evaluated for 1 frequency point. As was stated before in paragraph 2.4 not all elements of $[Z]$ have to be calculated due to the Toeplitz-type of symmetry of $[Z]$. The number of elements that have to be evaluated numerically is of order $K \times L$. Computation time can also be saved by calculating all elements of $[Z]$ simultaneously, because the Green's function needs to be evaluated only once in this case. More computation time can be saved if one neglects the coupling between patches that are far away from each other. The matrix $[Z]$ is in this case a sparse matrix. In paragraph 2.10 it will be shown that very accurate results can be obtained with this method even if only a few elements of $[Z]$ are unequal zero.

2.7 Efficient evaluation of the matrix $[V0]$

We shall use the same strategy here as was used in the previous section for the case of $[Z]$ matrix elements. An element of the matrix $[V0]$ is according to (2.16) given by

$$
\begin{aligned}
V0_{mj,i} &= \int_{-\infty}^{\infty}\int_{-\infty}^{\infty}\left[\int_0^{z_1'}\bar{\bar{Q}}_E(k_x,k_y,z_m,z)dz\cdot\vec{J}_{m1}(k_x,k_y,z_m)\right]\cdot\vec{e}_z J_0(a\sqrt{k_x^2+k_y^2}) \\
&\qquad e^{\jmath k_x(S_{xji}-x_s)}e^{\jmath k_y(S_{yji}-y_s)}dk_x dk_y \\
&= \int_{-\infty}^{\infty}\int_{-\infty}^{\infty}\left[\bar{\bar{Q}}_{vE}(k_x,k_y,z_m)\cdot\vec{J}_{m1}(k_x,k_y,z_m)\right]\cdot\vec{e}_z J_0(a\sqrt{k_x^2+k_y^2}) \\
&\qquad e^{\jmath k_x(S_{xji}-x_s)}e^{\jmath k_y(S_{yji}-y_s)}dk_x dk_y,
\end{aligned}
\tag{2.58}
$$

with

$$
\bar{\bar{Q}}_{vE}(k_x,k_y,z_m)=\int_0^{z_1'}\bar{\bar{Q}}_E(k_x,k_y,z_m,z)dz.
$$

Only 2 components of the dyadic function $\bar{\bar{Q}}_{vE}$ are needed in (2.58). The z-integrations can be performed analytically. The two components of $\bar{\bar{Q}}_{vE}$ are then given by

$$
\begin{aligned}
Q_{vEzx}(k_x,k_y,z_m) &= -\tfrac{\omega\mu_0 k_x\sin k_1 z_1'}{k_0^2 k_1\epsilon_r Tm}\left[\epsilon_r k_2\cos k_1(d-z_m)+\jmath k_1\sin k_1(d-z_m)\right], \\
Q_{vEzy}(k_x,k_y,z_m) &= -\tfrac{\omega\mu_0 k_y\sin k_1 z_1'}{k_0^2 k_1\epsilon_r Tm}\left[\epsilon_r k_2\cos k_1(d-z_m)+\jmath k_1\sin k_1(d-z_m)\right].
\end{aligned}
\tag{2.59}
$$

One infinite integral in (2.58) can be transformed into a finite integral by introducing a change to polar coordinates given by (2.21). The α-integration range can be reduced to the interval $[0,\frac{\pi}{2}]$ if one uses the even and odd properties of $\bar{\bar{Q}}_{vE}$ and of $\vec{J}_{m1}$. Using the set of basis functions defined in (2.19) we obtain the following result for the elements of $[V0]$

$$
\begin{aligned}
V0_{mj,i} &= \int_{-\pi}^{\pi}\int_0^{\infty}\left[\bar{\bar{Q}}_{vE}(\beta,\alpha,z_m)\cdot\vec{J}_{m1}(\beta,\alpha,z_m)\right]\cdot\vec{e}_z J_0(k_0\beta a) \\
&\qquad e^{\jmath k_0\beta\cos\alpha(S_{xji}-x_s)}e^{\jmath k_0\beta\sin\alpha(S_{yji}-y_s)}k_0^2\beta d\beta d\alpha \\
&= \int_0^{\frac{\pi}{2}}\int_0^{\infty}\left[\bar{\bar{Q}}_{vE}(\beta,\alpha,z_m)\cdot\vec{J}_{m1}(\beta,\alpha,z_m)\right]\cdot\vec{e}_z J_0(k_0\beta a)\;S_v(m,j,i,\beta,\alpha)k_0^2\beta d\beta d\alpha
\end{aligned}
\tag{2.60}
$$

with

1. $m_y = 0$, i.e. $\vec{J}_{m1} = J_{m1}\vec{e}_x$

$$S_v(m,j,i,\beta,\alpha) = \begin{cases} -4\jmath \sin k_x(S_{xji} - x_s)\cos k_y(S_{yji} - y_s) & m_x \text{ odd} \\ 4\cos k_x(S_{xji} - x_s)\cos k_y(S_{yji} - y_s) & m_x \text{ even} \end{cases}$$

2. $m_x = 0$, i.e. $\vec{J}_{m1} = J_{m1}\vec{e}_y$

$$S_v(m,j,i,\beta,\alpha) = \begin{cases} -4\jmath \cos k_x(S_{xji} - x_s)\sin k_y(S_{yji} - y_s) & m_y \text{ odd} \\ 4\cos k_x(S_{xji} - x_s)\cos k_y(S_{yji} - y_s) & m_y \text{ even} \end{cases}$$

The β-integration interval is divided in three sub-intervals, i.e. $[0,1]$, $[1,\sqrt{\epsilon_r}]$, and $[\sqrt{\epsilon_r},\infty]$. In the first interval the β-integrand has an infinite derivative at $\beta = 1$, which can be eliminated by using an appropriate change of variables with $\beta = \cos t$ (see (2.24)). In the second interval two numerical difficulties have to be conquered. The first numerical problem is caused by the infinite derivative at $\beta = 1$ and the second numerical problem is due to the existence of surface waves in the dielectric slab. The first problem is eleminated by a change of variables $\beta = \cosh t$ (see (2.25)) and the second problem can be treated with the singularity extraction technique described in paragraph 2.6. In order to accelerate the convergence of the numerical integration in the third interval, i.e. $[\sqrt{\epsilon_r},\infty]$, the source term extraction technique that was also used in paragraph 2.6 for $[Z]$ will be applied. The slowly converging β integral is then rewritten into a sum of a closed form expression and a relatively fast converging integral. This has already been described in [4] for the case of an isolated single patch microstrip antenna. The results of [4] can also be used here if one substitutes $(S_{xji} - x_s, S_{yji} - y_s)$ for (x_s, y_s) in the resulting expressions.
Fortunately not all elements of the matrix $[V0]$ have to be calculated, because of the Toeplitz type of symmetry of this matrix. It can be shown that only the $V0_{mj,1}$ elements of $[V0]$ have to be calculated for maximum four probe locations: 1) probe at (x_s, y_s), 2) probe at $(x_s, -y_s)$, 3) probe at $(-x_s, y_s)$ and 4) probe at $(-x_s, -y_s)$. Computation time can also be reduced if all elements of $[V0]$ are calculated simultaneously. More computation time can be saved when the elements of $[V0]$ corresponding to the interaction between probes and patches that are located far away from each other is neglected. The matrix $[V0]$ is in that case a sparse matrix. [12] only considers the interaction between probes and patches that are fysically connected to each other, i.e. probe and patch belonging to the same antenna element of the array. In paragraph 2.10 the influence on the calculated results when neglecting these elements of $[V0]$ is discussed.

2.8 Port impedance matrix and scattering matrix

One of the great advantages of a finite array approach (element by element approach) in order to analyse arrays, is the fact that the port impedance matrix $[Z^p]$ and the scattering

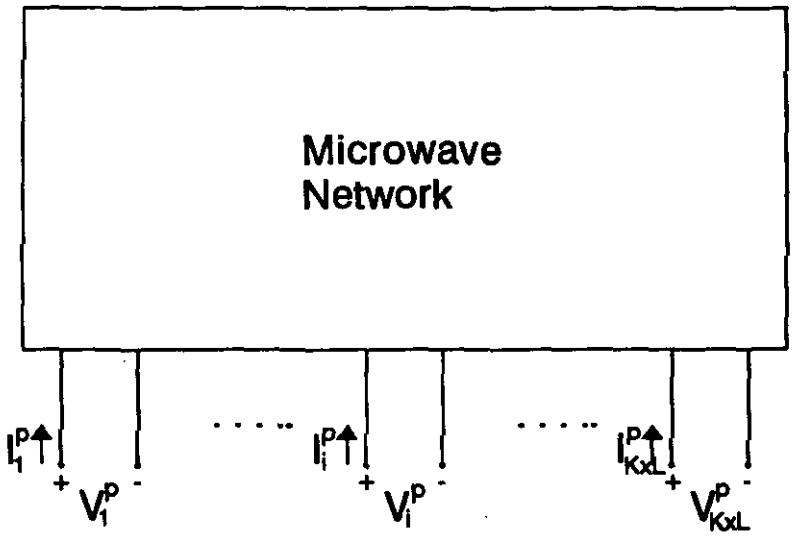

Figure 2.8: $K \times L$-*port network*

matrix $[S]$ can be calculated directly once the moment method matrices $[Z]$ and $[V0]$ are known. If one uses an infinite array approach [9],13],[14] only the active reflection coefficient is calculated for 1 scan angle. The elements of the scattering matrix can be calculated with an infinite array method if one performes an inverse Fourier transformation to the calculated active reflection coefficient. This means that the reflection coefficient has to be known over the full (θ_0, ϕ_0) range. This is of course a very cumbersome way in order to obtain the scattering matrix.
Figure 2.8 shows an $K \times L$ element array represented by an $K \times L$-port network. The relation between the port currents $[I^p]$ and port voltages $[V^p]$ is given by

$$[V^p] = [Z^p][I^p]. \tag{2.61}$$

According to [7] the relation between port voltage V_i^p and port current I_i^p is given by

$$V_i^p = \frac{P_{in}^i}{I_i^{p*}} = \frac{-1}{I_i^{p*}} \int\int\int_{source\ i} \vec{\mathcal{E}}^p \cdot \vec{J}^*_{source\ i} dV, \tag{2.62}$$

where $\vec{\mathcal{E}}^p$ is the total electric field and $\vec{J}^*_{source\,i}$ is the complex conjugate of the current distribution of source i. In our situation $\vec{\mathcal{E}}^p$ is the total electric field due to the currents on all the patches of the array. The contribution of the currents on the probes to the total electric field shall be neglected in this chapter. In chapter 3 where we look at microstrip arrays on thick substrates, this assumption is not made. The current distribution on the patches can be determined with the moment method procedure described in the previous

part of this chapter. The total electric field can then be expressed in terms of the current coefficients $[I]$:

$$\vec{\mathcal{E}}^p = \sum_{j=1}^{K\times L}\sum_{m=1}^{N_1+N_2} I_{mj}\vec{\mathcal{E}}^p_{mj}, \tag{2.63}$$

where $[I]$ is the solution of the matrix equation (2.14). Inserting the above expansion in (2.62) gives

$$\begin{aligned} V_i^p &= \frac{-1}{I_i^{p*}}\sum_{j=1}^{K\times L}\sum_{m=1}^{N_1+N_2} I_{mj}\int\int\int_{source\ i}\vec{\mathcal{E}}^p_{mj}\cdot\vec{\mathcal{J}}^*_{source\ i}dV \\ &= \frac{-1}{4\pi^2}[V0_{11,i}I_{11}+V0_{21,i}I_{21}+.....+V0_{mj,i}I_{mj}+.....+V0_{N_{max},i}I_{N_{max}}], \end{aligned} \tag{2.64}$$

with

$$N_{max} = (N_1+N_2)\cdot K\times L \quad \text{and} \quad i = 1,2,3....,K\times L.$$

Expression (2.64) can also be presented in a matrix form:

$$\begin{aligned} [V^p] &= \frac{-1}{4\pi^2}[V0]^T[I] \\ &= \frac{1}{4\pi^2}[V0]^T[Z]^{-1}[V0][I^p], \end{aligned} \tag{2.65}$$

where matrix equation (2.14) has been used. Matrix $[V0]^T$ is the transposed of $[V0]$ and $[Z]^{-1}$ is the inverse of $[Z]$. The port impedance matrix $[Z^p]$ is found by combining (2.61) with (2.65):

$$[Z^p] = \frac{1}{4\pi^2}[V0]^T[Z]^{-1}[V0]. \tag{2.66}$$

Note that $[Z^p]$ can be calculated without solving the method of moments matrix (2.14). At microwave frequencies one usually uses the scattering matrix rather than the port impedance matrix. At higher frequencies it is easier to work with incident and reflected power quantities than with impressed voltages and impressed currents. Incident power will usually remain constant under varying conditions, whereas it is very difficult to keep the impressed voltage or the impressed current constant [15]. The scattering matrix $[S]$ can be calculated by means of the well-known relation [15]

$$[S] = \{[Z^p]-[Z_0]\}\{[Z^p]+[Z_0]\}^{-1}, \tag{2.67}$$

where $[Z_0]$ is a diagonal matrix with elements equal to the characteristic impedance of the connecting coaxial cables, which is usually 50Ω. When scanning the main beam of the array at a certain scan angle (θ_0,ϕ_0), the elements of the excitation vector $[a]$ should have the form

$$a_j = e^{jk_0[(k-1)a_x u+(l-1)b_y v]}, \tag{2.68}$$

with

$$u = \sin\theta_0 \cos\phi_0, \quad v = \sin\theta_0 \sin\phi_0, \quad j = (l-1) \times K + k.$$

The active reflection coefficient of array element j can then be written in terms of the scattering matrix $[S]$:

$$R_i(\theta_0, \phi_0) = \sum_{j=1}^{K \times L} S_{ij} a_j. \tag{2.69}$$

Using (2.69) as an input signal at the terminals of all array elements means that the array is uniformly excitated. The amplitudes of the input signals are the same for each array element. When not only the phase of the input signals is used for scanning, but also the amplitude, one speaks of a tapered excitation of an array. In the following sections of this report we will assume that the array is uniformly excitated. Finally the active input impedance of array element i is given by

$$Z_{in}^{i}(\theta_0, \phi_0) = Z_0 \left[\frac{1 + R_i(\theta_0, \phi_0)}{1 - R_i(\theta_0, \phi_0)}\right] \tag{2.70}$$

2.9 Radiation pattern

Besides the port characteristics of antennas one is usually also interested in the radiation pattern since antennas are by definition made to radiate power into free space. In this section we shall assume that the elements of the method of moments matrices $[Z]$ and $[V0]$ have already been calculated. The easiest way to determine the far field pattern of an array is by using Huygens' principle. The sources, which are embedded in the grounded dielectric slab, are now replaced by an equivalent electric and magnetic current distribution on the upper surface S of the dielectric slab. We may assume [7] that the infinite plane S is a perfect electric conductor. In this case only the equivalent magnetic current distribution is nonzero on S (see figure (2.9). The magnetic current distribution on S is given by

$$\vec{J}_m = \vec{\mathcal{E}} \times \vec{n}. \tag{2.71}$$

In the far field region the electric field is given by [5]

$$\begin{aligned} \vec{\mathcal{E}}(\vec{r}) = \; & \frac{jk_0 e^{-jk_0 r}}{4\pi r} e^{jk_0 d \cos\theta} \vec{e}_r \times \\ & \int\int_S 2\vec{J}_m(x_0, y_0, d) e^{jk_0(x_0 \sin\theta\cos\phi + y_0 \sin\theta \sin\phi)} dx_0 dy_0, \end{aligned} \tag{2.72}$$

where $\vec{r}_0 = (x_0, y_0, d)$ represents a source point on the plane S and $\vec{r} = (x, y, z)$ an observation point in the far field region. The coordinate system is defined in figure 2.10.
Expression (2.72) can be written in terms of the spectral domain electric field with $k_x = k_0 \sin\theta\cos\phi$ and $k_y = k_0 \sin\theta \sin\phi$:

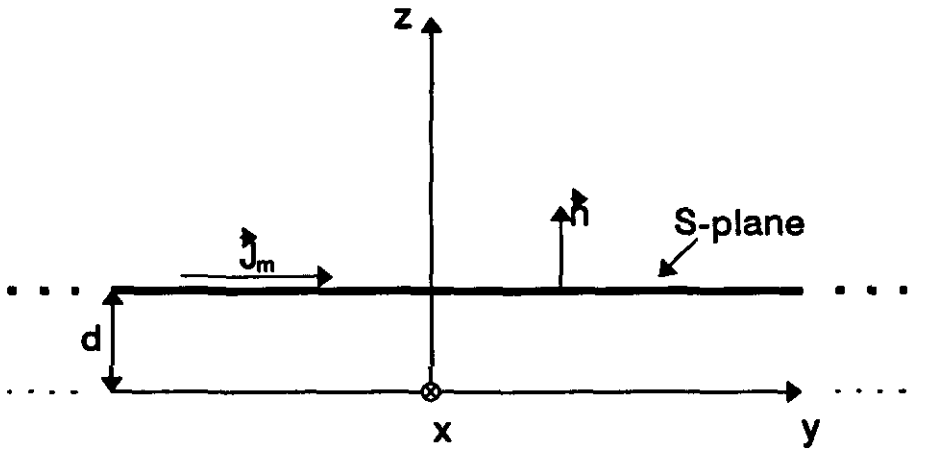

Figure 2.9: *Equivalent magnetic current source*

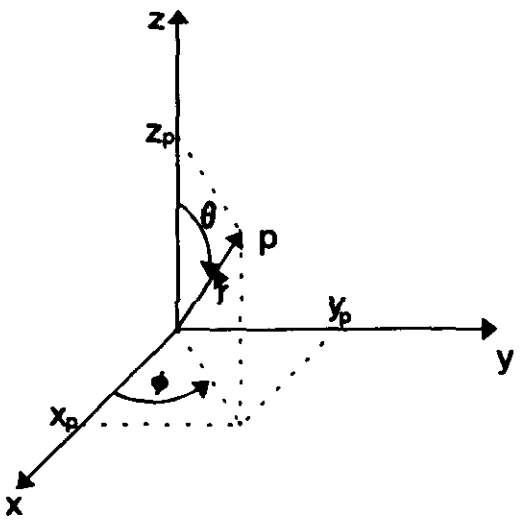

Figure 2.10: *Coordinate system*

$$\vec{\mathcal{E}}(\vec{r}) = \frac{jk_0 e^{-jk_0 r}}{2\pi r} e^{jk_0 d\cos\theta} \; \vec{e}_r \times \left[\vec{E}(k_x, k_y, d) \times \vec{e}_z\right]$$

$$= \frac{jk_0 e^{-jk_0 r}}{2\pi r} e^{jk_0 d\cos\theta} \; \vec{e}_r \times \left[\bar{\bar{Q}}(k_x, k_y, z_m, d) \cdot \sum_{j=1}^{K\times L} \sum_{m=1}^{N_1+N_2} I_{mj} \vec{J}_{mj}(k_x, k_y, z_m) \times \vec{e}_z\right], \tag{2.73}$$

with

$$z_m = \begin{cases} z_1' & m \leq N_1 \\ z_2' & m > N_1 \end{cases}.$$

In (2.73) use has been made of equation (2.4). So once the mode coefficient vector $[I]$ is known, the far field pattern can be calculated without any numerical difficulties from (2.73). $[I]$ can be determined from matrix equation (2.14) if one uses the relation

$$[I^p] = \{[UM] - [S]\}[a], \tag{2.74}$$

where $[UM]$ is the unity matrix. So the impressed port currents depend on the scattering parameters of the array. Note that for an infinite array $[I^p]$=c$[a]$, where c is a constant coefficient.

2.10 Results

2.10.1 7x7 single patch test array

In order to check the finite array theory which was presented in the previous sections, a test array was build of 7x7 square microstrip patches with a single patch layer, i.e. $z_1' = z_2'$. The array was designed to operate at L-band frequencies. The dimensions of this array are:

- patch location $z_1' = z_2' = 10mm$,
- substrate thickness $d = 10mm$,
- permittivity $\epsilon_r = 1.07 \;\; \tan\delta = 0.0008$,
- patch dimensions $W_{x1} = W_{y1} = 97.5mm$,
- inner radius coax $a = 1.5mm$,
- excitation point $X_s = 26mm$, $Y_s = 0$,
- array dimensions $a_x = b_y = 115.3mm$.

Figure 1 shows a photograph of the 7x7 test array. The overall size of the array is $1m \times 1m$. All S-parameter measurements were performed in an anechoic chamber and the measurements were made with a Hewlett Packard HP8510B network analyser. In this way the effect of reflections against objects in the environment is minimized. Because phase information is very important if one wants to determine the active reflection coefficient from the measured scattering parameters, one has to be sure that the reference plane is positioned very accurately. While measuring the S-parameter between two antenna elements, all the other antenna elements were terminated with 50Ω loads.

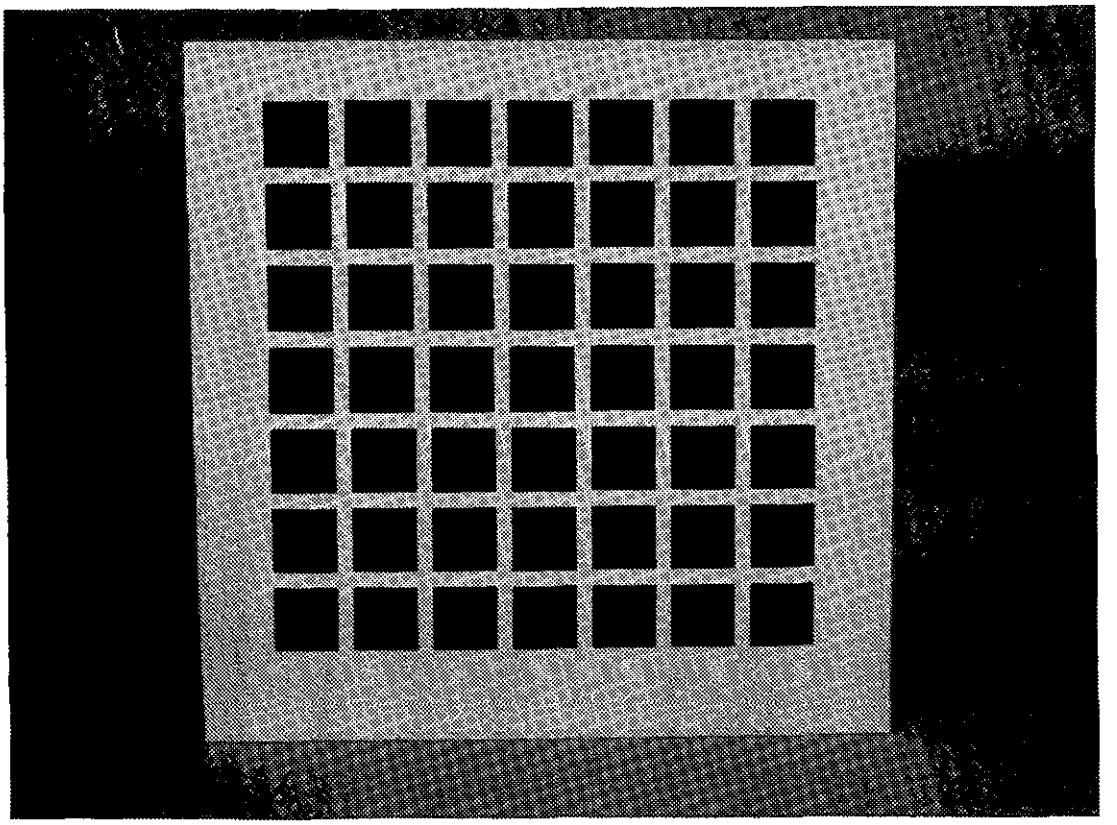

Figure 2.11: *Photograph of the* 7×7 *test array*

In figure 2.12 a plot is drawn of the calculated and measured amplitude of the coupling coefficient between the centre element ($k = l = 4, j = 25$) and elements along the $l = 4$ and $l = 3$ row with f =1.3 GHz. Calculations were made using three x-directed basis functions ($m_x = 1, 3, 5$; $m_y = 0$) and one y-directed basis function ($m_x = 0$; $m_y = 2$) for each array element (see also (2.19).
From figure 2.12 it is clear that there is some disagreement between measured and calculated S-parameter data. This is probably due to the finite size of the substrate and groundplane of the test array. Furthermore, the inaccuracy of the permittivity and the inaccuracy of the patch dimensions could be a potential source for errors. Another factor

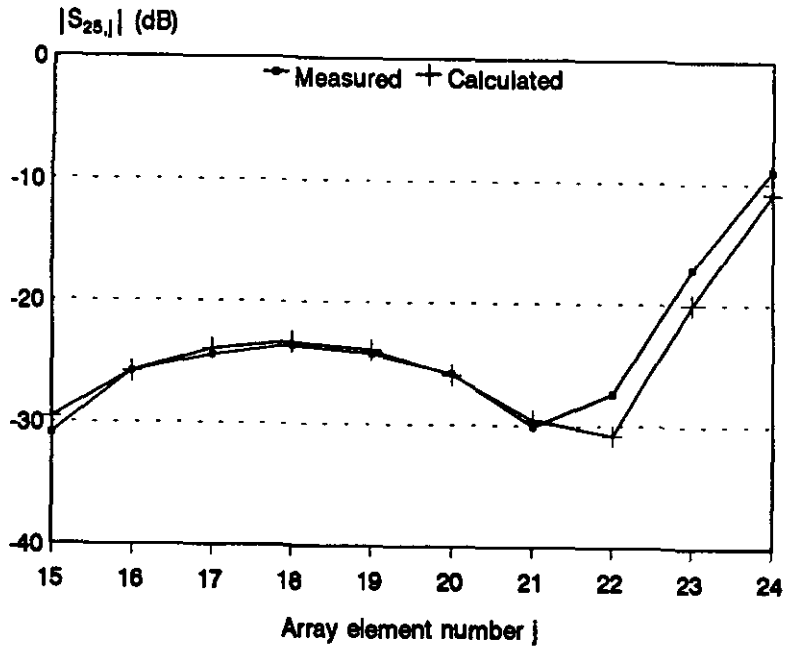

Figure 2.12: *Measured and calculated coupling coefficient between the centre element ($j = 25$) and elements of the $l = 4$ and $l = 3$ row of a 7x7 array with $j = (l-1)K + k$, $f = 1.3$ GHz*

could be the simple feed model that we have used in our theoretical model, i.e. the coupling between the coaxial probes was not included in the analysis. In chapter 3 a more sophisticated feed model will be used, including coupling between the coaxial probes of the array.

At this stage it is interesting to investigate how much computational effort has to be used in order to obtain accurate results for the calculated scattering matrix. We have used a numerical strategy that speeds up the numerical analysis: matrix elements of $[Z]$ corresponding to 2 array elements for which the distance in x-direction is larger than $k_{zmax} \times a_x$ and the distance in y-direction is larger than $l_{zmax} \times b_y$ are neglected. Similarly, matrix elements of $[V0]$ corresponding to 2 array elements for which the distance in x-direction and y-direction is larger than $k_{vmax} \times a_x$ respectively $l_{vmax} \times b_y$ are set to zero. In this way $[Z]$ and $[V0]$ become sparse matrices. First we shall examine what the influence is of this method if we apply this method only to the elements of $[V0]$. Figure 2.13 shows the calculated coupling coefficients between the centre element of our test array and array element $j = 24$, $j = 18$ and element $j = 1$ for various (k_{vmax}, l_{vmax}) values. Note that $k_{zmax} = l_{zmax} = 7$. Quite accurate results can be obtained even if $(k_{vmax}, l_{vmax}) = (1, 1)$.

Figure 2.14 shows calculated coupling coefficients between the centre element and array element $j = 24$, $j = 18$ and element $j = 1$ for various (k_{zmax}, l_{zmax}) values. The excitation matrix $[V0]$ is not altered so $k_{vmax} = l_{vmax} = 7$. From this figure it is clear that very accurate results can be obtained for the coupling between the centre element and all the

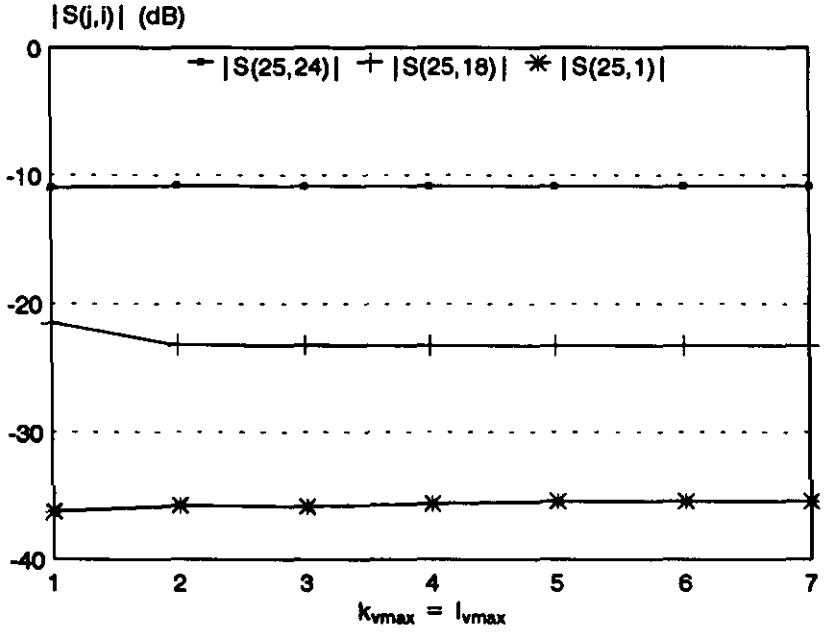

Figure 2.13: *Calculated S-parameters for various* (k_{vmax}, l_{vmax}) *values,* f *=1.3 GHz*

other array elements if we choose $(k_{zmax}, l_{zmax}) = (4,4)$. If one is only interested in the coupling between adjacent array elements $(k_{zmax}, l_{zmax}) = (2,2)$ can be used. In this way large arrays can be analysed while the overall computation time remains relatively short. Once the scattering matrix $[S]$ is known, we can calculate the active reflection coefficient from (2.69). Figure 2.15 shows the E- and H-plane active reflection coefficient of the centre element of our 7x7 test array, with f =1.3 GHz. The "measured" curve indicates that the measured S-parameter data was used whereas the "calculated" curve indicates that the calculated S-parameter data was used.
The disagreement between the measured curve and calculated curve is probably caused by phase errors in the measured S-parameter data. Phase errors of 10^0 are normal for this type of measurements [Pozar]. Another error causing factor could be the difference between the measured and calculated $S_{j,j}$ of the centre element $(j = 25)$. Figure 2.16 shows calculated and measured $S_{25,25}$ versus frequency. We think that the simple feed model which was used in the analysis is the cause of the disagreement.

2.10.2 Stacked-element microstrip array

In this section the results of a study of an array of stacked patch elements are presented. Again square microstrip elements are used on a square grid. The dimensions of the stacked array are

- patch location lower patch $z_1' = 1.57mm$,

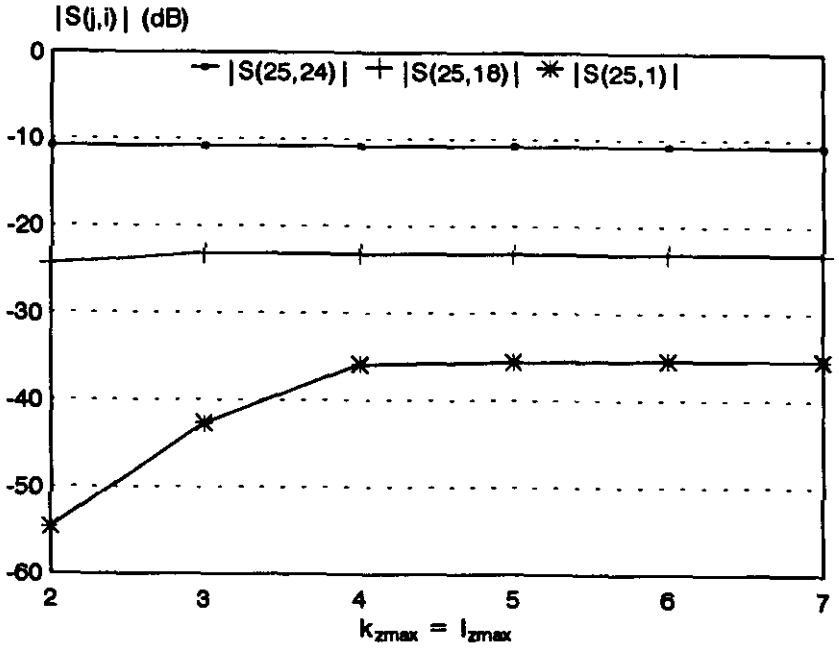

Figure 2.14: *Calculated S-parameters for various* (k_{zmax}, l_{zmax}) *values,* $f = 1.3$ *GHz*

- patch location upper patch $z_2' = 3.14mm$,
- substrate thickness $d = 3.14mm$,
- permittivity $\epsilon_r = 2.33 \quad \tan\delta = 0.001$,
- patch dimensions lower patch $W_{x1} = W_{y1} = 60mm$,
- patch dimensions upper patch $W_{x2} = W_{y2} = 59.7mm$,
- inner radius coax $a = 0.635mm$,
- excitation point $X_s = 15mm, \; Y_s = 0$,
- array dimensions $a_x = b_y = 91mm$.

In [14] this array has been used in order to compare results obtained from a finite array theory (presented in this report) with results obtained from an infinite array theory. For both theories 3 x-directed basis function ($m_x = 1, 3, 5 \; ; \; m_y = 0$) and one y-directed basis function ($m_x = 0 \; ; \; m_y = 2$) was used on each patch of the array. Figure 2.17 shows the calculated centre element active input impedance versus frequency with $\theta_0 = \phi_0 = 0^0$. This is done for various array sizes including an infinite array size. Two peaks can now be observed in the active resistance plot, because of the stacked configuration. The agreement between the finite and infinite theory is quite good for array sizes larger than 7x7.

In figure 2.18 a plot is shown of the centre element active reflection coefficient in the case of E-plane scanning ($\phi_0 = 0^0$) for various frequencies. Fig. 2.19 shows the active reflection coefficient of the centre element ($k = l = 4$) and of an edge array element ($k = l = 1$) in the case of an 7x7 array configuration. The calculated infinite array results are also shown in this plot. The agreement between the finite and infinite array approach is quite good if we consider the centre element, except for large scan angles ($\theta_0 > 60^0$). However, a significant difference is observed between the calculated reflection coefficient of the centre element and of an edge array element. So edge array elements can only be analysed properly if one uses a finite array approach.
In the last part of this chapter we shall take a closer look to the radiation patterns of stacked microstrip arrays. In paragraph 2.9 a method has been discussed to calculate the radiation charcteristics of such arrays. Figure 2.20 and 2.21 show the E-plane and H-plane radiation patterns for broadside scan ($\theta_0 = \phi_0 = 0^0$) of a 7x7 stacked microstrip array.
Note that we have used an uniform array excitation of the form (2.68). In fig. 2.22 the E-plane radiation pattern is given of a 7x7 stacked array in the case of E-plane scanning with $\theta_0 = 30^0$.

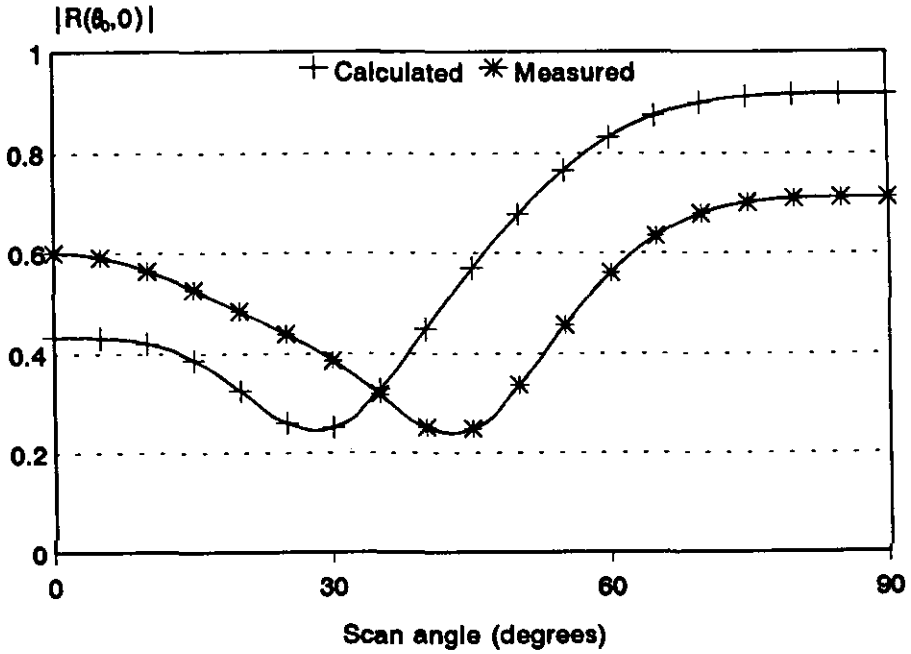

a. E-plane scanning ($\phi_0 = 0^0$)

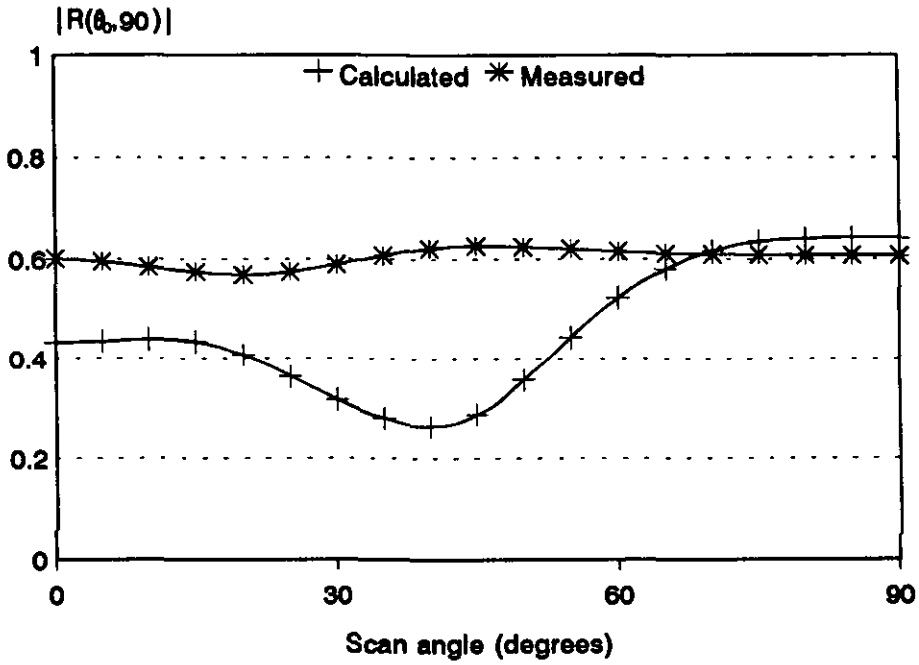

b. H-plane scanning ($\phi_0 = 90^0$)

Figure 2.15: *Centre element active reflection coefficient, f =1.3 GHz*

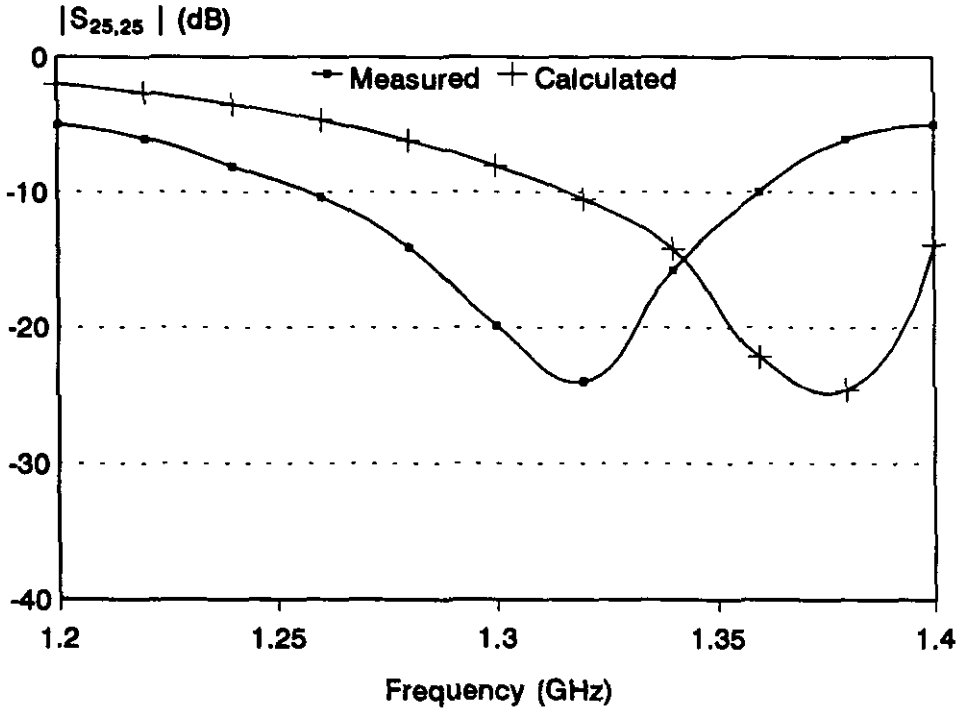

Figure 2.16: *Calculated and measured $S_{25,25}$ versus frequency*

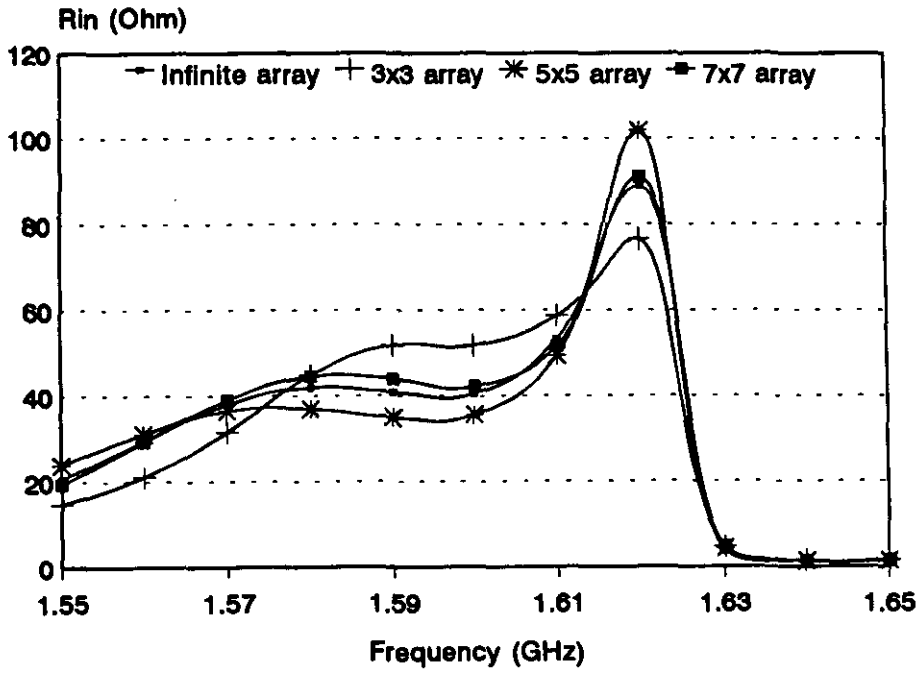

a. Real part input impedance

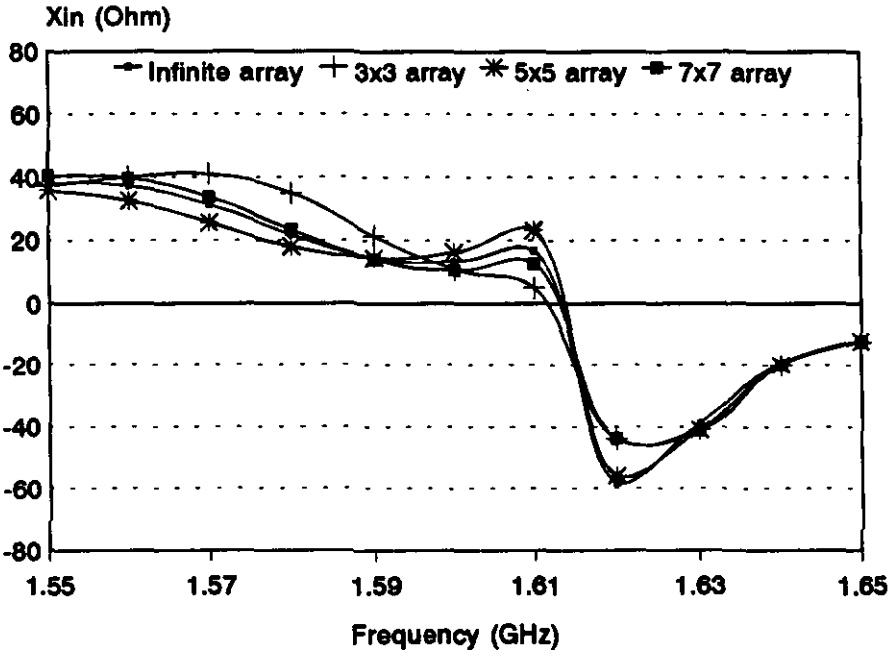

b. Imaginary part input impedance

Figure 2.17: *Centre element input impedance of a stacked array versus frequency,* $\theta_0 = \phi_0 = 0$

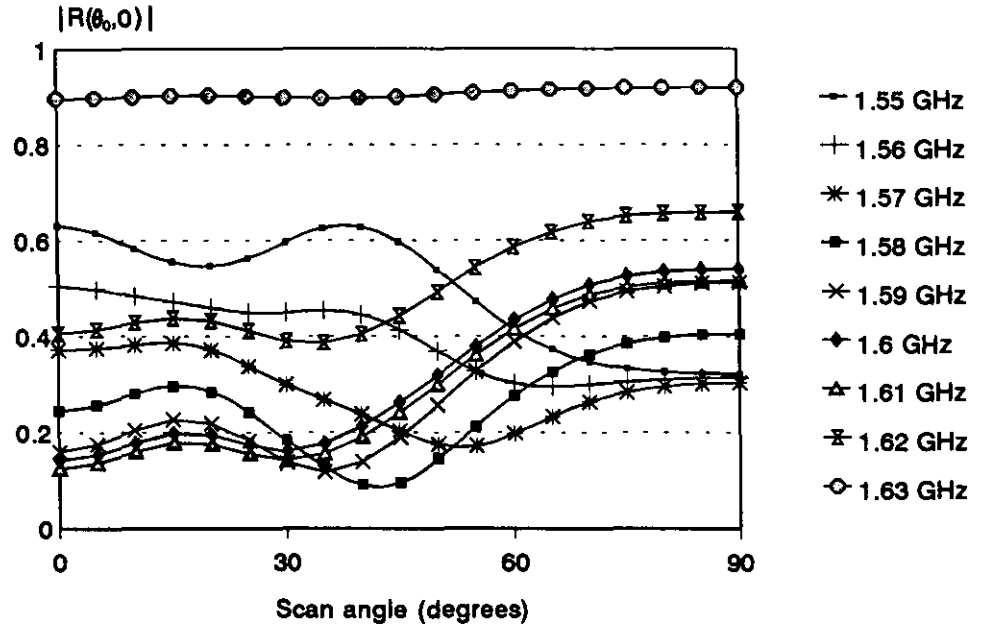

Figure 2.18: *Calculated centre element reflection coefficient of a 7x7 stacked microstrip array,* $\phi_0 = 0^0$

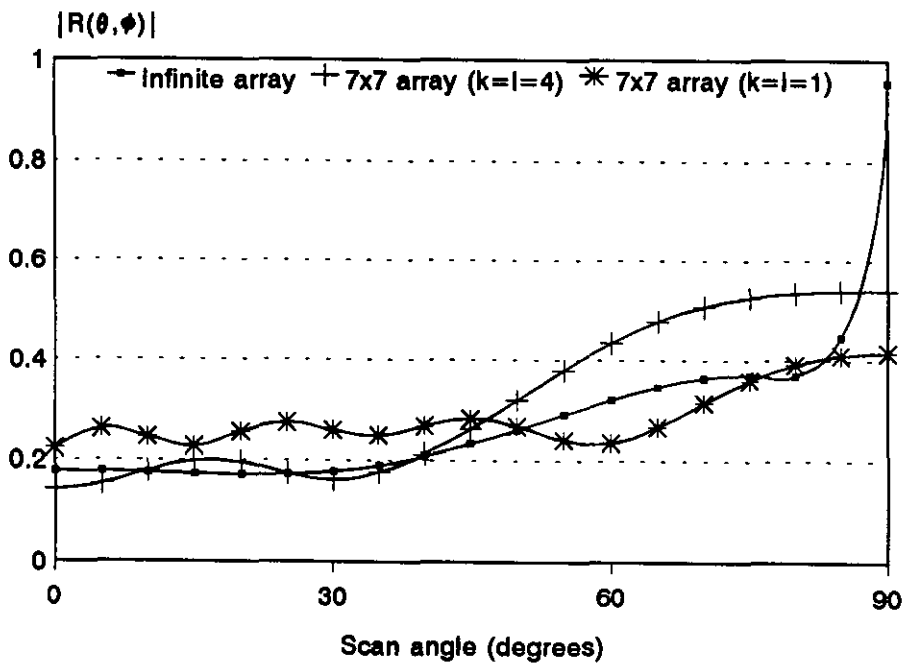

Figure 2.19: *Calculated reflection coefficient versus scan angle* θ *of a stacked microstrip array,* $f = 1.6$ *GHz,* $\phi_0 = 0^0$

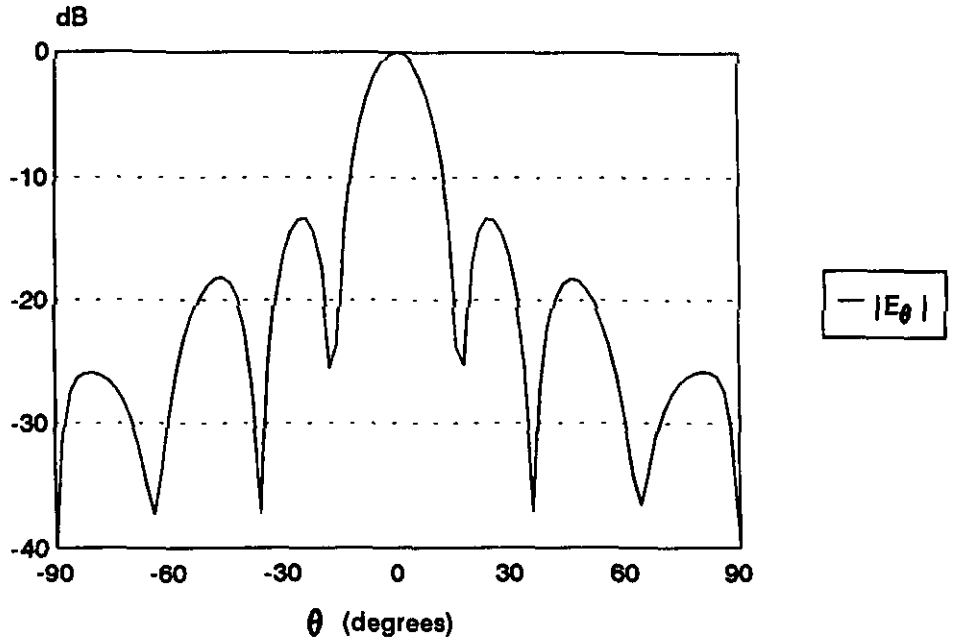

Figure 2.20: *E-plane* ($\phi = 0^0$) *radiation pattern of a 7x7 stacked microstrip array,* $\theta_0 = \phi_0 = 0^0$, $f = 1.6$ *GHz*

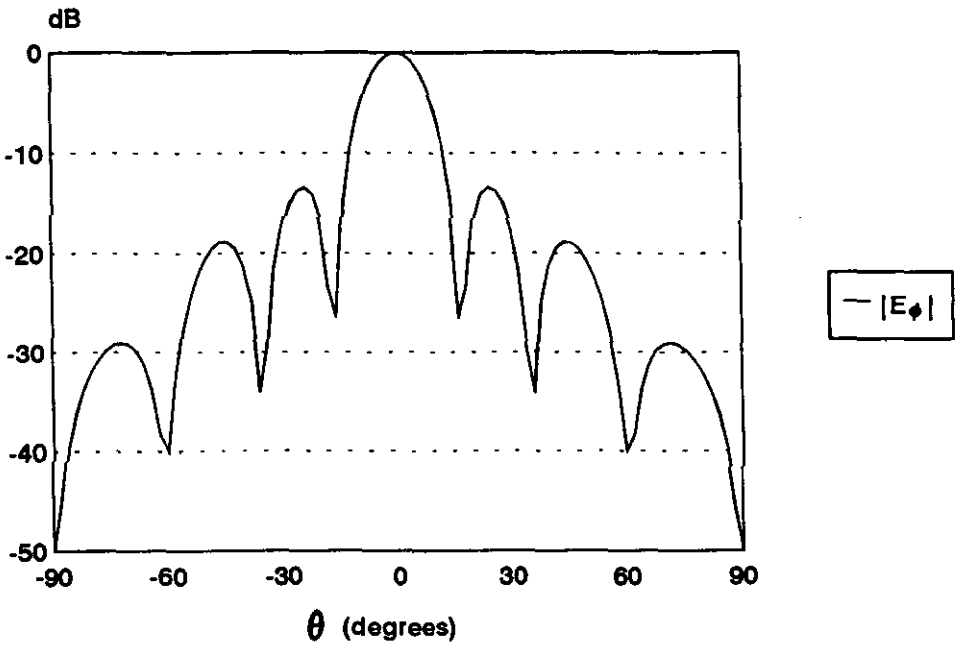

Figure 2.21: *H-plane* ($\phi = 90^0$) *radiation pattern of a 7x7 stacked microstrip array,* $\theta_0 = \phi_0 = 0^0$, $f = 1.6$ *GHz*

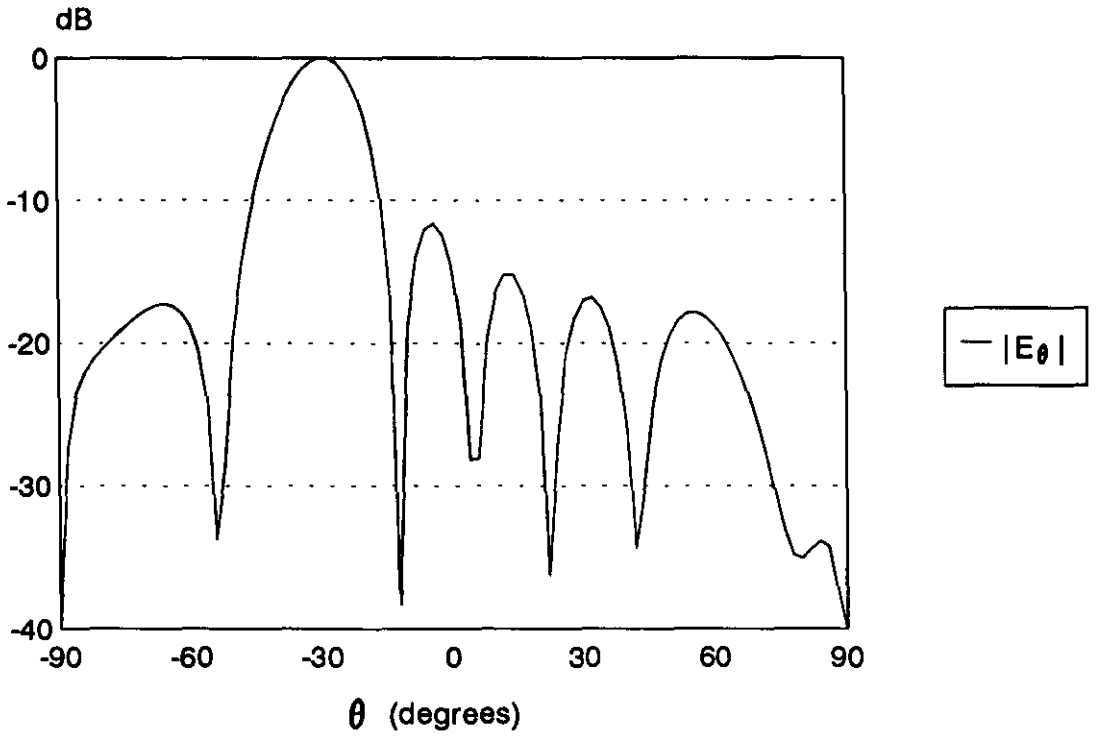

Figure 2.22: *E-plane* ($\phi = 0^0$) *radiation pattern of a 7x7 stacked microstrip array,* $\theta_0 = 30^0$, $\phi_0 = 0^0$, $f = 1.6$ *GHz*

Chapter 3

Finite stacked microstrip arrays with a thick substrate

3.1 Introduction

In chapter 2 of this report a method was presented for the analysis of finite stacked microstrip antennas based on an electrically thin dielectric substrate. Because of this thin substrate, the current distribution along the coaxial probes was almost constant and therefore a simple feed model could be used. This simple feed model fails however if one wants to analyse electrically thick microstrip arrays. In this case a more sophisticated model for the feeding coaxial cables has to be used that includes the variation of current along the probes. Furthermore, a special attachment mode has to be used in order to ensure continuity of current at the patch-probe transitions. In this chapter the model of chapter 2 is extended to the case of electrically thick substrates. A lot of attention will be paid to an efficient procedure for the evaluation of the elements of the method of moments matrices.

3.2 Model description

The geometry of a finite stacked microstrip array is shown in figure 2.1. The antenna is linearly polarised, so only one coaxial cable for each antenna element has to be used. The feeding coaxial cables, located at a distance (x_s, y_s) from the centre of each lower patch, are usually connected to the lower patch, but this is not necessary. The diameter of the inner conductor is $2a$ and the diameter of the outer conductor of each coaxial cable is equal $2b$. Figure 3.1 shows a more detailed view of the coaxial cable of antenna element 1. Figure 3.1a shows the most common construction where the probe is connected to the lower patch of each antenna element. Figure 3.1b shows a configuration where the probe is not fysically connected to the lower patch, i.e. $z_F < z_1'$. This "electromagnetically coupled" (EMC) microstrip structure has broadband characteristics [5,16].
The probes are represented by a cylinder with radius a and with perfectly conducting walls. It is assumed that the z-directed surface current on this cylinder only depends on the z-co-ordinate. The fields in the coaxial apertures of each array element act as sources. At frequencies for which $kb < 0.1$ ($k = \omega\sqrt{\epsilon\mu_0}$) only the groundmode, i.e. TEM-mode,

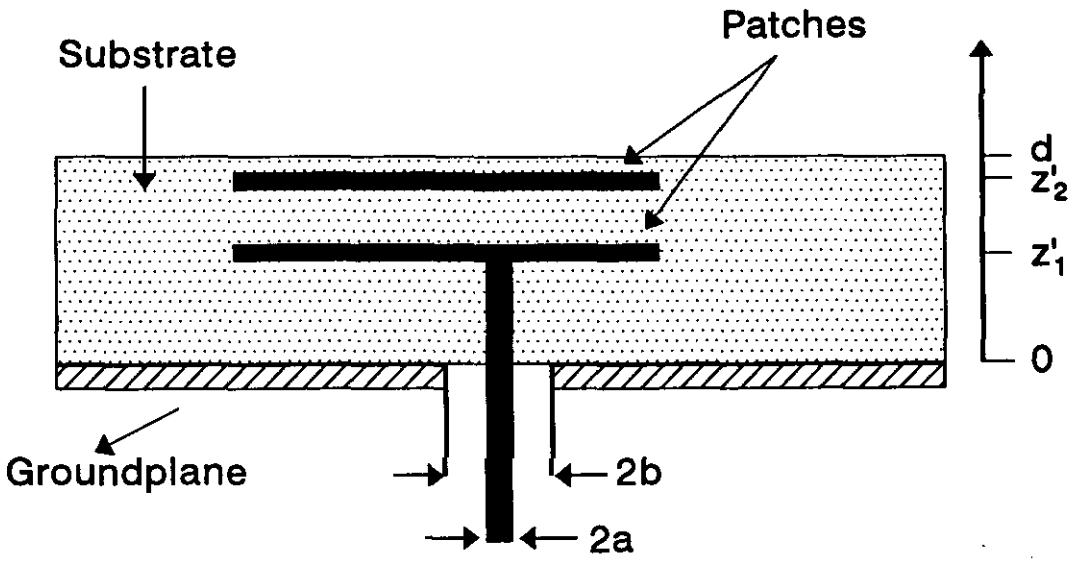

a. Probe connected to the lower patch

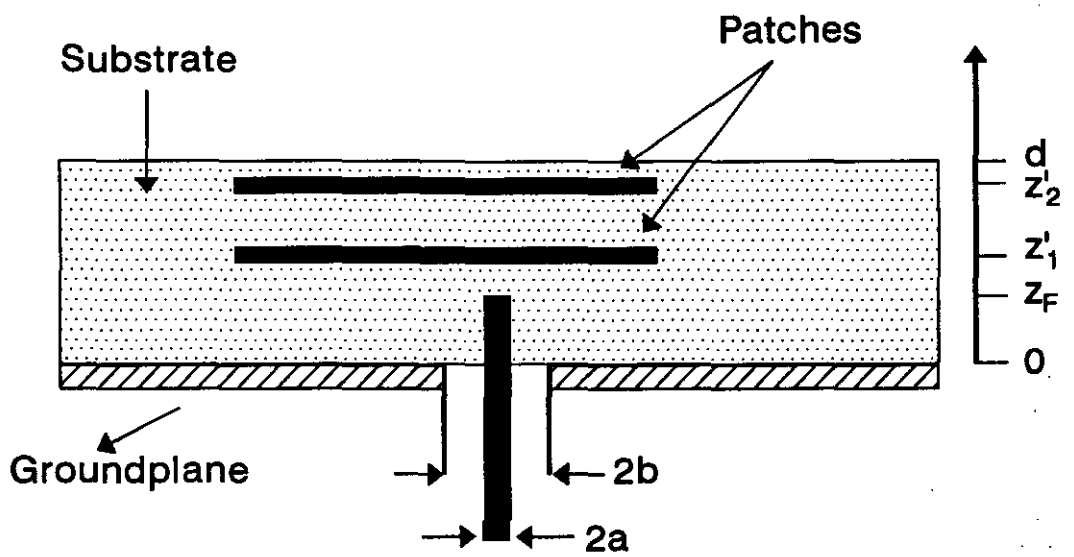

b. Probe not connected to the lower patch

Figure 3.1: *Feeding coaxial structure of antenna element 1*

exists in the coaxial cables. The field in the aperture of the coaxial cable connected to antenna element 1 is then given by

$$\vec{\mathcal{E}}_r(r) \approx \vec{\mathcal{E}}_{rTEM}(r) = \frac{V_1^p}{r' ln(\frac{b}{a})} \vec{e}_{r'} \quad a \leq r' \leq b$$

$$\vec{\mathcal{H}}_\phi(r) \approx \vec{\mathcal{H}}_{\phi TEM}(r) = \frac{I_1^p}{2\pi r'} \vec{e}_{\phi'} \quad a \leq r' \leq b \tag{3.1}$$

where $\vec{r'} = (x' \cos\phi', y' \sin\phi') = \vec{r} - \vec{r}_s$ with $\vec{r}_s = (x_s, y_s)$. V_1^p is the port voltage between the inner and outer conductor of the coaxial cable connected to antenna element 1 and I_1^p is the total current at the base ($z = 0$) of the probe. The electric fields in the coaxial apertures will be used as sources. So for a known set of port voltages V_j^p ($j = 1, 2, .., K \times L$) we have to determine the corresponding port currents I_j^p. The $K \times L$ sources can be represented by a magnetic current distribution at the aperture of each antenna element. For antenna element 1 this magnetic current distribution in the coaxial aperture takes the form

$$\vec{\mathcal{M}}_{frill1}^{tot} = \vec{\mathcal{M}}_{frill1} V_1^p = \vec{\mathcal{E}}_r \times \vec{e}_z = -\frac{V_1^p}{r' \ln(\frac{b}{a})} \vec{e}_{\phi'} \quad a \leq r' \leq b \tag{3.2}$$

In literature this source model is often called the "Magnetic frill excitation model".

3.3 Method of moments formulation

We can use the same strategy here as the one that was used in section 2.4. The only difference is that apart from x- and y-directed currents on the patches, we now also have to calculate the z-directed current distribution on the $K \times L$ coaxial probes. The boundary conditions on the $2 \times K \times L$ patches and on all the $K \times L$ probes of the stacked microstrip array are used in order to obtain an integral equation for the unknown currents on the patches and probes. The total tangential electric field has to be zero on all patches and on all probes:

$$\vec{\mathcal{E}}_{tan}^{tot}(x, y, z) = \vec{\mathcal{E}}_{tan}^{ex}(x, y, z) + \vec{\mathcal{E}}_{tan}^{s}(x, y, z) = \vec{0} \quad \text{on each patch and probe,} \tag{3.3}$$

where $\vec{\mathcal{E}}_{tan}^{ex}(x, y, z)$ is the excitation field which is excited by the magnetic current distribution at the coaxial apertures. The term $\vec{\mathcal{E}}_{tan}^{s}(x, y, z)$ represents the tangential component of the scattered field that results from the induced currents on all the patches and probes of the array. The unknown current distribution on each array element will now be expanded into a set of basis functions that exist on both patches and a set of basis functions that exist on the outer surface of the coaxial probe. In addition a special attachment mode shall be used that exists on the probe and on the lower patch of each array element. This attachment modes ensures continuity of current at the transition between the probe and

the lower patch. The expansion of the unknown current distribution on each array element can be written in the following form

$$\begin{aligned}\vec{J}(x,y,z) &= \sum_{j=1}^{K\times L} \vec{J}_j(x,y,z) = \sum_{j=1}^{K\times L} \sum_{m=1}^{1+N_z+N_1+N_2} \vec{J}_{mj}(x,y,z) \\ &= \sum_{j=1}^{K\times L} \left\{ I_{1j}\vec{J}^a_{1j}(x,y,z) + \sum_{m=2}^{N_z+1} I_{mj}\vec{J}^f_{mj}(x,y,z) \sum_{m=N_z+2}^{1+N_z+N_1+N_2} I_{mj}\vec{J}^p_{mj}(x,y,z_m) \right\},\end{aligned} \tag{3.4}$$

with

$$z_m = \begin{cases} z_1' & N_z+2 \le m \le N_z+1+N_1 \\ z_2' & m > N_z+1+N_1 \end{cases},$$

where the basis functions $\vec{J}^a_{1j}$ represent the attachment modes, $\vec{J}^f_{mj}$ are the basis functions on the probes and $\vec{J}^p_{mj}$ represent the N_1 basis functions on the lower patch and the N_2 basis functions on the upper patch of each array element. I_{mj} are the corresponding unknown mode coefficients of the basis functions. The total number of basis functions is $N_{max} = K \times L \times (1+N_z+N_1+N_2)$. More details about the type of basis functions that we shall use are given in section 3.4. The method of moments is applied to find the unknown mode coefficients I_{mj}. The method of moments has already been discussed in section 2.4. Using the strategy of section 2.4 we finally obtain a set of linear equations, which is in matrix form given by

$$[Z][I] + [V0][V^p] = [0], \tag{3.5}$$

with

$$\begin{aligned} Z_{mj,ni} &= 4\pi^2 \int\int\int_{S_{mj}} \vec{\mathcal{E}}^s_{ni}(x,y,z) \cdot \vec{J}_{mj}(x,y,z)\, dxdydz, \\ V0_{mj,i} &= 4\pi^2 \int\int\int_{S_{mj}} \vec{\mathcal{E}}^{ex}_i(x,y,z_m) \cdot \vec{J}_{mj}(x,y,z_m)\, dxdydz \\ &= -4\pi^2 \int\int\int_{frill\ i} \vec{\mathcal{H}}^s_{mj}(x,y,0) \cdot \vec{\mathcal{M}}_{frill\ i}(x,y,0)\, dxdy, \end{aligned} \tag{3.6}$$

where the reaction concept was used to rewrite $V0_{mj,i}$ [7]. $\vec{\mathcal{M}}_{frill\ i}(x,y,0)$ is the magnetic current distribution in the coaxial aperture of antenna element i and is given by expression (3.2). The matrix $[Z]$ contains $N_{max} \times N_{max}$ elements, $[I]$ is a vector containing the N_{max} unknown mode coefficients, $[V0]$ is the $N_{max} \times (K \times L)$ excitation matrix and $[V^p]$ is the $K \times L$-element column vector of port voltages. The difference between expression (3.5) and matrix equation (2.14) is that in (3.5) the port voltage vector $[V^p]$ is used whereas in (2.14) the port current vector $[I^p]$ was used. The method of moments matrices $[Z]$ and $[V0]$ have the following structure

$$[Z] = \begin{pmatrix} [Z^{aa}] & [Z^{af}] & [Z^{ap}] \\ [Z^{fa}] & [Z^{ff}] & [Z^{fp}] \\ [Z^{pa}] & [Z^{pf}] & [Z^{pp}] \end{pmatrix}, \tag{3.7}$$

and

$$[V0] = \begin{pmatrix} [V0^a] \\ [V0^f] \\ [V0^p] \end{pmatrix}, \tag{3.8}$$

where the superscript a denotes an attachment mode, f a basis function on one of the coaxial probes and p a basis function on one of the patches. Note that we have used current expansion (3.4). A method for the calculation of $[Z^{pp}]$ has already been discussed in chapter 2. In this chapter a method is presented in order to calculate the other submatrices of $[Z]$ and $[V0]$ in an efficient way. Note that $[V0^p]$ is not the same as the matrix $[V0]$ that was used in the previous chapter, because a different source model is used in this case. The matrix $[Z]$ is a symmetrical matrix because of the reciprocity concept. The elements of $[Z]$ can be expressed in terms of the spectral domain Green's function (see also (2.16))

$$
\begin{aligned}
Z^{aa}_{j,i} &= \int_{-\infty}^{\infty}\int_{-\infty}^{\infty}\int_{z}\int_{z_0}\left[\bar{\bar{Q}}_E(k_x,k_y,z_0,z)\cdot\vec{J}^{a}_{1}(k_x,k_y,z_0)\right]dz_0\cdot\vec{J}^{a*}_{1}(k_x,k_y,z)dz \\
&\quad e^{-jk_xS_{xji}}e^{-jk_yS_{yji}}dk_xdk_y, \\
Z^{fa}_{mj,i} &= \int_{-\infty}^{\infty}\int_{-\infty}^{\infty}\int_{z}\int_{z_0}\left[\bar{\bar{Q}}_E(k_x,k_y,z_0,z)\cdot\vec{J}^{a}_{1}(k_x,k_y,z_0)\right]dz_0\cdot\vec{J}^{f*}_{m1}(k_x,k_y,z)dz \\
&\quad e^{-jk_xS_{xji}}e^{-jk_yS_{yji}}dk_xdk_y, \\
Z^{ff}_{mj,ni} &= \int_{-\infty}^{\infty}\int_{-\infty}^{\infty}\int_{z}\int_{z_0}\left[\bar{\bar{Q}}_E(k_x,k_y,z_0,z)\cdot\vec{J}^{f}_{n1}(k_x,k_y,z_0)\right]dz_0\cdot\vec{J}^{f*}_{m1}(k_x,k_y,z)dz \\
&\quad e^{-jk_xS_{xji}}e^{-jk_yS_{yji}}dk_xdk_y, \\
Z^{pa}_{mj,i} &= \int_{-\infty}^{\infty}\int_{-\infty}^{\infty}\int_{z_0}\left[\bar{\bar{Q}}_E(k_x,k_y,z_0,z_m)\cdot\vec{J}^{a}_{1}(k_x,k_y,z_0)\right]dz_0\cdot\vec{J}^{p*}_{m1}(k_x,k_y,z_m) \\
&\quad e^{-jk_xS_{xji}}e^{-jk_yS_{yji}}dk_xdk_y, \\
Z^{pf}_{mj,ni} &= \int_{-\infty}^{\infty}\int_{-\infty}^{\infty}\int_{z_0}\left[\bar{\bar{Q}}_E(k_x,k_y,z_0,z_m)\cdot\vec{J}^{f}_{n1}(k_x,k_y,z_0)\right]dz_0\cdot\vec{J}^{p*}_{m1}(k_x,k_y,z_m) \\
&\quad e^{-jk_xS_{xji}}e^{-jk_yS_{yji}}dk_xdk_y, \\
Z^{pp}_{mj,ni} &= \int_{-\infty}^{\infty}\int_{-\infty}^{\infty}\left[\bar{\bar{Q}}_E(k_x,k_y,z_n,z_m)\cdot\vec{J}^{p}_{n1}(k_x,k_y,z_n)\right]\cdot\vec{J}^{p*}_{m1}(k_x,k_y,z_m) \\
&\quad e^{-jk_xS_{xji}}e^{-jk_yS_{yji}}dk_xdk_y,
\end{aligned}
\tag{3.9}
$$

where $\vec{J}^{a}_{1}(k_x,k_y,z)$ is the Fourier transform of the attachment mode on antenna element 1 and $\vec{J}^{f}_{n1}(k_x,k_y,z)$ represents the Fourier transform of the n-th basis function on the probe of antenna element 1. S_{xji} and S_{yji} are the distances in x respectively y-direction between the centre of antenna element j and antenna element i. Lateron it will be shown that the fourfold integrals in $Z^{aa}_{j,i}$, $Z^{fa}_{mj,i}$, $Z^{ff}_{mj,ni}$ can be reduced to a one dimensional integral. The z-integrations of $Z^{pa}_{mj,i}$ and $Z^{pf}_{mj,ni}$ can also be evaluated analytically. The elements of the excitation matrix $[V0]$ can also be expressed in terms of the spectral domain Green's function:

$$
\begin{aligned}
V0^a_{j,i} &= -4\pi^2 \int\int_{frill\ i} \vec{\mathcal{H}}^s_{mj}(x,y,0)\cdot\vec{\mathcal{M}}_{frill\ i}(x,y,0)\,dxdy \\
&= -4\pi^2 \int\int_{frill\ i} \left[\frac{1}{4\pi^2}\int_{-\infty}^{\infty}\int_{-\infty}^{\infty} \bar{\bar{Q}}_H(k_x,k_y,z_0,0)\cdot\vec{J}^a_j(k_x,k_y,z_0)dz_0 e^{-\jmath k_x x}e^{-\jmath k_y y}dk_x dk_y\right] \\
&\qquad \cdot\vec{\mathcal{M}}_{frill\ i}(x,y,0)dxdy \\
&= -\int_{-\infty}^{\infty}\int_{-\infty}^{\infty}\left[\int_{z_0}\bar{\bar{Q}}_H(k_x,k_y,z_0,0)\cdot\vec{J}^a_j(k_x,k_y,z_0)dz_0\right]\cdot\vec{M}^*_{frill\ i}(k_x,k_y)dk_x dk_y \\
&= -\int_{-\infty}^{\infty}\int_{-\infty}^{\infty}\left[\int_{z_0}\bar{\bar{Q}}_H(k_x,k_y,z_0,0)\cdot\vec{J}^a_1(k_x,k_y,z_0)dz_0\right]\cdot\vec{M}^*_{frill\ 1}(k_x,k_y) \\
&\qquad e^{\jmath k_x S_{xji}}e^{\jmath k_y S_{yji}}dk_x dk_y, \\
V0^f_{mj,i} &= -\int_{-\infty}^{\infty}\int_{-\infty}^{\infty}\left[\int_{z_0}\bar{\bar{Q}}_H(k_x,k_y,z_0,0)\cdot\vec{J}^f_{m1}(k_x,k_y,z_0)dz_0\right]\cdot\vec{M}^*_{frill\ 1}(k_x,k_y) \\
&\qquad e^{\jmath k_x S_{xji}}e^{\jmath k_y S_{yji}}dk_x dk_y, \\
V0^p_{mj,i} &= -\int_{-\infty}^{\infty}\int_{-\infty}^{\infty}\left[\bar{\bar{Q}}_H(k_x,k_y,z_m,0)\cdot\vec{J}^p_{m1}(k_x,k_y,z_m)\right]\cdot\vec{M}^*_{frill\ 1}(k_x,k_y)e^{\jmath k_x S_{xji}}e^{\jmath k_y S_{yji}}dk_x dk_y,
\end{aligned}
\tag{3.10}
$$

where $\vec{M}_{frill\ i}(k_x,k_y)$ is the Fourier transform of the magnetic current distribution in the coaxial aperture of antenna element i and is given by

$$
\begin{aligned}
\vec{M}_{frill\ i}(k_x,k_y) = \frac{1}{\ln\frac{b}{a}}e^{\jmath k_x((k_i-1)a_x+x_s)}e^{\jmath k_y((l_i-1)b_y+y_s)}\Bigg\{\vec{e}_x\frac{-2\pi\jmath\sin\alpha}{k_0\beta} \\
[J_0(k_0\beta b)-J_0(k_0\beta a)]+\vec{e}_y\frac{2\pi\jmath\cos\alpha}{k_0\beta}\left[J_0(k_0\beta b)-J_0(k_0\beta a)\right]\Bigg\},
\end{aligned}
\tag{3.11}
$$

with $k_x = k_0\beta\cos\alpha$, $k_y = k_0\beta\sin\alpha$ and where i is the array-element counter with $i = (l_i - 1)K + k_i$. Two of the three integrations in $V0^a_{j,i}$ and $V0^f_{mj,i}$ can be performed analytically (see section 3.6).

3.4 Basis functions

3.4.1 Attachment mode

An attachment mode is introduced to ensure continuity of current at the transition from probe to the lower patch of each antenna element. We shall use the attachment mode that was presented in [5] for the analysis of isolated thick substrate microstrip antennas. This attachment mode has an exact $\frac{1}{r}$ dependence near the patch-probe transition. In

[5] very good results have been obtained with this type of attachment mode. Another great advantage of this mode is the fact that the overall computation time is not increased significantly. The complicated attachment mode used by [17] needs a lot of computation time while the final results are not better then with our attachment mode. The attachment mode consists of two parts, namely a part on the probe and a part on the lower patch of each antenna element. If one considers only antenna element 1 then the attachment mode is given by

$$\vec{J}_1^a(x,y,z) = \vec{J}_1^{ap}(x,y,z_1') + \vec{J}_1^{af}(x,y,z) \tag{3.12}$$

with

$$\vec{J}_1^{ap}(x,y,z_1') = \begin{cases} -\dfrac{r'}{2\pi b_a^2}\vec{e}_{r'} & 0 \le r' \le a \\ \left(-\dfrac{r'}{2\pi b_a^2} + \dfrac{1}{2\pi r'}\right)\vec{e}_{r'} & a \le r' \le b_a \\ 0 & r' \ge b_a \end{cases},$$

$$\vec{J}_1^{af}(x,y,z) = \vec{e}_z \frac{1}{2\pi a}\delta\left(\sqrt{(x-x_s)^2+(y-y_s)^2} - a\right)\frac{2}{h}(z - z_1' + \frac{h}{2}) \quad z_1' - \tfrac{h}{2} \le z \le z_1',$$

where $\vec{r}' = \vec{r} - \vec{r}_s$, $\vec{r} = (x,y)$ and $\vec{r}_s = (x_s, y_s)$. A three-dimensional plot of the patch-part of the attachment mode is shown in figure 3.2.
The Fourier transform of the attachment mode is known in closed form and is given by

$$\vec{J}_1^a(k_x,k_y,z) = \vec{J}_1^{ap}(k_x,k_y,z_1') + \vec{J}_1^{af}(k_x,k_y,z), \tag{3.13}$$

with

$$\begin{aligned} \vec{J}_1^{ap}(k_x,k_y,z_1') &= [\vec{e}_x\cos\alpha + \vec{e}_y\sin\alpha]e^{\jmath k_x x_s}e^{\jmath k_y y_s}\left\{\frac{-2\jmath J_1(k_0\beta b_a)}{b_a k_0^2\beta^2} + \frac{\jmath J_0(k_0\beta a)}{k_0\beta}\right\} \\ \vec{J}_1^{af}(k_x,k_y,z) &= \vec{e}_z J_0(k_0\beta a)e^{\jmath k_x x_s}e^{\jmath k_y y_s}\frac{2}{h}(z - z_1' + \frac{h}{2}) \qquad z_1' - \tfrac{h}{2} \le z \le z \end{aligned}$$

3.4.2 Basis functions on the probes

On the $K \times L$ probes of the array piecewise linear subdomain basis functions (also called rooftop functions) will be used. On the probe of antenna element 1 these basis functions have the form

$$\vec{J}_{m1}^f(x,y,z) = \frac{1}{2\pi a}\delta\left(\sqrt{(x-x_s)^2+(y-y_s)^2} - a\right)g_m(z)\vec{e}_z, \tag{3.14}$$

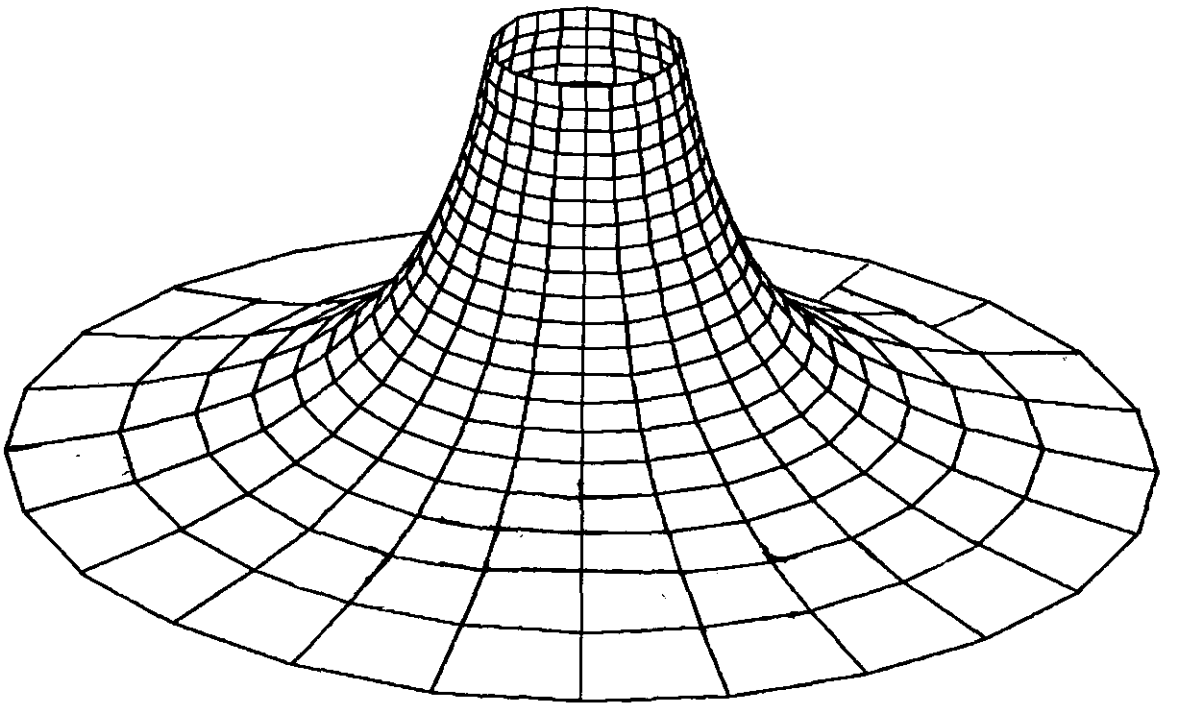

Figure 3.2: *Three dimensional representation of the patch-part of the attachment mode*

with

$$g_m(z) = \begin{cases} \frac{2}{h}(\frac{h}{2} - z) & m = 1 \quad 0 \leq z \leq \frac{h}{2} \\ \frac{2}{h}(z - z_{m-1}) & m \geq 2 \quad z_{m-1} \leq z \leq z_m \\ \frac{2}{h}(z_{m+1} - z) & m \geq 2 \quad z_m \leq z \leq z_{m+1} \end{cases} .$$

In figure 3.3 the z-dependent part of the basis functions is shown. The total number of basis functions on each probe equals N_z.
The Fourier transform of this set of basis functions is given by

$$\vec{J}^f_{m1}(k_x, k_y, z) = \vec{e}_z J_0(k_0 \beta a) g_m(z) e^{\jmath k_x x_s} e^{\jmath k_y y_s}, \tag{3.15}$$

with $k_0^2 \beta^2 = k_x^2 + k_y^2$.

3.4.3 Basis functions on the patches

The unknown current distribution on both patches of each array element are expanded into a set of entire domain basis functions. The set of basis functions that has also been used in chapter 2 will be applied here. So the basis functions and their corresponding Fourier transforms are given by expression (2.17) and (2.18) respectively.

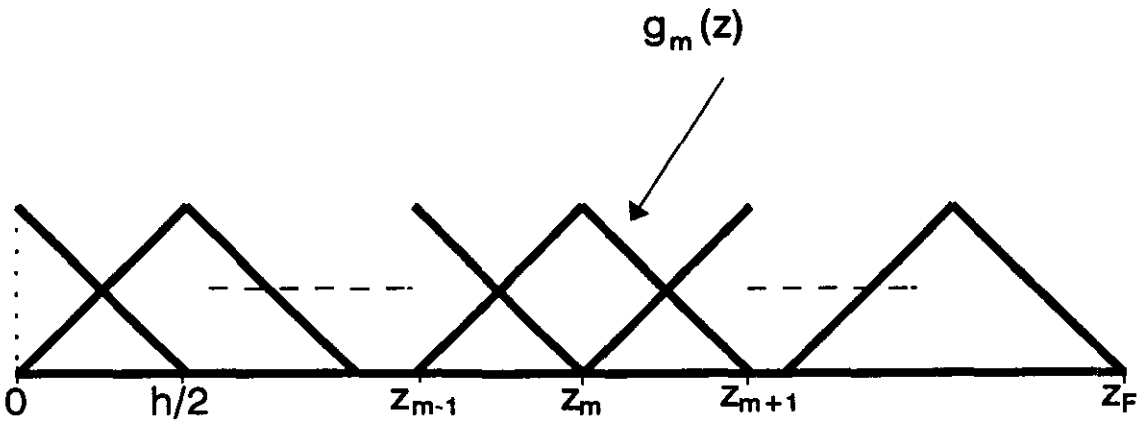

Figure 3.3: *Rooftop basis functions along the probe*

3.5 Calculation of the matrix $[Z]$

The structure of the method of moments matrix $[Z]$ is given by (3.7). Because $[Z]$ is a symmetrical matrix we only need to calculate 6 of the 9 submatrices. An efficient method to calculate the elements of the submatrix $[Z^{pp}]$ has already been discussed in chapter 2 of this report. In this section similar numerical techniques will be applied in order to calculate the elements of the remaining 5 submatrices, i.e. $[Z^{aa}]$, $[Z^{fa}]$, $[Z^{pa}]$, $[Z^{ff}]$ and $[Z^{pf}]$.

3.5.1 $[Z^{aa}]$: attachment modes $\longleftrightarrow$ attachment modes

This submatrix contains $(K \times L) \times (K \times L)$ elements. $[Z^{aa}]$ is symmetrical and has a Toeplitz structure. So only $K \times L$ elements need to be calculated. According to (3.9) an element of $[Z^{aa}]$ is given by

$$Z_{j,i}^{aa} = \int_{-\infty}^{\infty}\int_{-\infty}^{\infty}\int_{z}\int_{z_0}\left[\bar{\bar{Q}}_E(k_x,k_y,z_0,z)\cdot\vec{J}_1^{a}(k_x,k_y,z_0)\right]dz_0\cdot\vec{J}_1^{a*}(k_x,k_y,z)dz \\ e^{-jk_xS_{xji}}e^{-jk_yS_{yji}}dk_xdk_y, \tag{3.16}$$

where $\vec{J}_1^{a}(k_x,k_y,z)$ is given by expression (3.13). Now let's introduce a change to polar coordinates according to (2.21). This results in

$$Z_{j,i}^{aa} = \int_0^{\infty}\int_{-\pi}^{\pi}\int_z\int_{z_0}\left[\bar{\bar{Q}}_E(\beta,\alpha,z_0,z)\cdot\vec{J}_1^{a}(\beta,\alpha,z_0)\right]dz_0\cdot\vec{J}_1^{a*}(\beta,\alpha,z)dz \\ e^{-\jmath k_0\beta\cos\alpha S_{xji}}e^{-\jmath k_0\beta\sin\alpha S_{yji}}k_0^2\beta d\alpha d\beta, \tag{3.17}$$

The two z-integrations and the α-integration can be performed analytically [5]. An extra term $J_0(k_0\beta\sqrt{S_{xji}^2+S_{yji}^2})$ is introduced here compared with the case of an isolated microstrip antenna (see [5, section 3.7.1]). The resulting expression has the form

$$\begin{aligned} Z_{j,i}^{aa} = {} & 2\pi\int_0^{\infty}J_0(k_0\beta\sqrt{S_{xji}^2+S_{yji}^2})\left\{\frac{-\jmath\omega\mu_0 k_1\sin k_1 z_1'}{k_0^2\epsilon_r Tm}\right. \\ & [k_2\epsilon_r\cos k_1(d-z_1')+\jmath k_1\sin k_1(d-z_1')]\frac{1}{k_0^2\beta^2}\left[\frac{2J_1(k_0\beta b_a)}{b_a k_0\beta}-J_0(k_0\beta a)\right]^2 \\ & +\frac{4\jmath\omega\mu_0\beta}{hk_0\epsilon_r Tm}[\epsilon_r k_2\cos k_1(d-z_1')+\jmath k_1\sin k_1(d-z_1')] \\ & \left[\frac{h\sin k_1 z_1'}{2k_1}+\frac{\cos k_1 z_1'}{k_1^2}-\frac{\cos k_1(z_1'-\frac{h}{2})}{k_1^2}\right]J_0(k_0\beta a) \\ & \left.\frac{1}{k_0\beta}\left[\frac{2J_1(k_0\beta b_a)}{b_a k_0\beta}-J_0(k_0\beta a)\right]+I_{jf}^{aa}(\beta)J_0^2(k_0\beta a)\right\}k_0^2\beta d\beta, \end{aligned} \tag{3.18}$$

with

$$\begin{aligned} I_{jf}^{aa}(\beta) = {} & -\frac{\jmath\omega\mu_0 h}{6k_0^2(\beta^2-\epsilon_r)}-\frac{4\jmath\omega\mu_0\beta^2}{\epsilon_r h^2 k_1^3 Tm} \\ & \left\{\epsilon_r k_2\left(-\frac{h\cos k_1(d-z_1')\cos k_1(z_1'-\frac{h}{2})}{k_1}-\frac{2\sin k_1(d-z_1')\cos k_1(z_1'-\frac{h}{2})}{k_1^2}\right.\right. \\ & +\frac{\sin k_1(d-z_1'+\frac{h}{2})\cos k_1(z_1'-\frac{h}{2})}{k_1^2}+\frac{h\cos k_1(d-2z_1')}{2k_1} \\ & \left.+\frac{h^2\cos k_1(d-z_1')\sin k_1 z_1'}{4}+\frac{\sin k_1(d-z_1')\cos k_1 z_1'}{k_1^2}\right) \\ & -\jmath k_1\left(\frac{h\sin k_1(d-z_1')\cos k_1(z_1'-\frac{h}{2})}{k_1}-\frac{2\cos k_1(d-z_1')\cos k_1(z_1'-\frac{h}{2})}{k_1^2}\right. \\ & +\frac{\cos k_1(d-z_1'+\frac{h}{2})\cos k_1(z_1'-\frac{h}{2})}{k_1^2}-\frac{h\sin k_1(d-2z_1')}{2k_1} \\ & \left.\left.-\frac{h^2\sin k_1(d-z_1')\sin k_1 z_1'}{4}+\frac{\cos k_1(d-z_1')\cos k_1 z_1'}{k_1^2}\right)\right\}. \end{aligned}$$

In the derivation of the above expression the following relation has been used

$$\int_{-\pi}^{\pi}e^{\jmath k_0\beta R\sin\alpha}d\alpha = 2\int_0^{\pi}\cos(k_0\beta R\sin\alpha)d\alpha = 2\pi J_0(k_0\beta R). \tag{3.19}$$

Apparently an element of the submatrix $[Z^{aa}]$ can be calculated by performing only one infinite integration numerically. The numerical difficulties that occur when performing this integration are similar to the numerical problems that has been discussed in section 2.6 for the case of $[Z^{pp}]$ elements. Again the β-integration interval is divided in three sub intervals, i.e. $[0,1]$, $[1,\sqrt{\epsilon_r'}]$ and $[\sqrt{\epsilon_r'},\infty]$. In the first and second interval an infinite derivative occurs at $\beta = 1$, which can be eliminated by using an appropriate change of variables (2.24) and (2.25). In the second interval another numerical problem occurs due to surface waves that exist in the grounded dielectric slab. The numerical problems associated with these surface waves can be avoided if one uses the pole extraction technique of section 2.6. In the third integration interval a convergence acceleration technique will be applied. This technique was also used in section 2.6. Now let $Z_{j,i}^{aa}$ be given by

$$Z_{j,i}^{aa} = \int_0^\infty f_{j,i}^{aa}(\beta)d\beta. \tag{3.20}$$

This can also be written in the form

$$\begin{aligned} Z_{j,i}^{aa} &= \int_0^\infty f_{j,i}^{aa}(\beta)d\beta = \int_0^v f_{j,i}^{aa}(\beta)d\beta + \int_v^\infty f_{j,i}^{aa}(\beta)d\beta \\ &= \int_0^v f_{j,i}^{aa}(\beta)d\beta + \int_v^\infty \left[f_{j,i}^{aa}(\beta) - \widetilde{f}_{j,i}^{aa}(\beta)\right]d\beta + \int_v^\infty \widetilde{f}_{j,i}^{aa}(\beta)d\beta \\ &= \left[Z_{j,i}^{aa} - \widetilde{Z}_{j,i}^{aa}\right] + \widetilde{Z}_{j,i}^{aa}, \end{aligned} \tag{3.21}$$

with

$$\widetilde{Z}_{j,i}^{aa} = \int_v^\infty \widetilde{f}_{j,i}^{aa}(\beta)d\beta,$$

and $\widetilde{f}_{j,i}^{aa}(\beta)$ is the asymptotic form of the original β-integrand $f_{j,i}^{aa}(\beta)$ for large β-values. The asymptotic form of $f_{j,i}^{aa}(\beta)$ can be found by substituting $k_1 = -\jmath k_0\beta$ and $k_2 = -\jmath k_0\beta$ in the original expression. Doing this we finally obtain

$$\widetilde{Z}_{j,i}^{aa}(\beta) = \begin{cases} \displaystyle\int_v^\infty \frac{\jmath\omega\mu_0\pi J_0(k_0\beta R)}{k_0}\left(\frac{4J_1^2(k_0\beta b_a)}{\epsilon_r b_a^2 k_0^2\beta^2} - \frac{8J_1(k_0\beta b_a)J_0(k_0\beta a)}{\epsilon_r b_a h k_0^2\beta^2} + \frac{\epsilon_r J_0^2(k_0\beta a)}{\beta^4}\right. \\ \qquad \left. + \frac{4J_0^2(k_0\beta a)}{\epsilon_r h k_0\beta} - \frac{k_0 h J_0^2(k_0\beta a)}{3\beta} - \frac{8J_0^2(k_0\beta a)}{\epsilon_r h^2 k_0^2\beta^2}\right)d\beta & z_1' < \\ \displaystyle\int_v^\infty \frac{\jmath\omega\mu_0\pi J_0(k_0\beta R)}{k_0}\left(\frac{8J_1^2(k_0\beta b_a)}{(\epsilon_r+1) b_a^2 k_0^2\beta^2} - \frac{16J_1(k_0\beta b_a)J_0(k_0\beta a)}{(\epsilon_r+1) b_a h k_0^2\beta^2} + \frac{2\epsilon_r^2 J_0^2(k_0\beta a)}{(\epsilon_r+1)\beta^4}\right. \\ \qquad \left. + \frac{4J_0^2(k_0\beta a)}{\epsilon_r h k_0\beta} - \frac{k_0 h J_0^2(k_0\beta a)}{3\beta} - \frac{(4\epsilon_r+12)J_0^2(k_0\beta a)}{\epsilon_r(\epsilon_r+1)h^2 k_0^2\beta^2}\right)d\beta & z_1' = \end{cases} \tag{3.22}$$

where $R = \sqrt{S_{xji}^2 + S_{yji}^2}$ is the distance between the centre of antenna element j and antenna element i. In order to calculate $\widetilde{Z}_{j,i}^{aa}$ 5 types of integrals need to be known:

$$\begin{aligned} I_1 &= \int_v^\infty \frac{J_0^2(k_0\beta a)J_0(k_0\beta R)}{\beta} d\beta, \\ I_2 &= \int_v^\infty \frac{J_0^2(k_0\beta a)J_0(k_0\beta R)}{\beta^2} d\beta, \\ I_3 &= \int_v^\infty \frac{J_1^2(k_0\beta b_a)J_0(k_0\beta R)}{\beta^2} d\beta, \\ I_4 &= \int_v^\infty \frac{J_1(k_0\beta b_a)J_0(k_0\beta a)J_0(k_0\beta R)}{\beta^2} d\beta, \\ I_5 &= \int_v^\infty \frac{J_0^2(k_0\beta a)J_0(k_0\beta R)}{\beta^4} d\beta. \end{aligned} \tag{3.23}$$

All five integrals can be approximated by a closed form expression. As an example we will now take a closer look at the integral I_1. The other four integrals can be calculated with the same procedure. For large β values, the Bessel functions in the integrand of I_1 can be replaced by their asymptotic form, so

$$J_0(x) = \sqrt{\frac{2}{\pi x}} \left\{ \cos(x - \frac{\pi}{4}) + \frac{\sin(x - \frac{\pi}{4})}{8x} + \text{ higher order terms} \right\}. \tag{3.24}$$

For the sake of symplicity only the first term in the above expansion will be used here. However, more accurate results can be obtained if more terms of the asymptotic expansion of the Bessel funtions are being used. The number of terms that have to be used in order to obtain an accurate result for the integrals depends on R and a. Now using only the first term of (3.24) we get

$$\begin{aligned} I_1 &= \int_v^\infty \frac{J_0^2(k_0\beta a)J_0(k_0\beta R)}{\beta} d\beta \\ &= \int_v^\infty \frac{2}{\pi k_0 a} \sqrt{\frac{2}{\pi k_0 R}} \frac{\cos^2(k_0 a\beta - \frac{\pi}{4}) \cos(k_0 R\beta - \frac{\pi}{4})}{\beta^{\frac{5}{2}}} d\beta \\ &= \frac{2\sqrt{2}}{8\pi k_0 a} \sqrt{\frac{2}{\pi k_0 R}} (k_0 a)^{\frac{3}{2}} \\ &\quad \int_{k_0 va}^\infty \frac{2\sin\frac{Rx}{a} + 2\cos\frac{Rx}{a} + \cos x(\frac{R}{a} - 2) - \cos x(\frac{R}{a} + 2) + \sin x(\frac{R}{a} + 2) - \sin x(\frac{R}{a} - 2)}{x^{\frac{5}{2}}} dx, \end{aligned} \tag{3.25}$$

with

$$\begin{aligned} \int_{x_m}^\infty \frac{\sin\frac{Rx}{a}}{x^{\frac{5}{2}}} dx &= \frac{2\sin\frac{Rx_m}{a}}{3x_m^{\frac{3}{2}}} + \frac{4R\cos\frac{Rx_m}{a}}{3a\sqrt{x_m}} - \frac{4\sqrt{2\pi}\left(\frac{R}{a}\right)^2}{3\sqrt{\frac{R}{a}}} \left\{ \frac{1}{2} - S\left(\sqrt{\frac{Rx_m}{a}}\right) \right\}, \\ \int_{x_m}^\infty \frac{\cos\frac{Rx}{a}}{x^{\frac{5}{2}}} dx &= \frac{2\cos\frac{Rx_m}{a}}{3x_m^{\frac{3}{2}}} - \frac{4R\sin\frac{Rx_m}{a}}{3a\sqrt{x_m}} - \frac{4\sqrt{2\pi}\left(\frac{R}{a}\right)^2}{3\sqrt{\frac{R}{a}}} \left\{ \frac{1}{2} - C\left(\sqrt{\frac{Rx_m}{a}}\right) \right\}, \end{aligned}$$

where $S(x)$ and $C(x)$ are Fresnel integrals defined by

$$\begin{aligned} S(x) &= \int_0^x \sin\frac{\pi t^2}{2}dt \\ C(x) &= \int_0^x \cos\frac{\pi t^2}{2}dt. \end{aligned}$$

Fresnel integrals can be calculated with standard numerical routines [18]. When using more terms in the asymptotic expansion (3.24) we can also find a closed form expression for I_1, similar to the above result. If the distance between element j and i is zero, i.e. $R = 0$ and $j = i$, the integrals I_1 and I_2 can also be determined from [5]

$$\begin{aligned} I_1 &= \int_v^\infty \frac{J_0^2(k_0\beta a)}{\beta}d\beta \\ &= -\log\frac{1}{2}k_0va - C - \int_0^{k_0va}\frac{J_0^2(x)-1}{x}dx, \\ I_2 &= \int_v^\infty \frac{J_0^2(k_0\beta a)}{\beta^2}d\beta \\ &= \frac{J_0^2(k_0va)}{v} - \frac{4k_0a}{\pi} + 2k_0^2a^2v[J_1^2(k_0va)+J_0^2(k_0va)] \\ &\quad -2k_0aJ_0(k_0va)J_1(k_0va), \end{aligned} \tag{3.26}$$

with $C = 0.577215....$ is Euler's constant.

3.5.2 $[Z^{fa}]$: feed modes $\longleftrightarrow$ attachment modes

The submatrix $[Z^{fa}]$ contains $(K \times L \times N_z) \times (K \times L)$ elements. Fortunately this matrix has a Toeplitz type of symmetry. Therefore only $K \times L \times N_z$ elements need to be calculated. According to (3.9) an element of the matrix $[Z^{fa}]$ is given by

$$\begin{aligned} Z^{fa}_{mj,i} &= \int_{-\infty}^{\infty}\int_{-\infty}^{\infty}\int_z\int_{z_0}\left[\bar{\bar{Q}}_E(k_x,k_y,z_0,z)\cdot\vec{J}_1^a(k_x,k_y,z_0)\right]dz_0\cdot\vec{J}_{m1}^{f*}(k_x,k_y,z)dz \\ &\quad e^{-jk_xS_{xji}}e^{-jk_yS_{yji}}dk_xdk_y, \end{aligned} \tag{3.27}$$

where $\vec{J}_1^a(k_x,k_y,z)$ is given by (3.13) and the Fourier transform of a basis function on the probe, $\vec{J}_{m1}^f(k_x,k_y,z)$, is given by expression (3.15). Again a change to polar coordinates, given by (2.21) is introduced. Substituting this in the above expression gives

$$\begin{aligned} Z^{fa}_{mj,i} &= \int_0^{\infty}\int_{-\pi}^{\pi}\int_z\int_{z_0}\left[\bar{\bar{Q}}_E(\beta,\alpha,z_0,z)\cdot\vec{J}_1^a(\beta,\alpha,z_0)\right]dz_0\cdot\vec{J}_{m1}^{f*}(\beta,\alpha,z)dz \\ &\quad e^{-jk_0\beta\cos\alpha S_{xji}}e^{-jk_0\beta\sin\alpha S_{yji}}k_0^2\beta d\beta d\alpha. \end{aligned} \tag{3.28}$$

The α- and the two z-integrations can be performed analytically. Doing this, one finally arrives at the following expression for $Z^{fa}_{mj,i}$

$$Z^{fa}_{mj,i} = 2\pi \int_0^\infty J_0(k_0\beta\sqrt{S^2_{xji}+S^2_{yji}})J_0(k_0\beta a)\left(I^{fap}_m(\beta)+I^{faf}_m(\beta)J_0(k_0\beta a)\right)k_0^2\beta d\beta, \quad (3.29)$$

with

$$I^{fap}_m(\beta) = \frac{\jmath\omega\mu_0\beta}{k_0\epsilon_r Tm}\left[\epsilon_r k_2\cos k_1(d-z'_1)+\jmath k_1\sin k_1(d-z'_1)\right]\frac{1}{k_0\beta}\left[\frac{2J_1(k_0\beta b_a)}{b_a k_0\beta}-J_0(k_0\beta a)\right]$$
$$\begin{cases}\dfrac{2}{hk_1^2}\left[1-\cos(k_1\dfrac{h}{2})\right] & m=1\\ \dfrac{2}{hk_1^2}\left[2\cos k_1 z_m-\cos k_1 z_{m+1}-\cos k_1 z_{m-1}\right] & m\geq 2\end{cases},$$

and for $m \leq N_z - 1$

$$I^{faf}_m(\beta) = \frac{-2\jmath\omega\mu_0\beta^2}{\epsilon_r h^2 k_1^4 Tm}\left\{\epsilon_r k_2\left[h\cos k_1(d-z'_1)+\frac{2\sin k_1(d-z'_1)}{k_1}-\frac{2\sin k_1(d-z'_1+\frac{h}{2})}{k_1}\right]\right.$$
$$\left.+\jmath k_1\left[h\sin k_1(d-z'_1)-\frac{2\cos k_1(d-z'_1)}{k_1}+\frac{2\cos k_1(d-z'_1+\frac{h}{2})}{k_1}\right]\right\}$$
$$\begin{cases}\left[1-\cos(k_1\dfrac{h}{2})\right] & m=1\\ \left[2\cos k_1 z_m-\cos k_1 z_{m+1}-\cos k_1 z_{m-1}\right] & 2\leq m\leq N_z-1\end{cases},$$

and for $m = N_z$ (overlap between feed mode m and the attachment mode):

$$
\begin{aligned}
I_m^{faf}(\beta) \;=\; & \frac{j\omega\mu_0}{\epsilon_r}\Bigg\{-\frac{h\epsilon_r}{12k_0^2(\beta^2-\epsilon_r)}-\frac{2\beta^2}{h^2k_1^5Tm} \\
& [\epsilon_r k_2(-2\cos k_1 z_1'\sin k_1(d-z_1') - k_1 h\sin k_1 z_1'\sin k_1(d-z_1') \\
& +2\cos k_1(z_1'-h)\sin k_1(d-z_1'+\frac{h}{2}) - 4\cos k_1(z_1'-\frac{h}{2})\sin k_1(d-z_1'+\frac{h}{2}) \\
& -k_1 h\cos k_1(z_1'-h)\cos k_1(d-z_1') + 2k_1 h\cos k_1(z_1'-\frac{h}{2})\cos k_1(d-z_1') \\
& -2\cos k_1(z_1'-h)\sin k_1(d-z_1') + 6\cos k_1(z_1'-\frac{h}{2})\sin k_1(d-z_1')) \\
& -jk_1(-2\cos k_1 z_1'\cos k_1(d-z_1') - k_1 h\sin k_1 z_1'\cos k_1(d-z_1') \\
& +2\cos k_1(z_1'-h)\cos k_1(d-z_1'+\frac{h}{2}) - 4\cos k_1(z_1'-\frac{h}{2})\cos k_1(d-z_1'+\frac{h}{2}) \\
& +k_1 h\cos k_1(z_1'-h)\sin k_1(d-z_1') - 2k_1 h\cos k_1(z_1'-\frac{h}{2})\sin k_1(d-z_1') \\
& -2\cos k_1(z_1'-h)\cos k_1(d-z_1') + 6\cos k_1(z_1'-\frac{h}{2})\cos k_1(d-z_1'))]\Bigg\},
\end{aligned}
$$

where z_m, z_{m-1} and z_{m+1} are the z-coordinates of subdomain m on the probe of antenna element j (see section 3.4.2). If $m = 1$, i.e. $N_z = 1$ then $z_1' - h$ and $z_1' - \frac{h}{2}$ should be set to zero in the above expression for $I_m^{faf}(\beta)$. The numerical problems that occur when calculating the above infinite β-integral are similar to the numerical problems discussed in the previous section for $[Z^{aa}]$. We will therefore only discuss the asymptotic form extraction technique here for the integration interval $[\sqrt{\epsilon_r'}, \infty]$. Applying this extraction technique to $[Z_{mj,i}^{fa}]$ results in

$$
\begin{aligned}
Z_{mj,i}^{fa} &= \int_0^\infty f_{mj,i}^{fa}(\beta)d\beta = \int_0^v f_{mj,i}^{fa}(\beta)d\beta + \int_v^\infty f_{mj,i}^{fa}(\beta)d\beta \\
&= \int_0^v f_{mj,i}^{fa}(\beta)d\beta + \int_v^\infty \left[f_{mj,i}^{fa}(\beta) - \widetilde{f}_{mj,i}^{fa}(\beta)\right]d\beta + \int_v^\infty \widetilde{f}_{mj,i}^{fa}(\beta)d\beta \qquad (3.30) \\
&= \left[Z_{mj,i}^{fa} - \widetilde{Z}_{mj,i}^{fa}\right] + \widetilde{Z}_{mj,i}^{fa},
\end{aligned}
$$

with

$$
\widetilde{Z}_{mj,i}^{fa} = \int_v^\infty \widetilde{f}_{mj,i}^{fa}(\beta)d\beta,
$$

where $\widetilde{f}_{mj,i}^{fa}(\beta)$ is the asymptotic form of the original integrand for large β values. This asymptotic form is unequal zero only if subdomain m on the probe touches or overlaps the attachment mode:

$$\widetilde{Z}^{fa}_{mj,i} = \frac{2\jmath\omega\mu_0\pi}{\epsilon_r} \begin{cases} \displaystyle\int_v^\infty \frac{-2J_0(k_0\beta R)J_0^2(k_0\beta a)}{h^2k_0^3\beta^2}d\beta & m = N_z - 1 \\ \displaystyle\int_v^\infty \left(-\frac{\epsilon_r h J_0^2(k_0\beta a)}{12\beta} + \frac{2J_1(k_0\beta b_a)J_0(k_0\beta a)}{b_a h\beta^2 k_0^3} \right. & \\ \left. + \frac{6J_0^2(k_0\beta a)}{h^2\beta^2k_0^3} - \frac{2J_0^2(k_0\beta a)}{h\beta k_0^2} \right) J_0(k_0\beta R)d\beta & m = N_z \ \wedge \ d < z_1' \\ \displaystyle\int_v^\infty \left(-\frac{\epsilon_r h J_0^2(k_0\beta a)}{12\beta} + \frac{4\epsilon_r J_1(k_0\beta b_a)J_0(k_0\beta a)}{b_a h\beta^2 k_0^3(\epsilon_r+1)} \right. & \\ \left. + \frac{(4\epsilon_r+8)J_0^2(k_0\beta a)}{h^2\beta^2k_0^3(\epsilon_r+1)} - \frac{2J_0^2(k_0\beta a)}{h\beta k_0^2} \right) J_0(k_0\beta R)d\beta & m = N_z \ \wedge \ d = z_1' \end{cases} \tag{3.31}$$

with $R = \sqrt{S_{xji}^2 + S_{yji}^2}$. The three types of integrals in (3.31) can be approximated by a closed form expression. These three integrals are of the same type as the integrals of (3.23) and can be calculated with the same technique as discussed in the previous section.

3.5.3 $[Z^{pa}]$: patch modes $\longleftrightarrow$ attachment modes

The submatrix $[Z^{pa}]$ contains $(K \times L \times (N_1 + N_2)) \times (K \times L)$ elements. Due to the Toeplitz type of symmetry only $4 \times K \times L \times (N_1 + N_2)$ elements need to be calculated. An element of $[Z^{pa}]$ can be calculated from

$$\begin{aligned} Z^{pa}_{mj,i} \ = \ & \int_{-\infty}^{\infty}\int_{-\infty}^{\infty}\int_{z_0} \left[\bar{\bar{Q}}_E(k_x,k_y,z_0,z_m)\cdot\vec{J}_1^{\,a}(k_x,k_y,z_0)\right] dz_0 \cdot \vec{J}_{m1}^{\,p*}(k_x,k_y,z_m) \\ & e^{-\jmath k_x S_{xji}} e^{-\jmath k_y S_{yji}} dk_x dk_y, \end{aligned} \tag{3.32}$$

where $\vec{J}_1^{\,a}(k_x,k_y,z)$ is given by (3.13) and the Fourier transform of a patch basis function $\vec{J}_{m1}^{\,p}(k_x,k_y,z_m)$ is given by (2.18). Introduce a change to polar coordinates according to (2.21). The basis functions that are being used on the rectangular patches of the array do not have a radial symmetry and therefore the α-integration cannot be performed analytically. However, the α-integration can be reduced from $[-\pi,\pi]$ to the interval $[0,\frac{\pi}{2}]$, because of symmetry considerations. The z_0-integration in (3.32) can be performed analytically. Doing this, we finally get

$$\begin{aligned} Z^{pa}_{mj,i} \ = \ & \frac{\omega\mu_0}{\epsilon_r}\int_0^{\frac{\pi}{2}}\int_0^{\infty} \left\{ \frac{-\jmath k_1\beta\sin k_1 z_1'}{Tm}\left(\frac{-2\jmath J_1(k_0\beta b_a)}{b_a k_0^2\beta^2} + \frac{\jmath J_0(k_0\beta a)}{k_0\beta}\right) \right. \\ & \left. + \frac{2k_0\beta^2}{hk_1Tm}\left(\frac{h}{2}\sin k_1 z_1' + \frac{\cos k_1 z_1'}{k_1} - \frac{\cos k_1(z_1'-\frac{h}{2})}{k_1}\right) J_0(k_0\beta a)\right\} \\ & (k_2\epsilon_r\cos k_1(d-z_m) + \jmath k_1\sin k_1(d-z_m))\, S_{pf}(m,j,i,\beta,\alpha)d\beta d\alpha, \end{aligned} \tag{3.33}$$

with

$$z_m = \begin{cases} z_1' & \text{if basis function } m \text{ on lower patch} \\ z_2' & \text{if basis function } m \text{ on upper patch,} \end{cases}$$

and with

1. $m_y = 0$, i.e. $\vec{J}_{m1}^{p} = J_{m1}^{p}\vec{e}_x$

$$S_{pf}(m,j,i,\beta,\alpha) = \begin{cases} 4\jmath\cos\alpha\sin k_x(S_{xji}-x_s)\cos k_y(S_{yji}-y_s)J_{m1}^{p*}(\beta,\alpha,z_m) & m_x \text{ odd} \\ 4\cos\alpha\cos k_x(S_{xji}-x_s)\cos k_y(S_{yji}-y_s)J_{m1}^{p*}(\beta,\alpha,z_m) & m_x \text{ even} \end{cases}$$

2. $m_x = 0$, i.e. $\vec{J}_{m1}^{p} = J_{m1}^{p}\vec{e}_y$

$$S_{pf}(m,j,i,\beta,\alpha) = \begin{cases} 4\jmath\sin\alpha\cos k_x(S_{xji}-x_s)\sin k_y(S_{yji}-y_s)J_{m1}^{p*}(\beta,\alpha,z_m) & m_y \text{ odd} \\ 4\sin\alpha\cos k_x(S_{xji}-x_s)\cos k_y(S_{yji}-y_s)J_{m1}^{p*}(\beta,\alpha,z_m) & m_y \text{ even} \end{cases}$$

The β-integration interval is divided in three sub-intervals, i.e. $[0,1]$, $[1,\sqrt{\epsilon_r'}]$ and $[\sqrt{\epsilon_r'},\infty]$. In the first two intervals the same numerical techniques will be used as discussed in section 2.6. In the last interval the asymptotic-form extraction technique is applied in order to accelerate the convergence of the β-integral. $Z_{mj,i}^{pa}$ is rewritten in the following way:

$$\begin{aligned} Z_{mj,i}^{pa} &= \int_0^{\frac{\pi}{2}}\int_0^{\infty} f_{mj,i}^{pa}(\beta)d\beta d\alpha \\ &= \int_0^{\frac{\pi}{2}}\left(\int_0^{\infty}\left[f_{mj,i}^{pa}(\beta)-\widetilde{f}_{mj,i}^{pa}(\beta)\right]d\beta+\int_0^{\infty}\widetilde{f}_{mj,i}^{pa}(\beta)d\beta\right)d\alpha \\ &= \left[Z_{mj,i}^{pa}-\widetilde{Z}_{mj,i}^{pa}\right]+\widetilde{Z}_{mj,i}^{pa}, \end{aligned} \tag{3.34}$$

with

$$\widetilde{Z}_{mj,i}^{pa} = \int_0^{\frac{\pi}{2}}\int_0^{\infty}\widetilde{f}_{mj,i}^{pa}(\beta)d\beta d\alpha,$$

where $\widetilde{f}_{mj,i}^{pa}(\beta)$ is the asymptotic form of the original integrand for large β values. This asymptotic form is only unequal zero if $z_m = z_1'$ (basis function m on lower patch). By algebraic manipulations, it is rather simple to show that $\widetilde{Z}_{mj,i}^{pa}$ is given by

$$\widetilde{Z}_{mj,i}^{pa} = \begin{cases} \dfrac{\jmath\omega\mu_0}{\epsilon_{rh}}\displaystyle\int_0^{\frac{\pi}{2}}\int_0^{\infty}\left(-\frac{\jmath J_1(k_0\beta b_a)}{k_0 b_a}+\frac{\jmath J_0(k_0\beta a)}{k_0 h}\right. & \\ \qquad\left.-\dfrac{\jmath\epsilon_r J_0(k_0\beta a)}{2\beta}\right)S_{pf}(m,j,i,\beta,\alpha)d\beta d\alpha & z_m = z_1' \\ 0 & z_m = z_2' \end{cases}, \tag{3.35}$$

with

$$\epsilon_{rh} = \begin{cases} \epsilon_r & z_1' < d \\ \dfrac{\epsilon_r + 1}{2} & z_1' = d \end{cases}.$$

There are three types of integrals in expression (3.35):

$$\begin{aligned} I_1(\alpha) &= \int_0^\infty J_1(k_0\beta b_a) S_{pf}(m,j,i,\beta,\alpha) d\beta, \\ I_2(\alpha) &= \int_0^\infty J_0(k_0\beta a) S_{pf}(m,j,i,\beta,\alpha) d\beta, \\ I_3(\alpha) &= \int_0^\infty \frac{J_0(k_0\beta a)}{\beta} S_{pf}(m,j,i,\beta,\alpha) d\beta. \end{aligned} \tag{3.36}$$

Integral $I_1(\alpha)$ and integral $I_3(\alpha)$ can be calculated with the same procedure as the procedure that has been used in section 2.7. The remaining integral $I_2(\alpha)$ has to be calculated with an other technique, because the β-integrand of $I_2(\alpha)$ is an odd function of β. We shall present a method to calculate $I_2(\alpha)$ for the case of an x-directed basis function on the lower patch of antenna element j with m_x odd and $m_y = 0$. The procedure for the other basis functions is analogeous to the one presented here. Substituting (2.18) into expression (3.36) gives

$$I_2(\alpha) = \frac{A\cos\alpha}{\sin\alpha} \int_0^\infty J_0(k_0\beta a) \frac{\cos\frac{\beta\gamma}{2} \sin\frac{\beta\xi}{2} \sin\beta\nu \cos\beta\mu}{(m_x\pi - \beta\gamma)(m_x\pi + \beta\gamma)\beta} d\beta, \tag{3.37}$$

with

$$\begin{aligned} A &= \frac{16j\pi^2 m_x^2}{k_0 W_{y1}}, \\ \gamma &= k_0 \cos\alpha W_{x1}, \\ \xi &= k_0 \sin\alpha W_{y1}, \\ \nu &= k_0 \cos\alpha (S_{xji} - x_s), \\ \mu &= k_0 \sin\alpha (S_{yji} - y_s). \end{aligned}$$

The Bessel function $J_0(k_0\beta a)$ can be represented by an integral as

$$J_0(k_0\beta a) = \frac{1}{2\pi} \int_0^{2\pi} e^{jk_0\beta a \sin\theta} d\theta = \frac{1}{2\pi} \int_0^{2\pi} e^{j\beta\tau} d\theta,$$

with $\tau = k_0 a \sin\theta$. The $J_0(k_0\beta a) \cos\frac{\beta\gamma}{2} \sin\frac{\beta\xi}{2} \sin\beta\nu \cos\beta\mu$ term in (3.37) can be expanded into a set of exponential functions:

$$J_0(k_0\beta a) \cos\frac{\beta\gamma}{2} \sin\frac{\beta\xi}{2} \sin\beta\nu \cos\beta\mu = \frac{-1}{32\pi} \int_0^{2\pi} \{g(\beta,\theta) + g(-\beta,\theta)\} d\theta, \tag{3.38}$$

with

$$g(\beta,\theta) = \left(e^{j\beta(\frac{\gamma}{2}+\frac{\xi}{2}+\nu+\mu+\tau)}-1\right)+\left(e^{j\beta(\frac{\gamma}{2}+\frac{\xi}{2}+\nu-\mu+\tau)}-1\right)-\left(e^{j\beta(\frac{\gamma}{2}+\frac{\xi}{2}-\nu+\mu+\tau)}-1\right)$$
$$-\left(e^{j\beta(\frac{\gamma}{2}+\frac{\xi}{2}-\nu-\mu+\tau)}-1\right)-\left(e^{j\beta(\frac{\gamma}{2}-\frac{\xi}{2}+\nu+\mu+\tau)}-1\right)-\left(e^{j\beta(\frac{\gamma}{2}-\frac{\xi}{2}+\nu-\mu+\tau)}-1\right)$$
$$+\left(e^{j\beta(\frac{\gamma}{2}-\frac{\xi}{2}-\nu+\mu+\tau)}-1\right)+\left(e^{j\beta(\frac{\gamma}{2}-\frac{\xi}{2}-\nu-\mu+\tau)}-1\right),$$

where the integral representation for $J_0(k_0\beta a)$ has been used. The residue theorem of Cauchy and Jordan's Lemma [11] will now be applied in order to find a closed form expression for $I_2(\alpha)$. The modified integration path of figure 3.4 will be used here. The integral

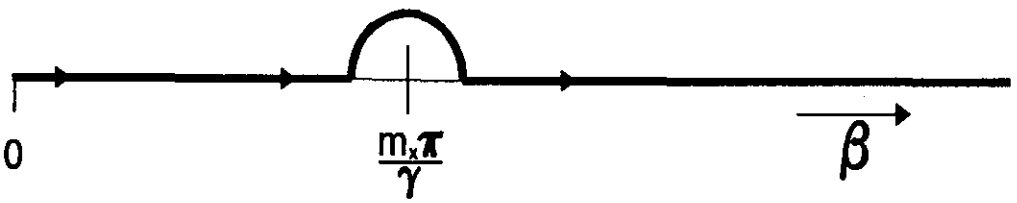

Figure 3.4: *Modified integration path for* $I_2(\alpha)$

$I_2(\alpha)$ is then given by

$$I_2(\alpha) = \frac{A\cos\alpha}{\sin\alpha}\oint_0^\infty J_0(k_0\beta a)\frac{\cos\frac{\beta\gamma}{2}\sin\frac{\beta\xi}{2}\sin\beta\nu\cos\beta\mu}{(m_x\pi-\beta\gamma)(m_x\pi+\beta\gamma)\beta}d\beta, \tag{3.39}$$

where $\oint_0^\infty$ denotes the integration path of figure 3.4. If we substitute expansion (3.38) into expression (3.39) and then divide this integral in 16 parts, we have to determine 16 integrals with the general form:

$$G(t) = \int_0^{\infty} \frac{e^{\jmath\beta t} - 1}{(m_x\pi - \beta\gamma)(m_x\pi + \beta\gamma)\beta} d\beta \tag{3.40}$$

Two situations can be distinguished in this case, namely i) $t \geq 0$ and ii) $t < 0$.

i) $t \geq 0$

The original integration path is closed with C_ρ^+ and with C_γ^+ as shown in figure 3.5.

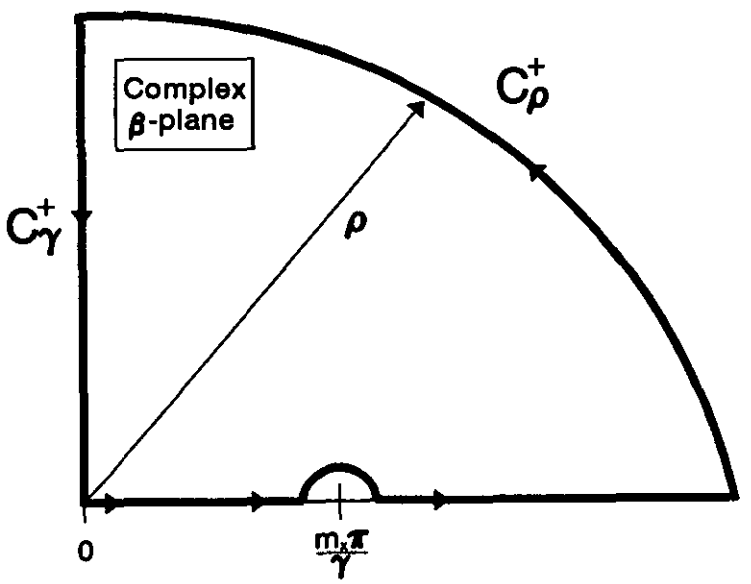

Figure 3.5: *Integration path for* $t \geq 0$

If $t \geq 0$ the integral over C_ρ^+ vanishes for $\rho \longrightarrow \infty$, because the integrand behaves as $\frac{1}{\rho^3}$ for large ρ values. Furthermore, there are no poles located within the area enclosed by the integration path of 3.5. So the only contribution to the integral $G(t)$ is the integration over C_γ^+:

$$G(t) = \int_{\jmath\infty}^{0} \frac{e^{\jmath\beta t} - 1}{(m_x\pi - \beta\gamma)(m_x\pi + \beta\gamma)\beta} d\beta \tag{3.41}$$

This may also be written in the form

$$
\begin{aligned}
G(t) &= \int_{j\infty}^{0} \frac{e^{j\beta t}-1}{(m_x\pi-\beta\gamma)(m_x\pi+\beta\gamma)\beta}d\beta \\
&= \int_{0}^{j\infty} \frac{1-e^{j\beta t}}{(m_x\pi-\beta\gamma)(m_x\pi+\beta\gamma)\beta}d\beta \\
&= \int_{0}^{\infty} \frac{1-e^{-ty}}{(m_x\pi-jy\gamma)(m_x\pi+jy\gamma)y}dy \\
&= \frac{1}{\gamma^2}\int_{0}^{\infty} \frac{1-e^{-ty}}{\left(\frac{m_x\pi}{\gamma}-jy\right)\left(\frac{m_x\pi}{\gamma}+jy\right)y}dy
\end{aligned}
\tag{3.42}
$$

Divide the integrand of the above integral in two parts and use relation 3.4.3.5 of [19]. This then gives

$$
\begin{aligned}
G(t) &= \frac{1}{\gamma^2}\int_{0}^{\infty} \frac{1-e^{-ty}}{\left(\frac{m_x\pi}{\gamma}-jy\right)\left(\frac{m_x\pi}{\gamma}+jy\right)y}dy \\
&= \frac{1}{\gamma^2}\left\{\frac{\gamma}{2m_x\pi}\int_{0}^{\infty}\frac{1-e^{-ty}}{y\left(\frac{m_x\pi}{\gamma}+jy\right)}dy + \frac{\gamma}{2m_x\pi}\int_{0}^{\infty}\frac{1-e^{-ty}}{y\left(\frac{m_x\pi}{\gamma}-jy\right)}dy\right\} \\
&= \frac{1}{2m_x^2\pi^2}\left\{2\mathcal{C}+\ln(-\frac{jm_x\pi t}{\gamma})+\ln(\frac{jm_x\pi t}{\gamma})-e^{-\frac{jm_x\pi t}{\gamma}}Ei(\frac{jm_x\pi t}{\gamma})-e^{\frac{jm_x\pi t}{\gamma}}Ei(-\frac{jm_x\pi t}{\gamma})\right\} \\
&= \frac{1}{m_x^2\pi^2}\left\{\mathcal{C}+\ln\left|\frac{m_x\pi t}{\gamma}\right|-ci\left|\frac{m_x\pi t}{\gamma}\right|\cos\left(\frac{m_x\pi t}{\gamma}\right)-si\left|\frac{m_x\pi t}{\gamma}\right|\sin\left|\frac{m_x\pi t}{\gamma}\right|\right\},
\end{aligned}
$$

for $t \geq 0$,

(3.43)

where $\mathcal{C}$ is Euler's constant and where $Ei(x)$ is the exponential-integral function [19, p. 925] and $si(x)$ and $ci(x)$ are the sine respectively cosine integrals [19, p. 928]. The exponential-integral function $Ei(x)$ can be expressed in terms of the sine and cosine integral:

$$Ei(x) = ci(x) \pm jsi(x). \tag{3.44}$$

This property has been used in (3.43).

ii) $t < 0$

The integration path for this situation is shown in figure 3.6.

There is one pole located within the area enclosed by the integration path. The contribution of the integral over C_ρ^- vanishes if $\rho \longrightarrow \infty$. So $G(t)$ can in this case be expressed in terms of the residue at $\beta = \frac{m_x\pi}{\gamma}$ and the integral over C_γ^-:

$$G(t) = -2\pi j \operatorname*{Res}_{\beta=\frac{m_x\pi}{\gamma}}\left(\frac{e^{j\beta t}-1}{(m_x\pi-\beta\gamma)(m_x\pi+\beta\gamma)\beta}\right) + \int_{-j\infty}^{0}\frac{e^{j\beta t}-1}{(m_x\pi-\beta\gamma)(m_x\pi+\beta\gamma)\beta}d\beta \tag{3.45}$$

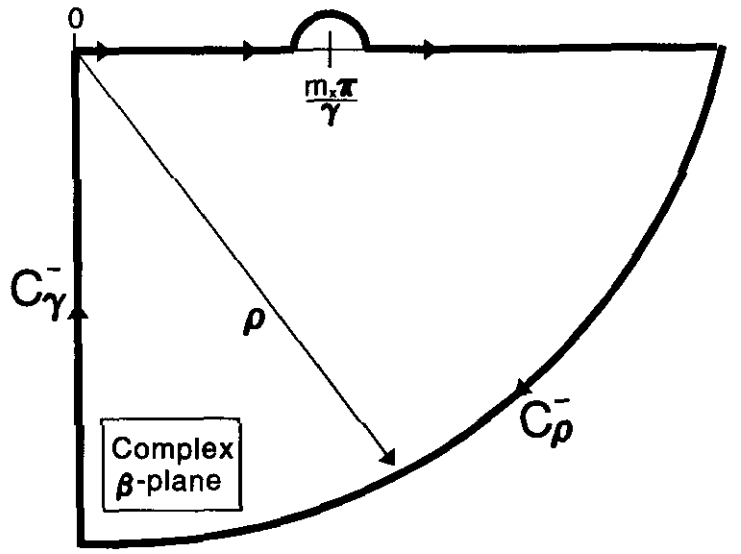

Figure 3.6: *Integration path for $t < 0$*

The residue at $\beta = \frac{m_x\pi}{\gamma}$ can be calculated with formula (2.45). Doing this we find

$$\operatorname*{Res}_{\beta = \frac{m_x\pi}{\gamma}} \left(\frac{e^{\jmath\beta t} - 1}{(m_x\pi - \beta\gamma)(m_x\pi + \beta\gamma)\beta} \right) = \frac{-1}{2m_x^2\pi^2} \left(e^{\frac{\jmath m_x\pi t}{\gamma}} - 1 \right). \tag{3.46}$$

The integration over C_γ^- can be rewritten in the following form

$$\int_{-\jmath\infty}^{0} \frac{e^{\jmath\beta t} - 1}{(m_x\pi - \beta\gamma)(m_x\pi + \beta\gamma)\beta} d\beta = \frac{1}{\gamma^2} \int_0^\infty \frac{1 - e^{ty}}{\left(\frac{m_x\pi}{\gamma} - \jmath y\right)\left(\frac{m_x\pi}{\gamma} + \jmath y\right) y} dy \tag{3.47}$$

This is exactly the same integral as in (3.42), because in this case $t < 0$. So we can use (3.43) as a result of the integral over C_γ^-. Combining (3.46) and (3.43) with (3.45) gives

$$G(t) = \frac{\jmath}{m_x^2\pi} \left(e^{\frac{\jmath m_x\pi t}{\gamma}} - 1 \right) + \frac{1}{m_x^2\pi^2} \left\{ C + \ln\left|\frac{m_x\pi t}{\gamma}\right| - ci\left|\frac{m_x\pi t}{\gamma}\right| \cos\left(\frac{m_x\pi t}{\gamma}\right) - si\left|\frac{m_x\pi t}{\gamma}\right| \sin\left|\frac{m_x\pi t}{\gamma}\right| \right\}, \tag{3.48}$$

for $t < 0$.

Define a help function $G'(t) = G(t) + G(-t)$. Then according to (3.43) and (3.48) $G'(t)$ is given by

$$G'(t) = \frac{J}{m_x^2\pi}\left(e^{-\frac{jm_x\pi|t|}{\gamma}} - 1\right) + \frac{2}{m_x^2\pi^2}\left\{C + \ln\left|\frac{m_x\pi t}{\gamma}\right| - ci\left|\frac{m_x\pi t}{\gamma}\right|\cos\left(\frac{m_x\pi t}{\gamma}\right) - si\left|\frac{m_x\pi t}{\gamma}\right|\sin\left|\frac{m_x\pi t}{\gamma}\right|\right\}. \tag{3.49}$$

The original integral $I_2(\alpha)$ given by (3.37) can now be expressed in terms of $G'(t)$

$$\begin{aligned} I_2(\alpha) &= \frac{A\cos\alpha}{\sin\alpha}\int_0^\infty J_0(k_0\beta a)\frac{\cos\frac{\beta\gamma}{2}\sin\frac{\beta\xi}{2}\sin\beta\nu\cos\beta\mu}{(m_x\pi-\beta\gamma)(m_x\pi+\beta\gamma)\beta}d\beta \\ &= \frac{-A\cos\alpha}{32\pi\sin\alpha}\int_0^{2\pi}\Big\{G'(\tfrac{\gamma}{2}+\tfrac{\xi}{2}+\nu+\mu+\tau)+G'(\tfrac{\gamma}{2}+\tfrac{\xi}{2}+\nu-\mu+\tau) \\ &\quad -G'(\tfrac{\gamma}{2}+\tfrac{\xi}{2}-\nu+\mu+\tau)-G'(\tfrac{\gamma}{2}+\tfrac{\xi}{2}-\nu-\mu+\tau) \\ &\quad -G'(\tfrac{\gamma}{2}-\tfrac{\xi}{2}+\nu+\mu+\tau)-G'(\tfrac{\gamma}{2}-\tfrac{\xi}{2}+\nu-\mu+\tau) \\ &\quad +G'(\tfrac{\gamma}{2}-\tfrac{\xi}{2}-\nu+\mu+\tau)+G'(\tfrac{\gamma}{2}-\tfrac{\xi}{2}-\nu-\mu+\tau)\Big\}d\theta \end{aligned} \tag{3.50}$$

with m_x odd and $m_y = 0$.

The θ-integration interval can be reduced to $[-\frac{\pi}{2}, \frac{\pi}{2}]$. From numerical tests we concluded that when $j \neq i$, the radius a in (3.37) can be set to zero. This then eliminates the θ integral in (3.50). Doing this very accurate results can be obtained for $I_2(\alpha)$ while the computation time is reduced significantly, because the θ-integral doesn't has to be calculated.

Now that we have found a way to compute $I_1(\alpha)$, $I_2(\alpha)$ and $I_3(\alpha)$, we can calculate $\widetilde{Z}^{pa}_{mj,i}$ by evaluating the remaining α integral in (3.35). By dividing the α integral properly into sub-intervals, only a few integration points are needed in order to obtain an accurate result. The boundaries of these sub-intervals correspond with zeros in the arguments of $G'(t)$ in expression (3.50). The α-integral needs only to be evaluated for 1 frequency point.

3.5.4 $[Z^{ff}]$: feed modes $\longleftrightarrow$ feed modes

The submatrix $[Z^{ff}]$ is a symmetric matrix containing $(K\times L\times N_z)\times(K\times L\times N_z)$ elements. This matrix has also a Toeplitz type of symmetry and therefore only $(K\times L\times N_z^2)$ elements need to be calculated. According to (3.9) an element of $[Z^{ff}]$ is given by

$$
\begin{aligned}
Z^{ff}_{mj,ni} &= \int_{-\infty}^{\infty}\int_{-\infty}^{\infty}\int_{z}\int_{z_0}\left[\bar{\bar{Q}}_E(k_x,k_y,z_0,z)\cdot\vec{J}^{f}_{n1}(k_x,k_y,z_0)\right]dz_0\cdot\vec{J}^{f*}_{m1}(k_x,k_y,z)dz \\
&\quad e^{-\jmath k_x S_{xji}}e^{-\jmath k_y S_{yji}}dk_x dk_y \\
&= \int_{-\infty}^{\infty}\int_{-\infty}^{\infty}\int_{z}\int_{z_0}\left[Q_{Ezz}(k_x,k_y,z_0,z)\vec{e}_z\cdot\vec{J}^{f}_{n1}(k_x,k_y,z_0)\right]dz_0\vec{e}_z\cdot\vec{J}^{f*}_{m1}(k_x,k_y,z)dz \\
&\quad e^{-\jmath k_x S_{xji}}e^{-\jmath k_y S_{yji}}dk_x dk_y,
\end{aligned}
\tag{3.51}
$$

where $\vec{J}^{f}_{n1}(k_x,k_y,z)$ is given by (3.15) and $\bar{\bar{Q}}_E(k_x,k_y,z_0,z)$ and $Q_{Ezz}(k_x,k_y,z_0,z)$ are defined in (2.4). Introduce a change to polar coordinates (2.21) and use relation (3.19) to eliminate the α-integral. The two z-integrations can also be done in closed form (see [5, chapter 2]). What remains is an one-dimensional integral that has to be calculated numerically:

$$
Z^{ff}_{mj,ni} = 2\pi\int_0^{\infty} J_0(k_0\beta\sqrt{S^2_{xji}+S^2_{yji}})J_0^2(k_0\beta a)k_0^2\beta I^{ff}_{m,n}(\beta)d\beta, \tag{3.52}
$$

where $I^{ff}_{m,n}(\beta)$ is calculated for three situations:

1. if $m = n$

$$
\begin{aligned}
I^{ff}_{m,m} &= \frac{\jmath\omega\mu_0}{\epsilon_r}\{\left(-\frac{h\epsilon_r}{3k_0^2(\beta^2-\epsilon_r)}+\frac{4\beta^2}{hk_1^2}\right)\epsilon_m-\frac{4\beta^2}{h^2k_1^5Tm} \\
&\quad [\epsilon_r k_2\left(\cos k_1 z_{m-1}\sin k_1(d-z_{m-1})-4\cos k_1 z_{m-1}\sin k_1(d-z_m)\right. \\
&\quad +2\cos k_1 z_{m-1}\sin k_1(d-z_{m+1})+4\cos k_1 z_m\sin k_1(d-z_m) \\
&\quad \left.-4\cos k_1 z_m\sin k_1(d-z_{m+1})+\cos k_1 z_{m+1}\sin k_1(d-z_{m+1})\right) \\
&\quad -\jmath k_1\left(\cos k_1 z_{m-1}\cos k_1(d-z_{m-1})-4\cos k_1 z_{m-1}\cos k_1(d-z_m)\right. \\
&\quad +2\cos k_1 z_{m-1}\cos k_1(d-z_{m+1})+4\cos k_1 z_m\cos k_1(d-z_m) \\
&\quad \left.-4\cos k_1 z_m\cos k_1(d-z_{m+1})+\cos k_1 z_{m+1}\cos k_1(d-z_{m+1})\right)\ ]\},
\end{aligned}
$$

with $\epsilon_m = 1$ for $m \geq 2$ and $\epsilon_m = \frac{1}{2}$ for $m = 1$. In the $m = 1$ case (half rooftop basis function) z_m and z_{m-1} should be set to zero.

2. if $n = m-1$

$$
\begin{aligned}
I^{ff}_{m,m-1} &= \frac{j\omega\mu_0}{\epsilon_r}\Big\{\Big(-\frac{h\epsilon_r}{12k_0^2(\beta^2-\epsilon_r)}-\frac{2\beta^2}{hk_1^2}\Big)-\frac{4\beta^2}{h^2k_1^5Tm} \\
&\quad [\epsilon_r k_2(\cos k_1 z_{m-2}\sin k_1(d-z_{m-1})-2\cos k_1 z_{m-2}\sin k_1(d-z_m) \\
&\quad +\cos k_1 z_{m-2}\sin k_1(d-z_{m+1})+5\cos k_1 z_{m-1}\sin k_1(d-z_m) \\
&\quad -2\cos k_1 z_{m-1}\sin k_1(d-z_{m-1})-2\cos k_1 z_{m-1}\sin k_1(d-z_{m+1}) \\
&\quad -2\cos k_1 z_m\sin k_1(d-z_m)+\cos k_1 z_m\sin k_1(d-z_{m+1})) \\
&\quad -jk_1(\cos k_1 z_{m-2}\cos k_1(d-z_{m-1})-2\cos k_1 z_{m-2}\cos k_1(d-z_m) \\
&\quad +\cos k_1 z_{m-2}\cos k_1(d-z_{m+1})+5\cos k_1 z_{m-1}\cos k_1(d-z_m) \\
&\quad -2\cos k_1 z_{m-1}\cos k_1(d-z_{m-1})-2\cos k_1 z_{m-1}\cos k_1(d-z_{m+1}) \\
&\quad -2\cos k_1 z_m\cos k_1(d-z_m)+\cos k_1 z_m\cos k_1(d-z_{m+1}))]\Big\}.
\end{aligned}
$$

If $m-1=1$, i.e. $m=2$, z_{m-2} and z_{m-1} should be set to zero.

3. if $n \leq m-2$

$$
\begin{aligned}
I^{ff}_{m,n} &= -\frac{j\omega\mu_0}{\epsilon_r}\frac{4\beta^2}{h^2k_1^5Tm}[2\cos k_1 z_n-\cos k_1 z_{n-1}-\cos k_1 z_{n+1}] \\
&\quad [\epsilon_r k_2(2\sin k_1(d-z_m)-\sin k_1(d-z_{m-1})-\sin k_1(d-z_{m+1})) \\
&\quad -jk_1(2\cos k_1(d-z_m)-\cos k_1(d-z_{m-1})-\cos k_1(d-z_{m+1}))].
\end{aligned}
$$

If $n=1$, z_n and z_{n-1} should be set to zero.
The β-integration interval is again divided into three regions, i.e. $[0,1]$, $[1,\sqrt{\epsilon_r'}]$ and $[\sqrt{\epsilon_r'},\infty]$. The numerical problems at $\beta=1$ and the problems caused by the surface waves can be avoided by using the techniques of section 2.6. The convergence of the numerical β-integration in the third integration interval can be accelerated if one uses the asymptotic-form extraction technique (see (3.21)). The extracted part is given by

$$
\widetilde{Z}^{ff}_{mj,ni} = 2\pi\int_v^\infty J_0(k_0\beta\sqrt{S_{xji}^2+S_{yji}^2})J_0^2(k_0\beta a)k_0^2\beta\widetilde{I}^{ff}_{m,n}(\beta)d\beta, \tag{3.53}
$$

with

1. if $m = n$

$$\tilde{I}^{ff}_{m,m} = \frac{j\omega\mu_0}{\epsilon_r} \begin{cases} -\frac{1}{h^2k_0^4\beta^2}\left(\frac{12}{k_0\beta} - 4h\right) - \frac{h\epsilon_r}{3\beta^2k_0^2} & m > 2 \wedge z_{m+1} < d \\ -\frac{1}{h^2k_0^4\beta^2}\left(\frac{10\epsilon_r + 14}{k_0\beta(\epsilon_r + 1)} - 4h\right) - \frac{h\epsilon_r}{3\beta^2k_0^2} & m > 2 \wedge z_{m+1} = d \\ -\frac{1}{h^2k_0^4\beta^2}\left(\frac{14}{k_0\beta} - 4h\right) - \frac{h\epsilon_r}{3\beta^2k_0^2} & m = 2 \wedge z_{m+1} < d \\ -\frac{1}{h^2k_0^4\beta^2}\left(\frac{12\epsilon_r + 16}{k_0\beta(\epsilon_r + 1)} - 4h\right) - \frac{h\epsilon_r}{3\beta^2k_0^2} & m = 2 \wedge z_{m+1} = d \\ -\frac{1}{h^2k_0^4\beta^2}\left(\frac{6}{k_0\beta} - 2h\right) - \frac{h\epsilon_r}{6\beta^2k_0^2} & m = 1 \wedge z_{m+1} < d \\ -\frac{1}{h^2k_0^4\beta^2}\left(\frac{4\epsilon_r + 8}{k_0\beta(\epsilon_r + 1)} - 2h\right) - \frac{h\epsilon_r}{6\beta^2k_0^2} & m = 1 \wedge z_{m+1} = d, \end{cases}$$

2. if $n = m - 1$,

$$\tilde{I}^{ff}_{m,m-1}(\beta) = \frac{j\omega\mu_0}{\epsilon_r}\left\{-\frac{1}{h^2k_0^4\beta^2}\left[2h - \frac{8}{k_0\beta}\right] - \frac{h\epsilon_r}{12\beta^2k_0^2}\right\},$$

3. if $n \leq m - 2$,

$$\tilde{I}^{ff}_{m,n}(\beta) = \begin{cases} -\frac{2j\omega\mu_0}{\epsilon_r h^2k_0^5\beta^3} & n = m - 2 \\ 0 & \text{otherwise.} \end{cases}$$

So $\tilde{Z}^{ff}_{mj,ni}$ is non-zero only if subdomain m overlaps or touches subdomain n. Apparently two types of integrals have to be calculated:

$$\begin{aligned} I_1 &= \int_v^\infty \frac{J_0^2(k_0\beta a)J_0(k_0\beta\sqrt{S_{xji}^2 + S_{yji}^2})}{\beta}d\beta \\ I_2 &= \int_v^\infty \frac{J_0^2(k_0\beta a)J_0(k_0\beta\sqrt{S_{xji}^2 + S_{yji}^2})}{\beta^2}d\beta. \end{aligned} \tag{3.54}$$

These integrals correspond with I_1 and I_2 of (3.23). A method to calculate I_1 and I_2 has already been presented in section 3.5.1.

3.5.5 $[Z^{pf}]$: patch modes $\longleftrightarrow$ feed modes

The submatrix $[Z^{pf}]$ contains $(K \times L \times (N_1 + N_2)) \times (K \times L \times N_z)$ elements and has a Toeplitz type of symmetry. Therefore only $4 \times K \times L \times (N_1 + N_2) \times N_z$ elements need to be calculated. According to (3.9) an element of $[Z^{pf}]$ is given by

$$Z^{pf}_{mj,ni} = \int_{-\infty}^{\infty}\int_{-\infty}^{\infty}\int_{z_0}\left[\bar{\bar{Q}}_E(k_x,k_y,z_0,z_m)\cdot\vec{J}^f_{n1}(k_x,k_y,z_0)\right]dz_0\cdot\vec{J}^{p*}_{m1}(k_x,k_y,z_m) \\ e^{-\jmath k_x S_{xji}}e^{-\jmath k_y S_{yji}}dk_x dk_y, \tag{3.55}$$

where $\vec{J}^f_{n1}(k_x,k_y,z)$ is given by expression (3.15) and the Fourier transform of a basis function on the patch, $\vec{J}^p_{m1}(k_x,k_y,z_m)$, is given by (2.18). Again a change to polar coordinates in introduced. The z_0-integration can be performed analytically. With some algebraic manipulations, it is relatively simple to show that an element of $[Z^{pf}]$ is given by

$$Z^{pf}_{mj,ni} = \int_0^{\frac{\pi}{2}}\int_0^{\infty}\frac{2\omega\mu_0 k_0\beta^2}{hk_1^2\epsilon_r Tm}\left(k_2\epsilon_r\cos k_1(d-z_m)+\jmath k_1\sin k_1(d-z_m)\right)J_0(k_0\beta a) \\ S_{pf}(m,j,i,\beta,\alpha)\begin{cases}\left[1-\cos(k_1\frac{h}{2})\right]d\beta d\alpha & n=1\\ \left[2\cos k_1 z_n-\cos k_1 z_{n-1}-\cos k_1 z_{n+1}\right]d\beta d\alpha & n\geq 2,\end{cases} \tag{3.56}$$

with

$$z_m = \begin{cases} z_1' & \text{if basis function } m \text{ on lower patch}\\ z_2' & \text{if basis function } m \text{ on upper patch,}\end{cases}$$

where $S_{pf}(m,j,i,\beta,\alpha)$ is given in (3.33). When evaluating the above integral numerically, the β-integration interval is divided in three parts, i.e. $[0,1]$, $[1,\sqrt{\epsilon_r}]$ and $[\sqrt{\epsilon_r},\infty]$. In the first two intervals the numerical techniques of section 2.6 will be applied. In the third interval the asymptotic-form extraction technique (see also (3.35)) is used in order to speed up the convergence of the β-integration. This technique has only to be used for the case that $n = N_z$ and $z_m = z_1'$, i.e. if the last subdomain on the probe touches the lower patch. For this situation the extracted part is given by

$$\tilde{Z}^{pf}_{mj,ni} = \begin{cases} 0 & z_{n+1} < z_m\\ \frac{\omega\mu_0}{h\epsilon_{rh}k_0}\int_0^{\frac{\pi}{2}}\int_0^{\infty}J_0(k_0\beta a)S_{pf}(m,j,i,\beta,\alpha)d\beta d\alpha & z_{n+1}=z_1',\end{cases} \tag{3.57}$$

with

$$\epsilon_{rh} = \begin{cases} \epsilon_r & z_1' < d \\ \dfrac{\epsilon_r + 1}{2} & z_1' = d \end{cases}.$$

The β-integral in (3.57) has exactly the same form as integral $I_2(\alpha)$ in (3.36). So we can use the method of section 3.5.3 to calculate the above β-integral. The remaining α-integration is performed with a standard numerical integration routine.

3.5.6 $[Z^{pp}]$: patch modes $\longleftrightarrow$ patch modes

The matrix $[Z^{pp}]$ contains $(K \times L \times (N_1 + N_2)) \times (K \times L \times (N_1 + N_2))$ elements. An efficient method for the calculation of the elements of this matrix has already been discussed in section 2.6 of the previous section.

3.6 Calculation of the excitation matrix $[V0]$

The general structure of the excitation matrix $[V0]$ is given by (3.10). The elements of $[V0]$ can be calculated in an efficient way if one uses the same numerical approach that has been used in the previous section for the calculation of $[Z]$.

3.6.1 $[V0^a]$: attachment modes

This submatrix contains $(K \times L) \times (K \times L)$ elements. $[V0^a]$ has a Toeplitz structure, so only $(K \times L)$ elements need to be calculated. According to (3.10) an element of $[V0^a]$ can be calculated with

$$V0^a_{j,i} = -\int_{-\infty}^{\infty}\int_{-\infty}^{\infty}\left[\int_{z_0} \bar{\bar{Q}}_H(k_x, k_y, z_0, 0) \cdot \vec{J}_1^a(k_x, k_y, z_0) dz_0\right] \cdot \vec{M}^*_{frill\ 1}(k_x, k_y) \; e^{jk_x S_{xji}} e^{jk_y S_{yji}} dk_x dk_y, \tag{3.58}$$

where $\vec{M}^*_{frill\ 1}(k_x, k_y)$ is given by expression (3.11) and the Fourier transform of the attachment mode, $\vec{J}_1^a(k_x, k_y, z_0)$, is given by (3.13). The magnetic field Green's function $\bar{\bar{Q}}_H$ has already been calculated in chapter 2 and is given by (2.5). If we use a change to polar coordinates (2.21), it can be easily shown that the α-integral can be performed analytically. Furthermore, the z_0-integration in (3.58) can also be done in closed form. We finally obtain the following expression for $V0^a_{j,i}$

$$
\begin{aligned}
V0^a_{j,i} \;=\; & \frac{4\pi^2 k_0}{ln(\frac{b}{a})}\int_0^\infty \frac{J_0(k_0\beta\sqrt{S^2_{xji}+S^2_{yji}})}{Tm}\left[J_0(k_0\beta b)-J_0(k_0\beta a)\right] \\
& \left[\frac{-2\beta k_0 J_0(k_0\beta a)}{k_1^3 h}\left\{\epsilon_r k_2[\frac{hk_1}{2}\cos k_1(d-z_1')-\sin k_1(d-z_1'+\frac{h}{2})+\sin k_1(d-z_1')\right]\right. \\
& \left.-\jmath k_1[\frac{-hk_1}{2}\sin k_1(d-z_1')-\cos k_1(d-z_1'+\frac{h}{2})+\cos k_1(d-z_1')]\right\} \\
& +\jmath\left\{\frac{-2\jmath J_1(k_0\beta b_a)}{b_a k_0^2\beta^2}+\frac{\jmath J_0(k_0\beta a)}{k_0\beta}\right\}(k_2\epsilon_r\cos k_1(d-z_1')+\jmath k_1\sin k_1(d-z_1'))\Big]\,d\beta,
\end{aligned}
\tag{3.59}
$$

where we have used relation (3.19) in order to eliminate the α integration. The remaining β-integral can be calculated with a numerical integration routine. The β-integration interval is divided in three parts, i.e. $[0,1]$, $[1,\sqrt{\epsilon_r'}]$ and $[\sqrt{\epsilon_r'},\infty]$. The numerical problems due to the infinite derivative at $\beta=1$ and due to surface waves in the interval $[1,\sqrt{\epsilon_r'}]$ can be avoided by using the techniques discussed in section 2.6. The β-integral in the third interval converges very quickly in most practical situations. However, if the probe part of the attachment mode touches the groundplane, i.e. if $\frac{h}{2}=z_1'(N_z=1)$, the β-integral converges very slowly. For this situation the asymptotic-form extraction technique will be used to speed up the convergence of the β-integration. $V0^a_{j,i}$ is now written in the form

$$
\begin{aligned}
V0^a_{j,i} &= \int_0^\infty f^a_{j,i}(\beta)d\beta=\int_0^v f^a_{j,i}(\beta)d\beta+\int_v^\infty f^a_{j,i}(\beta)d\beta \\
&= \int_0^v f^a_{j,i}(\beta)d\beta+\int_v^\infty\left[f^a_{j,i}(\beta)-\widetilde{f}^a_{j,i}(\beta)\right]d\beta+\int_v^\infty \widetilde{f}^a_{j,i}(\beta)d\beta \\
&= \left[V0^a_{j,i}-\widetilde{V0}^a_{j,i}\right]+\widetilde{V0}^a_{j,i},
\end{aligned}
\tag{3.60}
$$

with

$$
\widetilde{V0}^a_{j,i}=\int_v^\infty \widetilde{f}^a_{j,i}(\beta)d\beta,
$$

where $\widetilde{f}^a_{j,i}(\beta)$ is the asymptotic form of the original β-integrand for large β values. $\widetilde{V0}^a_{j,i}$ is unequal zero only if $\frac{h}{2}=z_1'$:

$$
\widetilde{V0}^a_{j,i}=\begin{cases}
0 & \frac{h}{2}<z_1' \\
\dfrac{-4\pi^2k_0^2}{ln(\frac{b}{a})}\displaystyle\int_v^\infty \frac{2J_0(k_0\beta a)J_0(k_0\beta\sqrt{S^2_{xji}+S^2_{yji}})}{hk_0^3\beta^2}\left[J_0(k_0\beta b)-J_0(k_0\beta a)\right]d\beta & \frac{h}{2}=z_1'
\end{cases}
\tag{3.61}
$$

The above integral has the same form as the integrals in (3.23). Therefore the same techniques as discussed in section 3.5.1 can be used in order to approximate the above integral with an analytical expression.

3.6.2 $[V0^f]$: feed modes

The submatrix $[V0^f]$ contains $(K \times L \times N_z) \times (K \times L)$ elements and has a Toeplitz type of symmetry, so only $(K \times L \times N_z)$ elements have to be calculated. According to (3.10) an element of $[V0^f]$ is given by

$$V0^f_{mj,i} = -\int_{-\infty}^{\infty}\int_{-\infty}^{\infty}\left[\int_{z_0}\bar{\bar{Q}}_H(k_x,k_y,z_0,0)\cdot\vec{J}^f_{m1}(k_x,k_y,z_0)dz_0\right]\cdot\vec{M}^*_{frill\ 1}(k_x,k_y) \\ e^{\jmath k_x S_{xji}}e^{\jmath k_y S_{yji}}dk_x dk_y, \tag{3.62}$$

where $\vec{J}^f_{m1}(k_x,k_y,z_0)$ is given by (3.15) and $\vec{M}^*_{frill\ 1}(k_x,k_y)$ is given by (3.11). Using a change to polar coordinates and after performing the α- and z_0-integrations analytically, we obtain the following expression for an element of $[V0^f]$

$$\begin{aligned} V0^f_{mj,i} = & -\frac{4\pi^2k_0^2}{ln(\frac{b}{a})}\int_0^{\infty}\frac{2\beta J_0(k_0\beta a)J_0(k_0\beta\sqrt{S^2_{xji}+S^2_{yji}})}{hk_1^3Tm}[J_0(k_0\beta b)-J_0(k_0\beta a)] \\ & \{\epsilon_r k_2[2\sin k_1(d-z_m)-\sin k_1(d-z_{m-1})-\sin k_1(d-z_{m+1})] \\ & -\jmath k_1[2\cos k_1(d-z_m)-\cos k_1(d-z_{m-1})-\cos k_1(d-z_{m+1})]\}d\beta, \end{aligned} \tag{3.63}$$

where z_m, z_{m-1} and z_{m+1} are the z-coordinates of subdomain m (see figure 3.3). If $m=1$, z_m and z_{m-1} are both equal zero. The β-integration interval is again divided into three regions, i.e. $[0,1]$, $[1,\sqrt{\epsilon_r^l}]$ and $[\sqrt{\epsilon_r^l},\infty]$. The numerical techniques used in the first two intervals are the same as those of section 2.6. In the third interval the asymptotic form extraction technique is used to speed up the convergence. The extracted part is given by

$$\widetilde{V0}^f_{mj,i} = -\frac{4\pi^2k_0^2}{ln(\frac{b}{a})}\int_v^{\infty}J_0(k_0\beta a)J_0(k_0\beta\sqrt{S^2_{xji}+S^2_{yji}})[J_0(k_0\beta b)-J_0(k_0\beta a)] \\ \begin{cases} \left(\frac{1}{k_0^2\beta}-\frac{2}{k_0^3\beta^2h}\right)d\beta & m=1 \\ \frac{2}{k_0^3\beta^2h}d\beta & m=2 \\ 0 & m\geq 3. \end{cases} \tag{3.64}$$

The extracted part is only unequal zero if subdomain m touches the groundplane. The β-integral in (3.64) has the same form as the integrals in (3.23) and can therefore be approximated by an analytical expression.

3.6.3 $[V0^p]$: patch modes

This matrix contains $(K \times L \times (N_1 + N_2)) \times (K \times L)$ elements. Again the Toeplitz type of symmetry can be used to reduce the number of elements that have to be calculated. An element of $[V0^p]$ is according to (3.10) given by

$$V0^p_{mj,i} = -\int_{-\infty}^{\infty}\int_{-\infty}^{\infty}\left[\bar{\bar{Q}}_H(k_x,k_y,z_m,0)\cdot\vec{J}^p_{m1}(k_x,k_y,z_m)\right]\cdot\vec{M}^*_{frill\ 1}(k_x,k_y) \\ e^{\jmath k_x S_{xji}}e^{\jmath k_y S_{yji}}dk_x dk_y, \tag{3.65}$$

where $\vec{J}^p_{m1}(k_x,k_y,z_m)$ is given by (2.18). If we use a change to polar coordinates given by (2.21), the α-integral can be reduced to the interval $[0,\frac{\pi}{2}]$. We finally obtain

$$V0^p_{mj,i} = \frac{2\jmath\pi k_0}{ln(\frac{b}{a})}\int_0^{\infty}\int_0^{\frac{\pi}{2}}\left[J_0(k_0\beta b)-J_0(k_0\beta a)\right]S^*_{pf}(m,j,i,\beta,\alpha) \\ \frac{1}{Tm}\left[k_2\epsilon_r\cos k_1(d-z_m)+\jmath k_1\sin k_1(d-z_m)\right]d\alpha d\beta, \tag{3.66}$$

where $S_{pf}(m,j,i,\beta,\alpha)$ is defined in (3.33). The β integration interval is again divided into three parts. The asymptotic form extraction technique doesn't has to be used now, because the β-integrand converges very fast to zero for large β-values ($\sim e^{-\beta}$).

3.7 Port admittance matrix and scattering matrix

If we compare matrix equation (3.5) with matrix equation (2.14), we see that in (3.5) the port-voltage vector $[V^p]$ is used while in (2.14) the port-current vector $[I^p]$ is used to excite the array. So instead of looking at the port impedance matrix $[Z^p]$ we are going to determine the port admittance matrix $[Y^p]$ in this section. The relation between port currents and port voltages is given by

$$[I^p] = [Y^p][V^p]. \tag{3.67}$$

The relation between port current I^p_i and port voltage V^p_i is given by [7]

$$I^p_i = \frac{P^{i*}_{in}}{V^p_i} = \frac{-1}{V^p_i}\int\int\int_{source\ i}\vec{\mathcal{H}}^t\cdot\vec{\mathcal{M}}^*_{source\ i}dV, \tag{3.68}$$

where $\vec{\mathcal{H}}^t$ is the total magnetic field and $\vec{\mathcal{M}}^*_{source\ i}$ is the complex conjugate of the magnetic current distribution in the coaxial aperture of source i (see (3.2). Note that $\vec{\mathcal{H}}^t$ is the magnetic field due to the currents on all the patches and probes of the array. We may therefore write

$$\vec{\mathcal{H}}^t = \sum_{j=1}^{K\times L}\left\{I_{1j}\vec{\mathcal{H}}^a_{1j}+\sum_{m=2}^{1+N_x}I_{mj}\vec{\mathcal{H}}^f_{mj}+\sum_{m=N_x+2}^{1+N_x+N_1+N_2}I_{mj}\vec{\mathcal{H}}^p_{mj}\right\}, \tag{3.69}$$

where the superscript a refers to an attachment mode, f to a basis function on a coaxial probe and p to a basis function on one of the patches. If we substitute the above expansion into expression (3.68) we get the matrix equation

$$[I^p] = -\frac{1}{4\pi^2}[V0]^T[Z]^{-1}[V0][V^p], \tag{3.70}$$

where matrix equation (3.5) has been used. The port admittance matrix can be calculated with

$$[Y^p] = -\frac{1}{4\pi^2}[V0]^T[Z]^{-1}[V0]. \tag{3.71}$$

In literature another approach is often used to calculate the admittance matrix. One often uses the formula

$$Y_{ji}^p = \frac{I_j(0)}{V_i} \text{ with } V_j = 0 \text{ for } j \neq i, \tag{3.72}$$

where $I_j(0)$ is the current at the base of probe j ($z = 0$) which can be determined by solving matrix equation (3.5). Formula (3.72) can be derived from (3.71) if one uses the approximation

$$\vec{\mathcal{H}}^t(x,y,z) = \frac{I_j(0)}{2\pi r}, \tag{3.73}$$

where r is the distance from the point (x,y,z) to the centre of probe j. In the case of electrically thick substrates formula (3.73) gives quite accurate results. However, the error between the exact expression (3.71) and (3.72) becomes very large ($> 25\%$) if the substrate of the antenna under consideration is thin. We shall therefore always use the exact expression (3.71). Once the port admittance matrix is known, we can also calculate the scattering matrix with the relation [15]

$$[S] = \{[Y_0] - [Y^p]\}\{[Y_0] + [Y^p]\}^{-1}, \tag{3.74}$$

where $[Y_0]$ is a diagonal matrix with elements equal to the characteristic admittance Y_0 of the coaxial cables. Usually $Y_0 = \frac{1}{Z_0} = \frac{1}{50}$ $(\frac{1}{\Omega})$. The main beam of the array can be scanned at a certain angle (θ_0, ϕ_0) by using the type of excitation vector given by (2.68). The active reflection coefficient and active input impedance can then be expressed in terms of the elements of the scattering matrix (see relation (2.69) and (2.70).

3.8 Radiation pattern

The radiation pattern of a thick stacked microstrip array can be determined with the method that was also used in section 2.9. The only difference is the fact that apart from currents on the patches we now also have to incorporate the current distribution on the coaxial probes.

3.9 Results

3.9.1 Convergence considerations

A great disadvantage of the rigorous method presented in this chapter for the analysis of electrically thick microstrip arrays, is the fact that a lot of one- and two-dimensional integrals have to be calculated numerically. It is therefore interesting to investigate how much computational effort has to be used in order to obtain accurate results. In section 2.10 a strategy was proposed that speeds up the numerical analyses. The idea behind this method is the fact that the coupling between array elements located far away from each other is negligible compared to the coupling between array elements that are located close to each other. In this way $[Z]$ and $[V0]$ become sparse matrices. We shall distinguish three sets of parameters

- (k_{vmax}, l_{vmax}): All interactions in the matrix $[V0]$ between modes and sources for which the distance in x- and y-direction is larger than $k_{vmax} \times a_x$ respectively $l_{vmax} \times b_y$ are zero. This affects $[V0^a]$, $[V0^f]$ and $[V0^p]$.

- $(k^{f+a}_{zmax}, l^{f+a}_{zmax})$: All interactions with modes on the probe or with attachment modes in the matrix $[Z]$ for which the distance in x- and y-direction is larger than $k^{f+a}_{zmax} \times a_x$ respectively $l^{f+a}_{zmax} \times b_y$ are zero. This affects sub matrix $[Z^{aa}]$, $[Z^{fa}]$, $[Z^{pa}]$, $[Z^{pf}]$ and $[Z^{ff}]$.

- (k^p_{zmax}, l^p_{zmax}): All interactions with modes on one of the patches in the matrix $[Z]$ for which the distance in x- and y-direction is larger than $k^p_{zmax} \times a_x$ respectively $l^p_{zmax} \times b_y$ are zero. This affects sub matrix $[Z^{pp}]$, $[Z^{pa}]$ and $[Z^{pf}]$.

The 7×7 array of section 2.10.1 will be used to investigate the above method. In figure 3.7, 3.8 and 3.9 the results are shown when varying one of the three sets of parameters while the other are equal (7,7).
From these three figures it is clear that a lot of computation time can be saved if not all the interactions between the basis functions are calculated. Quite accurate results for the calculated coupling coefficients can be obtained if one chooses $(k_{vmax}, l_{vmax}) = (1,1)$, $(k^{f+a}_{zmax}, l^{f+a}_{zmax}) = (1,1)$ and $(k^p_{zmax}, l^p_{zmax}) = (4,4)$ for the 7×7 single-patch array configuration. If one is only interested in the coupling between adjacent array elements, one can even use $(k^p_{zmax}, l^p_{zmax}) = (2,2)$. The above method results in a dramatic reduction of computation time. If we look at the above example with $(k_{vmax}, l_{vmax}) = (1,1)$, $(k^{f+a}_{zmax}, l^{f+a}_{zmax}) = (1,1)$ and $(k^p_{zmax}, l^p_{zmax}) = (4,4)$, the total number of elements of $[Z]$ and $[V0]$ that have to be calculated is reduced from approximately $49(2 + 2N_z + N_z^2 + 2(N_1 + N_2) + N_z(N_1 + N_2) + (N_1 + N_2)^2)$ to $2 + 2N_z + N_z^2 + 2(N_1 + N_2) + N_z(N_1 + N_2) + 16(N_1 + N_2)^2$. With $N_z = 3$, $N_1 = 5$ and $N_2 = 0$ this corresponds to a reduction of the total number of non-zero elements in $[Z]$ and $[V0]$ by a factor $\frac{3283}{442} \approx 7.5$. Using this method relatively large finite arrays can be analysed while the overall computation time remains limited.

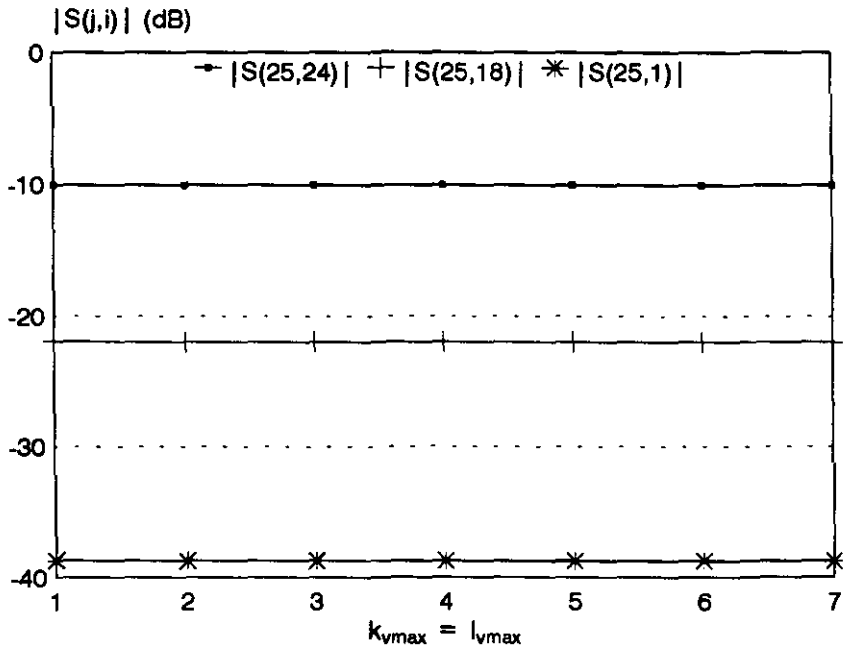

Figure 3.7: *Calculated S-parameters for various* (k_{vmax}, l_{vmax}) *values,* $f = 1.3$ *GHz*

3.9.2 Single patch layer arrays

So far as we know no measured data is available from literature concerning finite stacked-element microstrip arrays made on electrically thick substrates. We will therefore validate our model with measured data from microstrip arrays with only one patch-layer, i.e. with $z_1' = z_2'$. The first array that will be investigated is the 8×1 linear array presented in [23]. This array is based on foam material and has a relatively thick substrate with $(\frac{d}{\lambda_0} = 0.08)$. The array dimensions are given by

- patch location patch $z_1' = z_2' = 7.03mm$,
- substrate thickness $d = 7.03mm$,
- permittivity $\epsilon_r = 1.089 \quad \tan\delta = 0.0008$,
- patch dimensions $W_{x1} = W_{y1} = 31.9mm$,
- dimensions coax $a = 0.635mm$, $b = 2.1mm$,
- excitation point $X_s = 11mm$, $Y_s = 0$,
- array dimensions $a_x = 60mm$, $b_y = 0$,
- number of elements $K = 8$, $L = 1$.

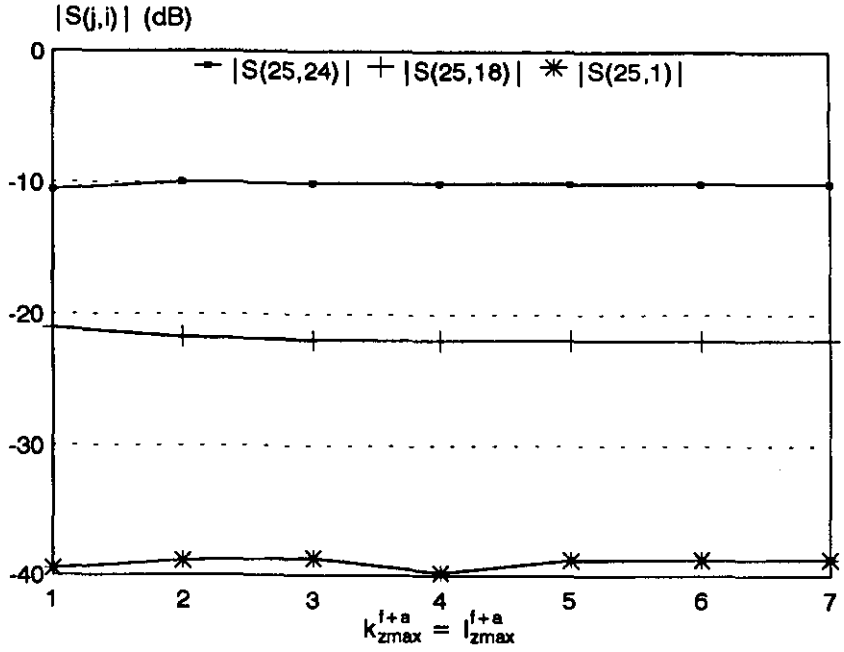

Figure 3.8: *Calculated S-parameters for various* $(k^{f+a}_{zmax}, l^{f+a}_{zmax})$ *values,* f *=1.3 GHz*

This configuration is often called an E-plane array configuration. Figure 3.10 shows a plot of the calculated and measured coupling coefficient $|S_{1,i}|$ between the last element ($j = 8$) and the other 7 elements of the linear array. The frequency is 3.3 GHz. The agreement between the calculated data and measured data is excellent. Note that the spacing between the elements of this array is approximately $0.66\lambda_0$. So if one wants to use this antenna as an active phased array, a grating lobe will appear at $\theta = 42^o$.
Next the 7×7 array of section 2.10.1 is analysed. This array has been measured in the antenna laboratory at the Eindhoven University of Technology. More details about this array can be found in section 2.10.1. The array is also based on foam and has a relatively thickness of ($\frac{d}{\lambda_0} = 0.04$). The spacing between the elements is approximately $0.5\lambda_0$. Figure 3.11 shows the calculated and measured coupling coefficients between the centre element ($j = 25$) and the elements along the $l = 4$ and $l = 3$ row, with f =1.3 GHz.

3.9.3 Stacked-element arrays

In this section an example is presented of a stacked-element finite microstrip array, based on a relatively thick dielectric substrate. One could use the model of chapter 2 if the distance between the first patch layer and the groundplane, i.e. z'_1, is very short. However, the array that we are going to investigate in this section has a long probe, so we have to use a sophisticated model for the coaxial cables. The antenna dimensions are

- patch location lower patch $z'_1 = 1.57mm$,

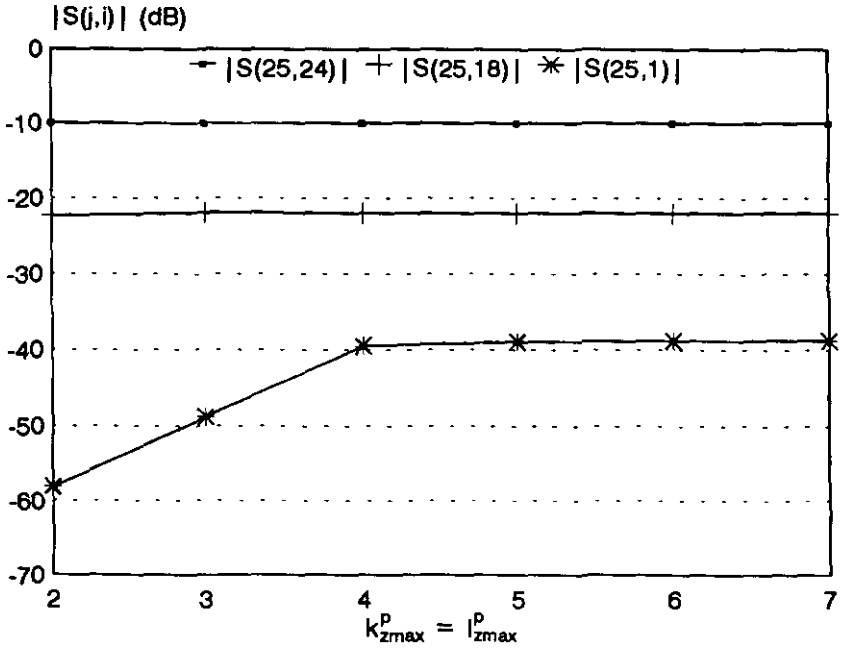

Figure 3.9: *Calculated S-parameters for various* (k^p_{zmax}, l^p_{zmax}) *values,* f *=1.3 GHz*

- patch location lower patch $z_2' = 3.14mm$,
- substrate thickness $d = 3.14mm$,
- permittivity $\epsilon_r = 2.33$ $\tan\delta = 0.001$,
- lower patch dimensions $W_{x1} = W_{y1} = 24mm$,
- upper patch dimensions $W_{x2} = W_{y2} = 23.9mm$,
- dimensions coax $a = 0.635mm$, $b = 2.1mm$,
- excitation point $X_s = 6mm$, $Y_s = 0$,
- array dimensions $a_x = 37.5mm$, $b_y = 37.5mm$,
- number of elements $K = 5$, $L = 5$.

Figure 3.12 shows a plot of the calculated input impedance versus frequency of the centre element when the array is not scanned, so $(\theta_0, \phi_0) = (0°, 0°)$. Two peaks in the input resistance plot can be observed, because of the stacked configuration. In figure 3.13 a plot is shown of the calculated mutual coupling coefficients between the centre element and the other elements of this 5 × 5 array (see figure 2.1 for the element numbering).
The H-plane coupling is far stronger than the E-plane coupling for this configuration. Compare this with the results of the 7 × 7 single patch layer array, where the E-plane coupling was more dominant.

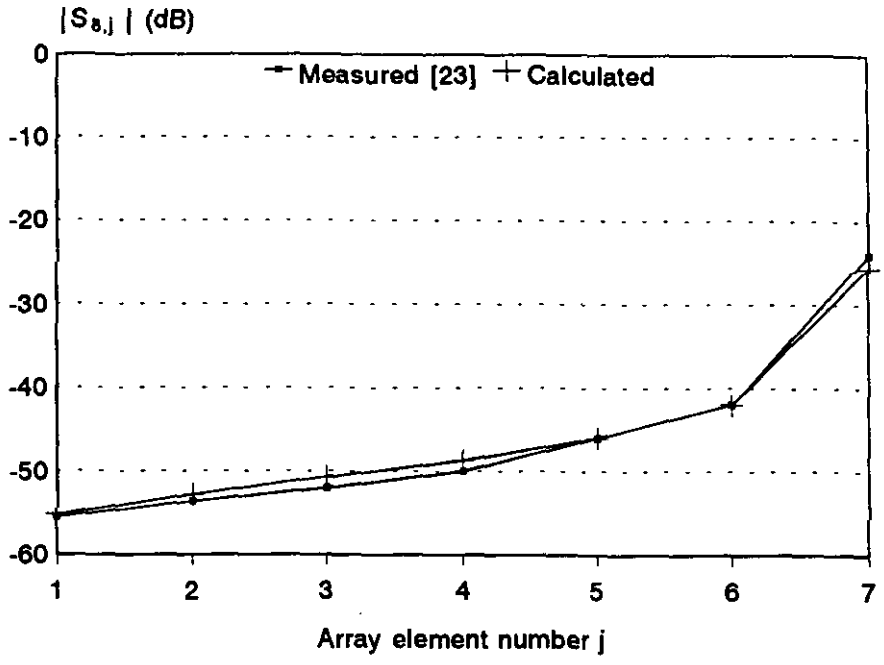

Figure 3.10: *Measured [23] and calculated coupling coefficient between element 8 and the other elements of a* 8×1 *linear E-plane array,* f *=3.3 GHz.*

3.9.4 Arrays with EMC-coupled microstrip elements

One way to improve the bandwidth of a microstrip antenna or -array is by using thick substrates. However, electrically thick substrates give rise to an inductive shift in the input impedance and therefore the use of a compensating network would be necessary. A solution for this problem could be the so-called electromagnetically coupled (EMC) microstrip structure [5]. In this case the patch is not fysically connected to the probe, i.e. $z_F < z_1'$ (see figure 3.1). We will now investigate if such an element can be used in an array configuration. A 7×1 E-plane linear array is considered with dimensions:

- patch location $z_1' = z_2' = 6.61mm$,
- substrate thickness $d = 6.61mm$,
- length of probe $z_F = 6.36mm$,
- permittivity $\epsilon_r = 2.33 \quad \tan\delta = 0.001$,
- lower patch dimensions $W_{x1} = W_{y1} = 11.5mm$,
- dimensions coax $a = 0.635mm$, $b = 2.1mm$,
- excitation point $X_s = 4.6mm$, $Y_s = 0$,

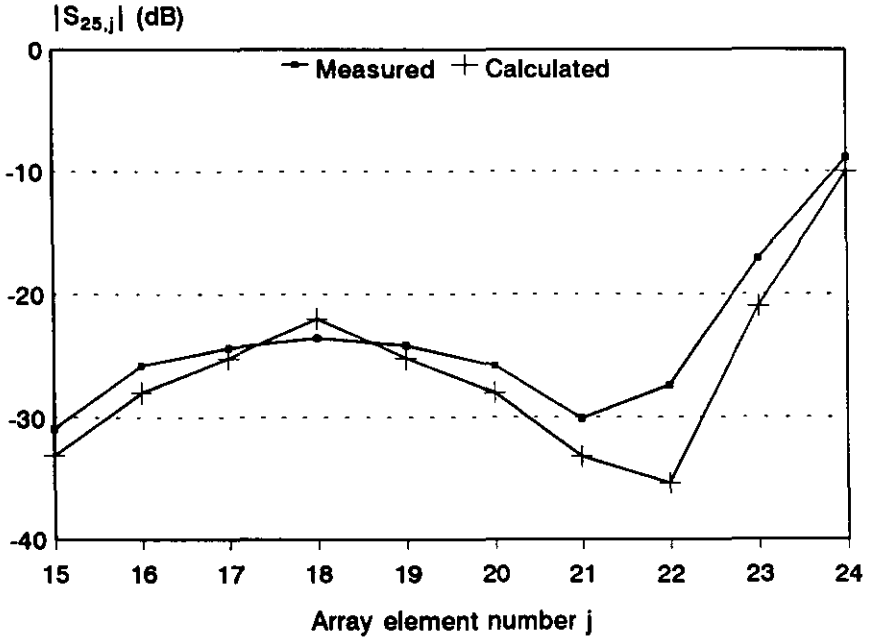

Figure 3.11: *Measured and calculated (thick substrate model) coupling coefficient between the centre element ($j = 25$) and elements of the $l = 4$ and $l = 3$ row of a 7x7 array with $j = (l-1)K + k$, $f = 1.3$ GHz*

- array dimensions $a_x = 32.mm$,
- number of elements $K = 7$, $L = 1$.

Figure 3.14 shows a plot of the calculated coupling coefficient between the first element of the array ($k = 1$) and the other six array elements for three frequencies. Figure 3.15 shows the corresponding active reflection coefficient of array element 1. From these figures it is clear that this EMC-coupled microstrip structure can be used in order to design a broadband microstrip array.

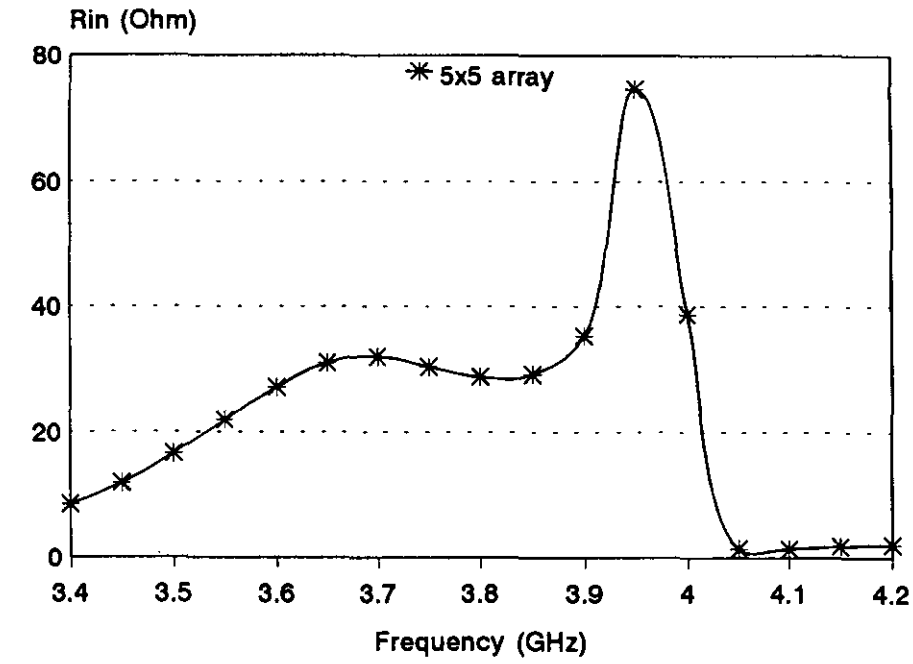

a. Real part input impedance

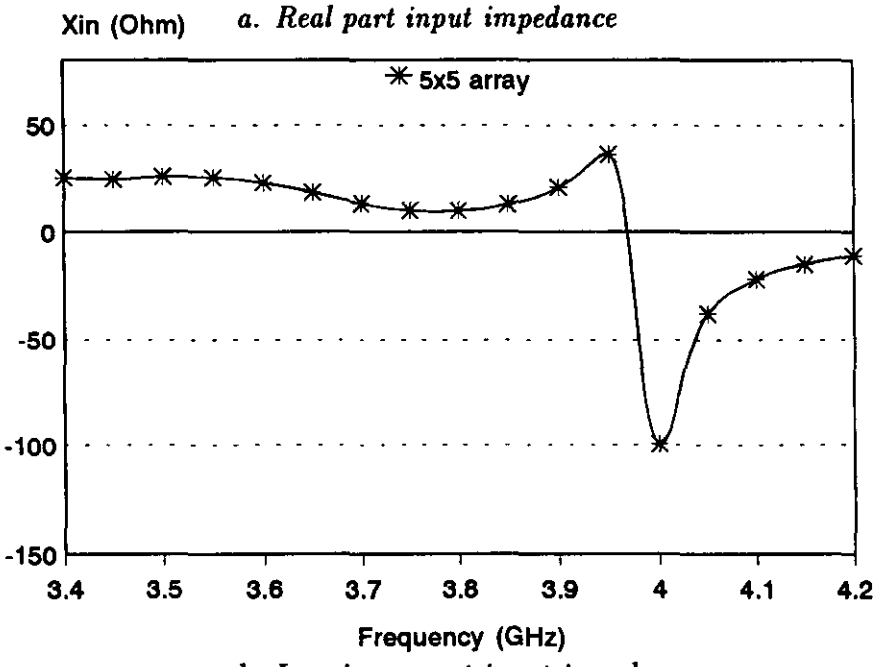

b. Imaginary part input impedance

Figure 3.12: *Centre element input impedance of a* 5×5 *stacked array versus frequency,* $\theta_0 = \phi_0 = 0$

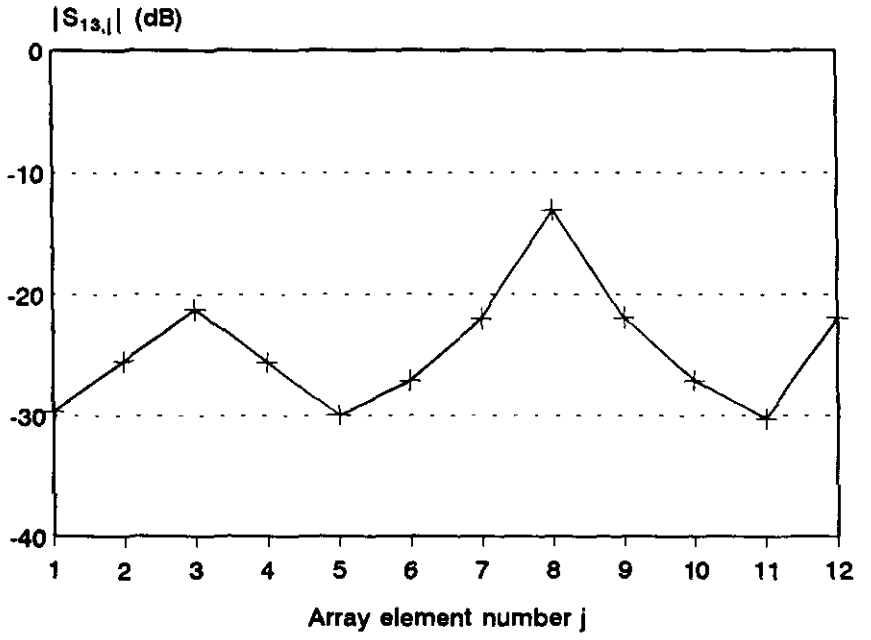

Figure 3.13: *Calculated coupling coefficient between the centre element ($j = 13$) and elements of the $l = 1$, $l = 2$ and $l = 3$ row of a 5×5 array with $j = (l-1)K + k$, $f = 3.75$ GHz*

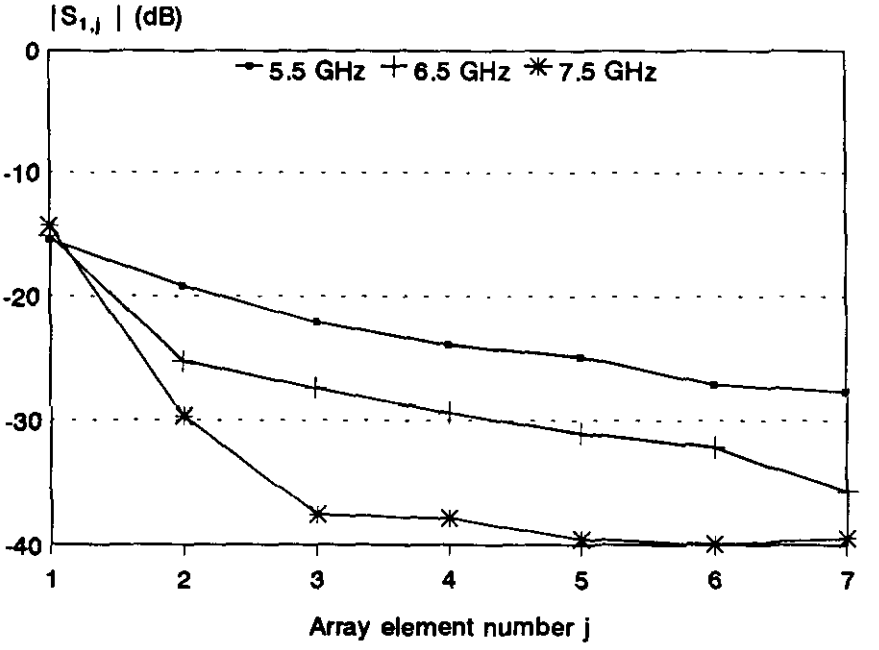

Figure 3.14: *Calculated coupling coefficient between element 1 ($k = 1$) and the other elements of a 7×1 linear EMC-array.*

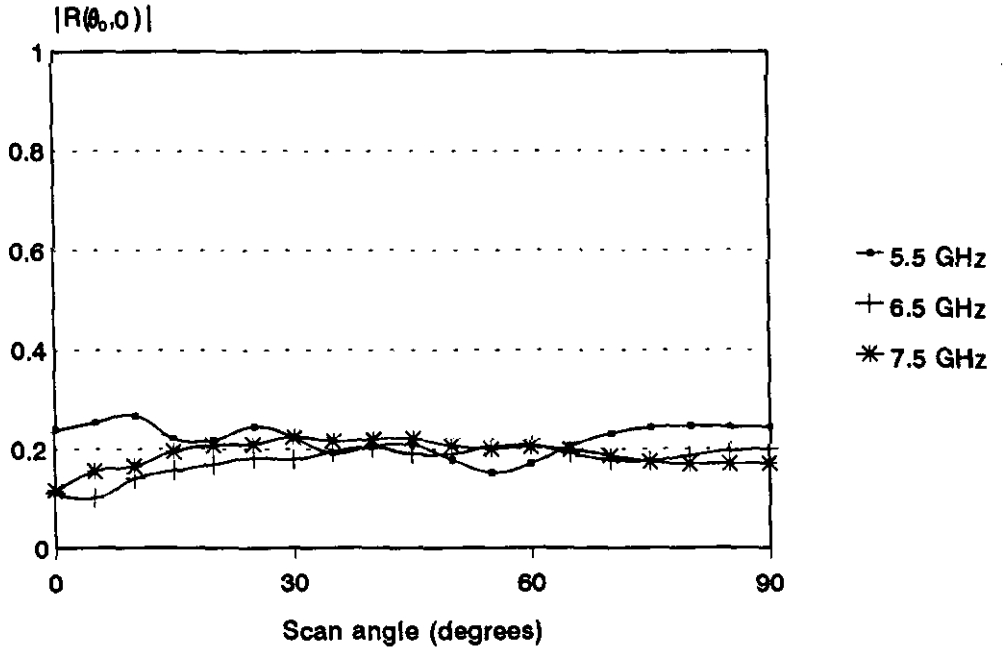

Figure 3.15: *Calculated active reflection coefficient of the first array element of a* 7×1 *linear EMC-array*

Chapter 4

Finite array of monopoles embedded in a grounded dielectric slab

Note: *This section was published as a paper in Electronics Letters, Vol.28 (1992), p.2079-2080. The numbering of its equations and references has been changed, so that they correspond with the numbering of the previous part of this report*

Finite array of monopoles embedded in a grounded dielectric slab.

Indexing terms: Phased array, monopoles

Abstract

A finite array of monopoles embedded in a dielectric slab is studied using a rigorous yet efficient spectral domain moment method. Computed input impedance data are compared with data from an infinite array analysis. Significant differences are observed, even for relatively large arrays.

Introduction

In this letter a method is presented for the analysis of finite two-dimensional arrays of vertical monopoles embedded in a grounded dielectric slab. The radiation pattern of such an array has a null at broadside. Previously, this type of arrays has been investigated by Pozar [20], who analysed an infinite array of monopoles. Fenn [21] studied a finite array of monopoles in free space. We have investigated finite arrays of monopoles embedded in a dielectric slab by using a spectral domain moment method. A sophisticated magnetic frill source model is used in order to account for the feeding coaxial cables. Both Pozar [20] and Fenn [21] use a more simple and less accurate source model.

Theory

In figure 4.1 the geometry of a finite two-dimensional array of monopoles embedded in a grounded dielectric slab is shown. The length of a monopole is d.

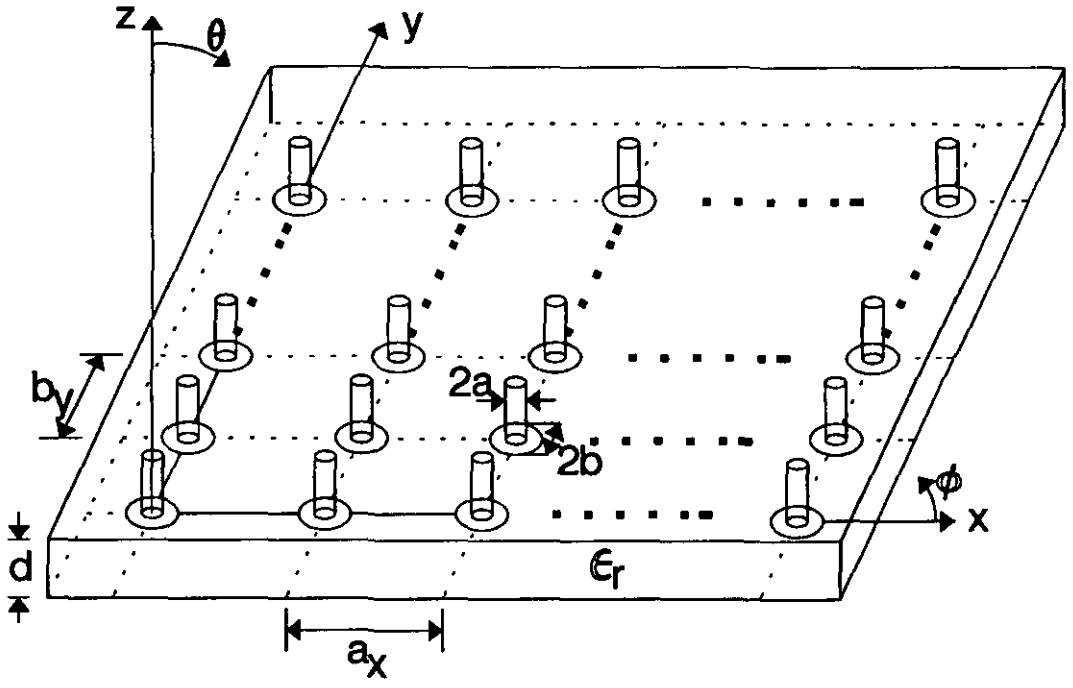

Figure 4.1: *Geometry of a finite array of vertical monopoles embedded in a grounded dielectric slab*

An antenna element is represented by a cylinder with radius a and with perfectly conducting walls. It is assumed that the z-directed surface current on this cylinder only depends on the z-coordinate. The fields corresponding to the TEM-mode in the coaxial aperture act as a source. The electric field in the coaxial aperture of antenna element 1 then takes the form [5,7]:

$$\vec{\mathcal{E}}_r^1(\vec{r}) = \frac{V_1^p}{r \ln \frac{b}{a}} \vec{e}_r, \quad a \leq r \leq b \tag{4.1}$$

where V_1^p represents the impressed port voltage at monopole 1 (=port 1). The unknown currents on the antenna elements can be found by applying the well known method of moments. The problem is formulated in the spectral domain, i.e. all quantities are transformed according to $\{x, y\} \longrightarrow \{k_x, k_y\}$. This finally results in the matrix equation:

$$[Z][I] + [V] = [0] \tag{4.2}$$

with

$$Z_{mjni} = 2\pi \int_0^\infty k_0^2 \beta J_0(k_0 \beta R_{ji}) J_0^2(k_0 \beta a) \int_z \left[\int_{z_0} Q_{Ezz}(\beta, z_0, z) g_{ni}(z_0) dz_0 \right] g_{mj}(z) dz d\beta$$

$$V_{mj} = -\frac{4\pi^2 k_0^2 V_j^p}{ln(\frac{b}{a})} \int_0^\infty \frac{\beta}{k_1 Tm} J_0(k_0 \beta R_{ji}) J_0(k_0 \beta a) \left[J_0(k_0 \beta b) - J_0(k_0 \beta a) \right]$$
$$\int_{z_0} g_{mj}(z_0) [\epsilon_r k_2 \sin k_1(d - z_0) - \jmath k_1 \cos k_1(d - z_0)] dz_0 d\beta$$

$$Q_{Ezz}(\beta, z_0, z) = \frac{\jmath \omega \mu_0}{\epsilon_r k_0^2} \delta(z - z_0)$$
$$- \frac{\jmath \omega \mu_0 \beta^2}{\epsilon_r k_1 Tm} \begin{cases} \cos k_1 z_0 \left[\epsilon_r k_2 \sin k_1(d - z) - \jmath k_1 \cos k_1(d - z) \right] & z_0 \leq z \\ \cos k_1 z \left[\epsilon_r k_2 \sin k_1(d - z_0) - \jmath k_1 \cos k_1(d - z_0) \right] & z_0 \geq z \end{cases}$$

$$Tm = k_2 \epsilon_r \cos k_1 d + \jmath k_1 \sin k_1 d$$

$$k_1^2 = \epsilon_r k_0^2 - k_x^2 - k_y^2$$

$$k_2^2 = k_0^2 - k_x^2 - k_y^2$$

$$k_0^2 \beta^2 = k_x^2 + k_y^2 \qquad k_0^2 = \omega^2 \epsilon_0 \mu_0$$

R_{ji} is the distance between monopole j and i. $g_{mj}(z)$ represents the z-dependent part of the m-th basis function on monopole j. Subdomain rooftop basis functions are used. The two z-integrations can be performed analytically for this type of basis function. The mode coefficients $[I]$ are found by solving equation (4.2). The main disadvantage of the spectral domain moment method for the analysis of finite arrays is the long computation time needed to evaluate the elements of $[Z]$ and $[V]$. Especially when the distance between monopole j and i is large. This problem is mainly due to the numerical evaluation of infinite integrals over slowly decaying and strongly oscillating functions. Fortunately we have found a way to rewrite these infinite integrals as a sum of a closed form expression and a relatively fast converging integral. In Smolders [22] this approach was used for the analysis of microstrip patch antennas. Using this analytical method, the computation time can be reduced significantly. Once the elements of $[Z]$ and $[V]$ are known the port admittance matrix $[Y^p]$ can be easily calculated. An element of the port admittance matrix is given by:

$$Y_{ji}^p = \frac{I_j^p}{V_i^p}, \qquad with \quad V_m^p = 0 \quad for \quad m \neq i \tag{4.3}$$

where I_j^p is the current at the base of monopole j and is calculated with (4.3), V_i^p is the impressed port voltage at monopole i. Once the port admittance matrix is known, the scattering matrix $[S^p]$ and the active reflection coefficient can be determined. Note that with the infinite array approach of [20], the scattering matrix cannot be calculated.

Results

We have checked our method and computer program with the results obtained by Fenn [21], who analysed finite arrays of monopoles in free space ($\epsilon_r = 1$). The agreement between our calculations and the measurements of Fenn [21] is excellent. Next we considered the array configuration of Pozar ([20], fig. 4), with $\epsilon_r = 2.5$, $d = 10mm$, $a = 0.565mm$, $a_x = b_y = 60.6mm$ and $\phi = 45^0$. Pozar [20] measured the input impedance using a waveguide simulator in the TM_{11} mode, with $\theta = \arcsin \frac{\lambda}{\sqrt{2}a_x}$. In fig. 4.2 the calculated centre element reflection coefficient against frequency for this configuration is shown for three array sizes. The characteristic impedance is 50Ω. Note that the reflection coefficient of the centre element can become larger than 1 for a finite array.

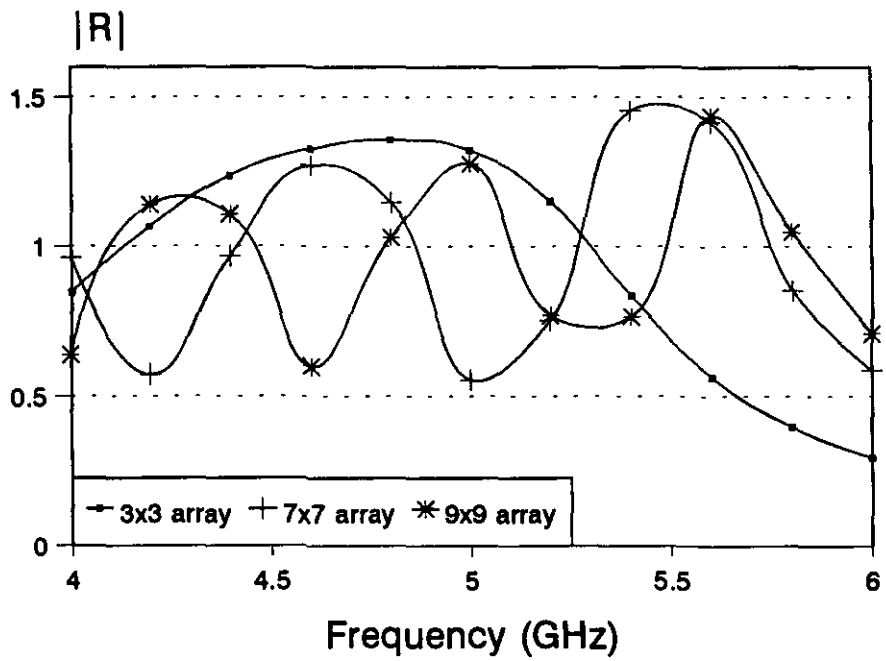

Figure 4.2: *Calculated centre element reflection coefficient magnitude versus frequency for three finite arrays of monopoles embedded in a dielectric slab*

A significant difference can be observed between the calculated reflection coefficient of figure 4.2 and the results obtained by Pozar ([20], fig. 4) using an infinite array approach, even for relatively large arrays. In Fig. 4.3, the corresponding calculated coupling coefficients between the center element and the elements of row 5 (see fig. 4.1 of a 9×9 array are given.

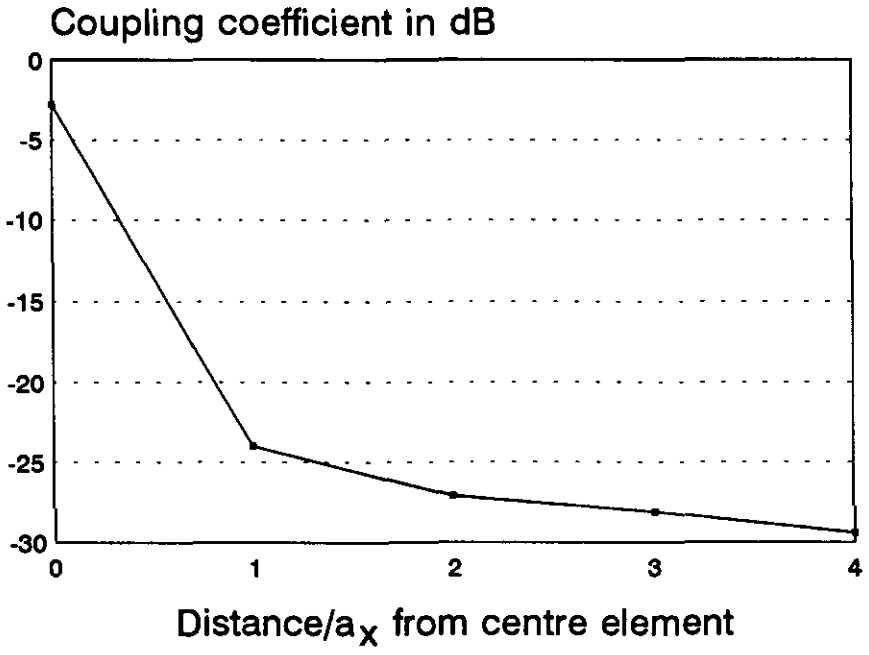

Figure 4.3: *Coupling coefficient of center element and the elements of row 5 in a* 9×9 *array of monopoles embedded in a dielectric slab,* $f = 4$ *GHz*

Conclusion

A rigorous yet efficient method is presented for the analysis of a finite array of monopoles embedded in a dielectric slab. Significant differences in calculated input impedance data between our finite array method and the infinite array approach of Pozar [20] are observed, even for relatively large arrays.

Acknowledgements

This research was supported by the Technology Foundation (STW). The author wishes to acknowledge Dr. M.E.J. Jeuken for the helpful discussions.

Chapter 5

Conclusions

Chapter 2 has dealt with finite stacked microstrip arrays based on electrically thin dielectric substrates, whereas in chapter 3 we investigated finite stacked microstrip arrays on thick substrates. In the case of an electrically thick substrate a proper model for the feeding coaxial cables has to be incorporated in the analysis, including an attachment mode between the probes and patches.
A lot of computation time can be saved if one uses the asymptotic form extraction technique. Without this analytical technique it would be almost impossible to analyse large finite arrays, because the overall computation time would become extremely long. More computation time can be saved if interactions in the method of moments matrices between basis functions that are located far away from each other are neglected. In this way these matrices become sparse matrices.
Mutual coupling measurements were made on a 7×7 planar array with a single patch layer. The measurements agreed quite well with our calculations. Two broadband microstrip structures have been investigated, namely a stacked array on a thick substrate and an array with electromagnetically coupled (EMC) microstrip elements. As could be expected, the mutual coupling deteriorates when thick substrates are being used. Despite of this, it seems that an EMC-microstrip antenna is a very good candidate for the design of broadband microstrip arrays.

Bibliography

[1] Bailey, D.M. and M.D. Deshpande
INTEGRAL EQUATION FORMULATION OF MICROSTRIP ANTENNAS.
IEEE Trans. on Antennas and Propagation, Vol. AP-30 (1982), p.651-656.

[2] Pozar, D.M.
INPUT IMPEDANCE AND MUTUAL COUPLING OF RECTANGULAR MICROSTRIP ANTENNAS.
IEEE Trans. on Antennas and Propagation, Vol. AP-30 (1982), p.1191-1196.

[3] Gronau, G.
THEORETISCHE UND EXPERIMENTELLE UNTERSUCHUNG DER VERKOPPLUNG IN STREIFENLEITUNGSANTENNEN.
Ph.D. Thesis, Duisburg University, 1987.

[4] Smolders, A.B.
AN EFFICIENT METHOD FOR ANALYZING MICROSTRIP ANTENNAS WITH A DIELECTRIC COVER USING A SPECTRAL DOMAIN MOMENT METHOD.
Eindhoven: Faculty of Electrical Engineering,
Eindhoven University of Technology, 1991.
EUT Report 91-E-255.

[5] Smolders, A.B.
RIGOROUS ANALYSIS OF THICK MICROSTRIP ANTENNAS AND WIRE ANTENNAS EMBEDDED IN A SUBSTRATE.
Eindhoven: Faculty of Electrical Engineering,
Eindhoven University of Technology, 1992
EUT Report 92-E-263.

[6] Smolders, A.B.
ANALYSIS OF MICROSTRIP ANTENNAS IN THE SPECTRAL DOMAIN USING A MOMENT METHOD.
Professional group Electromagnetism, Faculty of Electrical Engineering,
Eindhoven University of Technology, 1989.
M. Sc. Thesis, divisional no. ET-15-89.

[7] Harrington, R.F.
TIME HARMONIC FIELDS.
New York: McGraw-Hill, 1961.

[8] Carver, K.R. and J.W. Mink
MICROSTRIP ANTENNA TECHNOLOGY.
IEEE Trans. on Antennas and Propagation, Vol. AP-29 (1981), p.2-24.

[9] Pozar, D.M. and D.H. Schaubert
ANALYSIS OF AN INFINITE ARRAY OF RECTANGULAR MICROSTRIP PATCHES WITH IDEALISED PROBE FEEDS.
IEEE Trans. on Antennas and Propagation, Vol. AP-32 (1984), p. 1101-1107.

[10] Mosig, J.R. and T.K. Sarkar
COMPARISON OF QUASI-STATIC AND EXACT ELECTROMAGNETIC FIELDS FROM A HORIZONTAL ELECTRIC DIPOLE ABOVE A LOSSY DIELECTRIC BACKED BY AN IMPERFECT GROUND PLANE.
IEEE Trans. Microwave Theory and Tech., Vol. MTT-34 (1986), p. 379-387.

[11] Watson, G.N.
COMPLEX INTEGRATION AND CAUCHY'S THEOREM.
New York: Hafner, 1914.

[12] Pozar, D.M.
FINITE PHASED ARRAYS OF RECTANGULAR MICROSTRIP PATCHES.
IEEE Trans. on Antennas and Propagation, Vol. AP-34 (1986), p. 658-665.

[13] Deshpande, M.D. and P.D. Rufus Prabhakar
ANALYSIS OF DIELECTRIC COVERED INFINITE ARRAY OF RECTANGULAR MICROSTRIP ANTENNAS.
IEEE Trans. on Antennas and Propagation, Vol. AP-32 (1984), p. 1101-1107.

[14] Arts, M.J. and A.B. Smolders
STUDY OF STACKED MICROSTRIP PHASED ARRAYS.
Microwave and Optical Technology Letters, vol. 6, to be published in June 1993.

[15] Altman, J.L.
MICROWAVE CIRCUITS.
New York: Van Nostrand, 1964.

[16] Smolders, A.B. and M.E.J. Jeuken
EFFICIENT AND RIGOROUS ANALYSIS OF BROADBAND MICROSTRIP PATCH ANTENNAS USING A SPECTRAL DOMAIN MOMENT METHOD.
In: Proc. JINA'92 Int. Symp. Antennas, Nice (France) 12-14 November 1992.
Nice: Nice university, 1992. p. 75-78.

[17] Pozar, D.M.
ANALYSIS OF INFINITE ARRAYS OF PROBE-FED RECTANGULAR MICROSTRIP ANTENNAS USING A RIGOROUS FEED MODEL.
IEE Proceedings-H, Vol. 136 (1989), p. 110-119.

[18] Spanier,J and K.B. Oldham
AN ATLAS OF FUNCTIONS.
Berlin: Springer, 1987 .

[19] Gradsteyn, I.S. and I.M. Ryzhik
TABLE OF INTEGRALS, SERIES AND PRODUCTS.
New York: Academic Press, 1965.

[20] Pozar, D.M.
PERFORMANCE OF AN INFINITE ARRAY OF MONOPOLES IN A GROUNDED DIELECTRIC SLAB.
IEE Proceedings H, Vol. 137 (1990), p.117-120.

[21] Fenn, A.J.
THEORETICAL AND EXPERIMENTAL STUDY OF MONOPOLE PHASED ARRAY ANTENNAS.
IEEE Trans. on Antennas and Propagation, Vol. AP-33 (1985), p. 1118-1126.

[22] Smolders, A.B.
EFFICIENT ANALYSIS OF MICROSTRIP ANTENNAS USING A SPECTRAL DOMAIN MOMENT METHOD.
In: Proc. COST 223 workshop on active antennas, Noordwijk (Netherlands) 11-12 June 1992.
Noordwijk: ESTEC, 1992. p. 11.1-11.8.

[23] Nauwelears, B. and A. van de Capelle
DEVELOPMENT OF AN ANALYSIS TOOL FOR MICROSTRIP (PHASED) ARRAY ANTENNAS WITH RECTANGULAR ELEMENTS.
Katholieke Universiteit Leuven, ESAT-TELEMIC Report (ESTEC/Contract No. 8593/89/NL/PB(SC)).
Leuven: Leuven University, 1991.

Eindhoven University of Technology Research Reports ISSN 0167-9708
Coden: TEUEDE

Faculty of Electrical Engineering

(249) Zhu, Y.C. and A.C.P.M. Backx, P. Eykhoff
MULTIVARIABLE PROCESS IDENTIFICATION FOR ROBUST CONTROL.
EUT Report 91-E-249. 1991. ISBN 90-6144-249-4

(250) Pfaffenhöfer, F.M. and P.J.M. Cluitmans, H.M. Kuipers
EMDABS: Design and formal specification of a datamodel for a clinical research database system.
EUT Report 91-E-250. 1991. ISBN 90-6144-250-8

(251) Eijndhoven, J.T.J. van and G.G. de Jong, L. Stok
THE ASCIS DATA FLOW GRAPH: Semantics and textual format.
EUT Report 91-E-251. 1991. ISBN 90-6144-251-6

(252) Chen, J. and P.J.I. de Maagt, M.H.A.J. Herben
WIDE-ANGLE RADIATION PATTERN CALCULATION OF PARABOLOIDAL REFLECTOR ANTENNAS: A comparative study.
EUT Report 91-E-252. 1991. ISBN 90-6144-252-4

(253) Haan, S.W.H. de
A PWM CURRENT-SOURCE INVERTER FOR INTERCONNECTION BETWEEN A PHOTOVOLTAIC ARRAY AND THE UTILITY LINE.
EUT Report 91-E-253. 1991. ISBN 90-6144-253-2

(254) Velde, M. van de and P.J.M. Cluitmans
EEG ANALYSIS FOR MONITORING OF ANESTHETIC DEPTH.
EUT Report 91-E-254. 1991. ISBN 90-6144-254-0

(255) Smolders, A.B.
AN EFFICIENT METHOD FOR ANALYZING MICROSTRIP ANTENNAS WITH A DIELECTRIC COVER USING A SPECTRAL DOMAIN MOMENT METHOD.
EUT Report 91-E-255. 1991. ISBN 90-6144-255-9

(256) Backx, A.C.P.M. and A.A.H. Damen
IDENTIFICATION FOR THE CONTROL OF MIMO INDUSTRIAL PROCESSES.
EUT Report 91-E-256. 1991. ISBN 90-6144-256-7

(257) Maagt, P.J.I. de and H.G. ter Morsche, J.L.M. van den Broek
A SPATIAL RECONSTRUCTION TECHNIQUE APPLICABLE TO MICROWAVE RADIOMETRY.
EUT Report 92-E-257. 1992. ISBN 90-6144-257-5

(258) Vleeshouwers, J.M.
DERIVATION OF A MODEL OF THE EXCITER OF A BRUSHLESS SYNCHRONOUS MACHINE.
EUT Report 92-E-258. 1992. ISBN 90-6144-258-3

(259) Orlov, V.B.
DEFECT MOTION AS THE ORIGIN OF THE 1/F CONDUCTANCE NOISE IN SOLIDS.
EUT Report 92-E-259. 1992. ISBN 90-6144-259-1

(260) Rooijackers, J.E.
ALGORITHMS FOR SPEECH CODING SYSTEMS BASED ON LINEAR PREDICTION.
EUT Report 92-E-260. 1992. ISBN 90-6144-260-5

(261) Boom, T.J.J. van den and A.A.H. Damen, Martin Klompstra
IDENTIFICATION FOR ROBUST CONTROL USING AN H-infinity NORM.
EUT Report 92-E-261. 1992. ISBN 90-6144-261-3

Eindhoven University of Technology Research Reports ISSN 0167-9708
Coden: TEUEDE

Faculty of Electrical Engineering

(262) Groten, M. and W. van Etten
LASER LINEWIDTH MEASUREMENT IN THE PRESENCE OF RIN AND USING THE RECIRCULATING SELF HETERODYNE METHOD.
EUT Report 92-E-262. 1992. ISBN 90-6144-262-1

(263) Smolders, A.B.
RIGOROUS ANALYSIS OF THICK MICROSTRIP ANTENNAS AND WIRE ANTENNAS EMBEDDED IN A SUBSTRATE.
EUT Report 92-E-263. 1992. ISBN 90-6144-263-X

(264) Freriks, L.W. and P.J.M. Cluitmans, M.J. van Gils
THE ADAPTIVE RESONANCE THEORY NETWORK: (Clustering-) behaviour in relation with brainstem auditory evoked potential patterns.
EUT Report 92-E-264. 1992. ISBN 90-6144-264-8

(265) Wellen, J.S. and F. Karouta, M.F.C. Schemmann, E. Smalbrugge, L.M.F. Kaufmann
MANUFACTURING AND CHARACTERIZATION OF GAAS/ALGAAS MULTIPLE QUANTUMWELL RIDGE WAVEGUIDE LASERS.
EUT Report 92-E-265. 1992. ISBN 90-6144-265-6

(266) Cluitmans, L.J.M.
USING GENETIC ALGORITHMS FOR SCHEDULING DATA FLOW GRAPHS.
EUT Report 92-E-266. 1992. ISBN 90-6144-266-4

(267) Józwiak, L. and A.P H. van Dijk
A METHOD FOR GENERAL SIMULTANEOUS FULL DECOMPOSITION OF SEQUENTIAL MACHINES: Algorithms and implementation.
EUT Report 92-E-267. 1992. ISBN 90-6144-267-2

(268) Boom, H. van den and W. van Etten, W.H.C. de Krom, P. van Bennekom, F. Huijskens, L. Niessen, F. de Leijer
AN OPTICAL ASK AND FSK PHASE DIVERSITY TRANSMISSION SYSTEM.
EUT Report 92-E-268. 1992. ISBN 90-6144-268-0

(269) Putten, P.H.A. van der
MULTIDISCIPLINAIR SPECIFICEREN EN ONTWERPEN VAN MICROELEKTRONICA IN PRODUKTEN (in Dutch).
EUT Report 93-E-269. 1993. ISBN 90-6144-269-9

(270) Bloks, R.H.J.
PROGRIL: A language for the definition of protocol grammars.
EUT Report 93-E-270. 1993. ISBN 90-6144-270-2

(271) Bloks, R.H.J.
CODE GENERATION FOR THE ATTRIBUTE EVALUATOR OF THE PROTOCOL ENGINE GRAMMAR PROCESSOR UNIT.
EUT Report 93-E-271. 1993. ISBN 90-6144-271-0

(272) Yan, Keping and E.M. van Veldhuizen
FLUE GAS CLEANING BY PULSE CORONA STREAMER.
EUT Report 93-E-272. 1993. ISBN 90-6144-272-9

(273) Smolders, A.B.
FINITE STACKED MICROSTRIP ARRAYS WITH THICK SUBSTRATES.
EUT Report 93-E-273 1993. ISBN 90-6144-273-7